MANIPULATING THE ELECTROSTATIC PROPERTIES OF NUCLEIC ACIDS FOR APPLICATIONS IN SENSING AND DRUG DELIVERY

by

Amberlyn Megan Peterson

A dissertation submitted to the faculty of
The University of Utah
in partial fulfillment of the requirements for the degree of

Doctor of Philosophy

Department of Chemistry

The University of Utah

August 2016

Copyright © Amberlyn Megan Peterson 2016

All Rights Reserved

The University of Utah Graduate School

STATEMENT OF DISSERTATION APPROVAL

The dissertation of **Amberlyn Megan Peterson**

has been approved by the following supervisory committee members:

Jennifer M. Heemstra	, Chair	**Dec 2, 2015** Date Approved
Hamidreza S. Ghandehari	, Member	**Dec 2, 2015** Date Approved
Joel Mark Harris	, Member	**Dec 2, 2015** Date Approved
Marc D. Porter	, Member	**Dec 2, 2015** Date Approved
Ilya Zharov	, Member	**Dec 2, 2015** Date Approved

and by **Cynthia Burrows** , Chair/Dean of

The Department/College/School of **Chemistry**

and by David B. Kieda, Dean of The Graduate School.

ABSTRACT

Electrostatics are a major driving force for many phenomena at the molecular level, where tuning polarity is vital for achieving control of assembly properties. For example, micelle formation and manipulation are governed by these forces. Negatively charged DNA can act as the polar headgroup of a monomer and, when attached to a hydrophobic polymer, the DNA can be responsive to a complementary sequence, nuclease, or molecular target. Using multiplier DNA-tocopherol conjugates, we designed micelles and characterized these structures. Micelle stability was monitored through the exchange of a FRET pair, DiI and DiO. We found that the presence of the highly charged DNA corona slows guest exchange compared to SDS or Tween80.

While characterizing the CMCs with the commonly used NR dye, we observed inconsistent results. Working with DiO, we found that its emission spectrum changes upon sequestration in a micelle, and consequently decided to test its efficiency in CMC measurement. In a parallel experiments using a variety of surfactants, we found that DiO and NR give accurate CMCs; however, DiO was more reproducible and user-friendly.

Next we investigated aptameric biosensor function in micelle solutions and found that target binding is maintained in the presence of neutral and negatively charged surfactants. Further, we found that the presence of micelles can

modulate substrate binding. We hypothesize that hydrophobic molecules are taken into the micelle core, preventing them from binding to the aptamer. Concurrently, aptamer binding with more hydrophilic molecules is only slightly affected.

Finally, we explored the ability of DNA to stabilize PNA-AuNP conjugates. Since the PNA backbone is neutral, it causes agglomeration when conjugated to AuNP. We found that if DNA is attached to the AuNPs, PNA can then be hybridized to the DNA-AuNP without causing agglomerates. Electrostatics remain important since the inclusion of a single positively charged lysine reside can cause AuNP aggregation despite the highly negatively charged DNA. We determined that PNA can gives a dose-dependent response to a target nucleic acid, and these conjugates can enter cells. Additionally, since PNA is not degraded by proteases or nucleases, this provides biological stability.

To my family, teachers, and friends who have inspired
me through the years and helped make this possible.

TABLE OF CONTENTS

LIST OF ABBREVIATIONS

λ_{em}	emission wavelength
λ_{ex}	excitation wavelength
A	adenine
ATRP	atom-transfer radical-polymerization
AuNP	gold nanoparticle
Apt	aptamer
BE	β-estradiol
BHQ1	black hole quencher 1
°C	Celsius degrees
C	cytosine
CCMV	cowpea chlorotic mottle virus
CD	circular dichroism
cf	carboxyfluorescein
CHAPS	3-[(3-cholamidopropyl)dimethylammonio]-1propanesulfonate
CMC	critical micelle concentration
CS	complementary strand
CTAB	cetyl trimethylammonium bromide
D	displacement

DCA	deoxycholic acid sodium salt
DiI	1,1'-dioctadecyl-3,3,3'3'-tetramethylindocarbocyanine perchlorate
DiO	3,3’-dioctadecyloxacarbocyanine perchlorate
DIS	dehydroisoandrosterone 3-sulfate sodium salt
DLS	dyamic light scattering
DNA	2’-deoxyribonucleic acid
DOA	deoxycorticosterone acetate
DOX	doxorubicin
DPC	DNA polymer conjugate
DPH	1,6-diphenyl-1,3,5-hexatriene
DTAB	dodecyltrimethylammonium bromide
DTT	dithiothreitol
EPR	enhanced permeability and retention
F	fluorescence
FACS	fluorescence-activated cell sorting
FAM	fluorescein
FRET	Förster resonance energy transfer
G	guanine
h	hours
HBPO-star-PEO	hyperbranchedpoly [3-ethyl-3-oxetanemeth- anol)-star-poly(ethylene oxide)] (HBPO-star-PEO)

HSA	human serum albumin
LCST	lower critical solution temperature
mRNA	messenger ribonucleic acid
N_{agg}	monomers per assembly
NaGC	sodium glycocholate
NaTC	sodium taurocholate
NR	nile red
PAGE	polyacrylamide gel electrophoresis
PBnMA	poly(benzyl methacrylate)
PBS	phosphate buffer saline
PDI	polydispersity index
PEG	polyethylene glycol
PLGA	poly(D,L-lactic-co-glycolic acid)
PNIPAAm	poly(N-isopropylacrylamide)
PNA	peptide nucleic acid
POEMA	poly[oligo(ethyleneoxide) methacrylate]
PPO	poly(propylene oxide)
pTriEGMA	poly[tri(ethylene glycol)ethyl ether methacrylate]
PX	paclitaxel
ROMP	ring-opening metathesis polymerization
SDS	sodium dodecyl sufate
SELEX	systematic evolution of ligands by exponential enrichment

T	thymine
TCEP	tris(2-carboxyethyl)phosphine
TEM	transmission electron microscopy
THF	tetrahydrofuran
U	uracil
v	volume
w	weight
XRD	X-ray diffraction

LIST OF TABLES

ACKNOWLEDGEMENTS

I am very grateful to my advisor, Prof. Jennifer M. Heemstra, for her support and guidance through this journey. I appreciate her enthusiasm for research and science.

I would also like to thank my committee members for their time and support through my graduate career. I thank those helped me with procedures and instruments, including Shelley Minteer, Jim Muller, George Sutherland, David Belnap, Hamid Ghandehari, and Marc Porter. I'd also like to thank Jo Hoovey and Cindy Burrows for helping me get into the program and navigate it.

I am also extraordinarily grateful for my group members, who helped keep me going through the hard days and troubleshoot my science. During my time in lab, I have had the opportunity to work with many great graduate students and postdocs, including Trevor Feagin, Kirsten Meek, Alex Rangel, Tilani de Costa, Ashwani Sharma, David Olsen, Nicholas Spiropulos, Tewoderos Ayele, Collin Swenson, Petr Simonov, Zhe Chen, and Zhesen Tan. I'd also like to thank the undergraduate students - Annika Pecchia-Bekkum, Nick Farrall, Evelyn Kimbrough, Erin Price, Zach Headman, Alexandra Kent, and April Anamisis,

Finally, I would like to thank my family, teachers, and friends who helped me find my passions in life and supported me through my graduate school experience. I wouldn't have been able to do it without you!

CHAPTER 1

CONTROLLING SELF-ASSEMBLY OF DNA-POLYMER CONJUGATES FOR APPLICATIONS IN IMAGING AND DRUG DELIVERY

Introduction

DNA is virtually unrivaled in its capacity for digital information storage.[1] One copy of human genomic DNA weighs only a few picograms, but encodes nearly all of the information necessary for life. Given this highly information-rich architecture, it is not surprising that researchers have found numerous applications for DNA that extend beyond its canonical biological role. These tasks include the construction of nanoscale objects in two and three dimensions, the detection of protein and small-molecule analytes, and the programming of computation and logic operations.[2-4] In many cases, these applications utilize unfunctionalized or minimally funtionalized DNA and rely on Watson-Crick or Hoogsteen base pairing interactions to drive assembly and function. However,

---

[1] Reprinted with permission from Peterson, A. M.; Heemstra, J. M. Controlling self-assembly of DNA-polymer conjugates for applications in imaging and drug delivery. *WIREs Nanomed. Nanobiotechnol.* **2014**, 282-297. Copyright 2014 John Wiley & Sons, Inc

DNA can also be attached to organic polymers or lipids to provide DNA-polymer conjugates (DPCs), which combine the information storage capability of DNA with the unique chemical properties of the polymer, opening the door to new modes of assembly and function.[5] DPCs functionalized with a water-soluble polymer such as poly(ethylene glycol) (PEG) or poly-L-lysine remain dispersed in solution, and have been used for antiviral activity,[6] nucleotide separation,[7] DNA detection,[8] and antisense delivery.[9] In contrast, this review will primarily focus on DPCs having moderately to strongly hydrophobic polymers or lipids, as these amphiphilic macromolecules are capable of assembling into nanoscale architectures such as micelles, tubes, and vesicles (Figure 1.1).[10] Each of these assembled structures has unique properties, and the type of assembly formed is largely defined by the three-dimensional shape of the monomer units. Micelles and tubes are composed of a single amphiphile layer, and in aqueous environments assemble to display a hydrophilic corona surrounding an internal hydrophobic pocket. In contrast, vesicles are composed of an amphiphilic bilayer, in which the internal and external surfaces are hydrophilic and a hydrophobic layer exists between the two hydrophilic regions. Micelles and tubes primarily bind hydrophobic guest molecules. However, vesicles are capable of binding to both hydrophobic and hydrophilic guest molecules, as hydrophilic molecules can be sequestered in the aqueous interior pocket, and hydrophobic molecules can bind in the interior of the bilayer. In these DPC architectures, the DNA serves not only as the hydrophilic portion of the amphiphile, but also stores information that can be used to further direct assembly, change the structure of the assembly, or trigger guest release.[11]

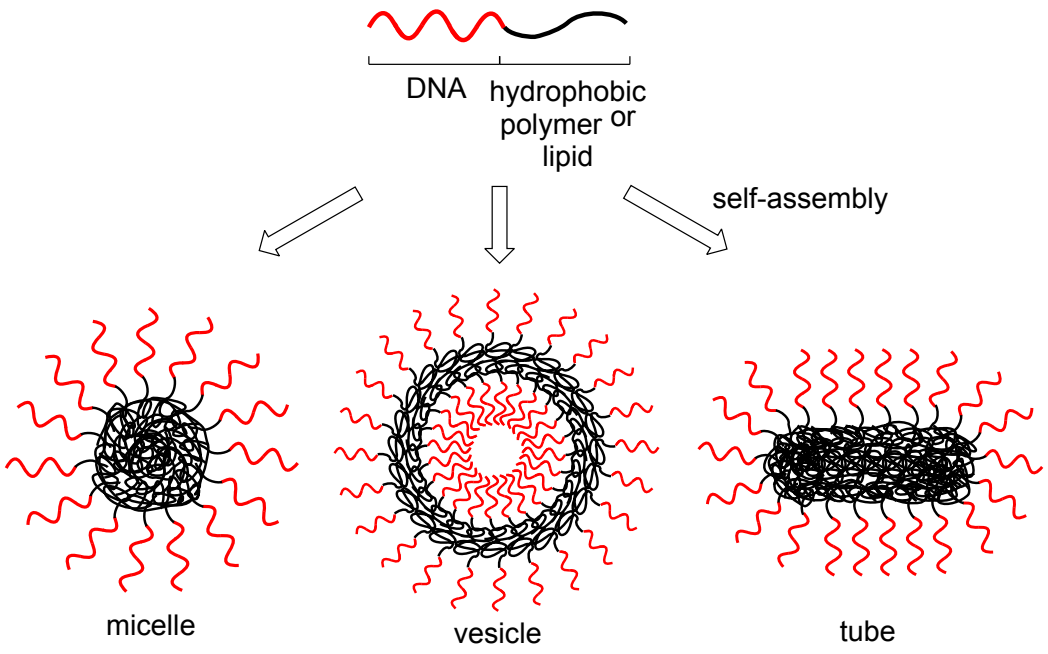

Figure 1.1. DPC monomers can self-assemble to provide a variety of architectures including micelles, vesicles, and tubes.

The earliest example of an amphiphilic DPC capable of well-ordered assembly was reported by Park and coworkers in 2001.[12] This report describes the conjugation of poly(D,L-lactic-co-glycolic acid) (PLGA) to a 15 nucleotide DNA sequence. In aqueous solvent, the monomers were designed to undergo phase-driven assembly into micellar structures in which the hydrophobic polymer is shielded from the polar solvent while the DNA is well-solvated by the aqueous environment. The amphiphilic monomers synthesized by Park and coworkers assembled into micelles having an average diameter of 65 nm. Excitingly, these micelles were also found to be cell permeable, enabling the nucleic acid segment to act as an antisense therapeutic. Since this initial report, the scope of both structure and function for DPCs has rapidly expanded, providing fundamental insights into the biophysical properties for these amphiphilic molecules, and also

significantly advancing the fields of nanoscience and nanomedicine through practical applications. The current review is divided into four sections, each covering a key aspect of DPCs. In the first section, we will discuss strategies for synthesizing DPCs, which can be challenging due to the orthogonal solubilities of DNA and organic polymers. Next, we will explore the types of architectures that can be formed by modulating the size and shape of the DNA and polymer components in the DPCs. Third, we will investigate how assembly impacts the properties of DNA such as nuclease resistance and binding affinity with other nucleic acids. Finally, we will highlight key applications in chemistry, biology, and medicine that have been made possible using DPCs.

Synthesis of DPCs

The geometry of the DNA and polymer units, as well as the connectivity between the two have a large impact on the properties of the resulting DPC assemblies, so these aspects must be taken into consideration during the design process. Typically, the DNA and polymer are covalently linked, but noncovalent conjugation using an intercalating moiety attached to the polymer has also been reported recently.[13] A broad range of chemical functionalities can be incorporated into DNA and organic polymers, enabling conjugation via a diverse array of chemical coupling reactions. Additionally, DNA can be easily modified either terminally or internally, enabling attachment of the polymer to a variety of sites along the length of the DNA strand.[14] Three general strategies have been reported for the synthesis of DPCs (Figure 1.2): (1) independent synthesis of DNA and polymer followed by solution-phase conjugation; (2) attachment of the

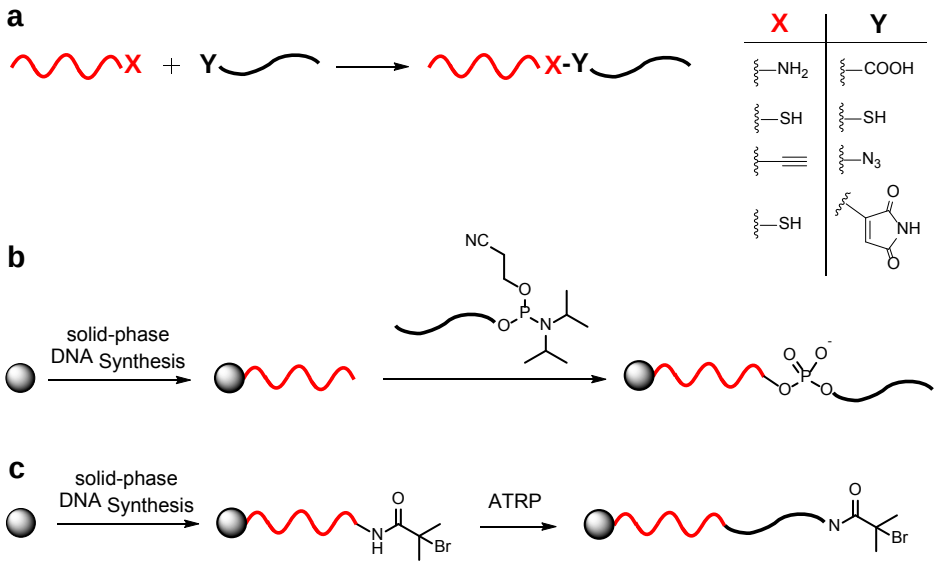

Figure 1.2. General methods for the synthesis of DPCs: (a) independent synthesis of DNA and polymer followed by solution-phase conjugation; (b) attachment of the polymer to DNA during solid-phase DNA synthesis; (c) incorporation of an initiator during solid-phase DNA synthesis followed by polymer growth.

polymer to DNA through a phosphoramidite linkage during solid-phase DNA synthesis; (3) incorporation of a polymerization initiator during solid-phase DNA synthesis followed by polymer growth from the DNA strand.[10,15] Once the DNA has been conjugated to the polymer, further modifications can be made such as enzymatic DNA extension or polymer cross-linking to stabilize the assembly.

Solution-phase conjugation of DNA and polymer

The most common method for generating DPCs involves separate synthesis of the DNA and polymer followed by solution-phase conjugation (Figure 1.2a). The polymer can be synthesized using a variety of polymerization methods including ring-opening metathesis polymerization (ROMP)[16] or atom-

transfer radical-polymerization (ATRP)[17] to give linear or branched polymers. Depending upon the structure and properties desired, the composition of the polymer can be adjusted to tune hydrophobicity, which in turn modulates the assembly properties of the resulting DPCs.[18] One strategy to accomplish such tuning employs diblock copolymers, which are synthesized from two monomers having differing polarities. The chemical properties of these polymers are dictated by the composition ratio of the two monomers, enabling fine-tuning of the overall hydrophobicity.[19]

Once the DNA and polymer are synthesized, a large number of chemical conjugation reactions can be utilized for coupling of the two to generate a DPC. The two key requirements for these reactions are that they must be compatible with the relatively polar solvents required to dissolve DNA, and they must not use reagents that are damaging to the DNA or polymer. Among the most commonly utilized coupling reactions are copper-catalyzed azide-alkyne cycloaddition,[20] Michael addition,[21] disulfide bond formation,[17] and amide bond formation.[22] In some cases, additional reagents must be added to prevent polymer or DNA degradation. For example, the copper (I) catalyst employed in azide-alkyne cycloaddition can degrade DNA via oxidative strand cleavage. However, a number of ligands have been reported that are capable of binding to copper to prevent DNA degradation, and in some cases these ligands have the added benefit of improving reaction efficiency.[23]

In carrying out conjugation reactions, the DNA and polymer do not necessarily have to be conjugated using a 1:1 stoichiometry. DPC monomers can be synthesized having varying stoichiometries of polymer to DNA if multiple

reactive groups are incorporated into one of the subunits. In one study, multiple reactive groups were appended to poly(*N*-isopropylacrylamide) (PNIPAAm) to enable attachment of several DNA strands to each polymer. By synthesizing monomers having this brush-type architecture, the authors were able to generate capsule-shaped assemblies.[24]

The solution-phase conjugation strategy for generating DPCs has the benefit of providing excellent flexibility with regard to polymer structure and chemical functionality at the DNA-polymer linkage. However, finding a solvent that is capable of dissolving both the DNA and polymer, while still facilitating the desired chemical reaction in good yield, can be extremely challenging.

Attachment of polymer during DNA synthesis

The second approach to DPC synthesis involves attachment of the polymer during solid-phase DNA synthesis (Figure 1.2b). Among the earliest reported examples of this is the "syringe method," in which the DNA is synthesized using standard solid-phase methods, then the synthesis cartridge is removed and a syringe is used to manually inject the reactants required to conjugate the polymer to the DNA.[25] While effective, early iterations of this approach often suffered from inconsistency of reaction yields. However, Gianesschi and coworkers have recently demonstrated that conjugation can be achieved with high efficiency on the solid support using amide bond forming conditions. [26]

To avert this challenge, fully automated phosphoramidite chemistry has been developed in which the polymer is directly attached to the DNA during solid-

phase synthesis. In this method, the polymer is functionalized as a phosphoramidite, enabling attachment to the 5' terminus, or is attached to the nucleobase of a standard DNA phosphoramidite monomer, enabling internal modification. A key benefit of this method is that solid-phase synthesis enables multiple polymer units to be incorporated at specific sites along the DNA sequence. For example, a recent report by Sleiman and coworkers demonstrated that hydrophobic hexaethylene and hydrophilic hexaethylene glycol blocks could be incorporated into a DNA strand in a sequence-defined manner.[27] By controlling the location and number of polymers added to the DNA strand, they were able to tune the overall hydrophobicity as well as the assembly properties. Sleiman and coworkers reported incorporation of up to 12 polymer units in a single DNA sequence. However, due to the excellent yields achieved and facile purification, they predict that a larger number of polymer units could be incorporated if desired. Sequence-controlled polymer addition during DNA synthesis has also been reported using a modified uracil base functionalized with a hydrophobic dodec-1-yne strand.[18]

Polymerization from an initiator in the DNA sequence

In the previous two strategies, the polymer must be fully formed prior to attachment to the DNA. However, solubility can present a challenge in these cases, as hydrophobic polymers often have limited solubility in the solvents used for DNA synthesis. The third strategy for DPC synthesis averts this limitation by incorporating an ATRP initiator into the DNA sequence during solid-phase synthesis (Figure 1.2c). Das and coworkers recently reported a phosphoramidite

monomer containing a bromoisobutyryl ATRP initiator, and showed that polymers including poly[oligo(ethyleneoxide) methacrylate] (POEOMA) or poly(benzyl methacrylate) (PBnMA) could be synthesized on a DNA strand either before or after cleavage of the DNA from the solid support.[15] Synthesis of the polymer prior to cleavage from the solid support enables facile purification of the DPC from excess monomers, but does require that the polymer be stable to the high pH conditions used in the cleavage step.[28]

Post-synthetic modification

Following synthesis, DPCs can be further modified in order to increase functionality or control assembly. For example, the DNA can be extended through PCR[29] or enzymatic primer extension.[30,31] Rather than creating a single continuous DNA strand, Vebert-Nardin and coworkers used DNA origami to generate a hydrophilic corona composed of two-dimensional DNA structures.[32] In this case, the polymer was conjugated to a short DNA primer using copper-catalyzed azide-alkyne cycloaddition, then the origami structure assembled from the primer. Interestingly, if the DNA origami was assembled prior to attaching the polymer, the conjugation reaction did not proceed. This highlights the role that sterics can play in determining the efficiency of DNA-polymer conjugation reactions.

The dynamic nature of noncovalently assembled DPCs can be a benefit in certain applications, but stabilization of the assembled structure may also be desirable. This can be achieved by incorporating photoreactive groups into the polymer, which react with one another upon irradiation with UV light. Reaction

between functional groups on different monomers provides covalent crosslinks which prevent dissociation of the assembled structures (Figure 1.3).[31 32]

Controlling Assembly of DNA-Polymer Conjugates

The majority of DPCs assemble to form micelles,[28] and while these architectures have found many uses, the ability to access alternative morphologies further expands the scope of potential applications. In 2007, the first DPC capable of assembling into vesicles was reported,[33] and DPCs have also been incorporated into liposomes in order to enhance function.[34] The phase-driven assembly of DPCs is controlled in large part by the monomer structure, including factors such as DNA and polymer volume,[18] hydrophilic to hydrophobic ratio,[35] geometric shape, and electrostatics.[36] Assembly can also be controlled by environmental factors such as ionic strength, temperature, and solvent polarity, or by the addition of specific chemical or biological stimuli.[37] DPCs form dynamic structures in which monomers experience fluidity within the structure, and are capable of reversible assembly and disassembly.[22] This dynamic nature of DPCs enables them to respond to changes in structure or environmental conditions with a change in assembly morphology. As such, the reversibility of assembly and transformation between morphologies has drawn much interest.

Controlling assembly through polymer and DNA modification

DPC assembly is in large part driven by minimizing contact between the hydrophobic polymer regions and the aqueous solvent. Thus, thermoresponsive

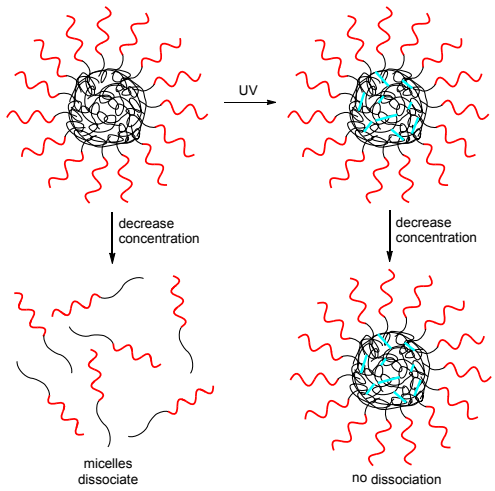

Figure 1.3. As the monomer concentration is reduced below the CMC, the micelles dissociate. However, cross-linking of the polymer segments stabilizes the micelle assemblies, preventing dissociation at low concentrations.

polymers such as PNIPAAm or poly[tri(ethylene glycol)ethyl ether methacrylate] (pTriEGMA) can be employed to control assembly as a function of temperature.[17,38,39] Below a lower critical solution temperature (LCST), these polymers are water soluble; however, once the solution temperature is raised above the LCST, the polymers become hydrophobic, initiating assembly. Maeda and coworkers found that for PNIPAAm-containing DPCs, both polymer size and structure influence assembly behavior.[40] DPCs having either linear or branched PNIPAAm form micelles at temperatures above the LCST, and increasing PNIPAAm content decreases the LCST. However, linear PNIPAAm provided micelles having larger overall diameter and number of monomers per assembly (N_{agg}) compared to branched PNIPAAm.

The hydrophobic:hydrophilic balance of the DPCs can also be modulated using modified nucleobases having an appended hydrophobic group. Herrmann

and coworkers synthesized DNA strands containing dodec-1-yne modified uracil nucleotides, and explored the effect of the number and location of the modified nucleotides on assembly properties.[18] By increasing the number of hydrophobic groups at the terminus of the DNA strand from two to four, the critical micelle concentration (CMC) decreased from 8.1 mgL^{-1} to 5.4 mgL^{-1} and the micelle diameter decreased by approximately 15%. Interestingly, however, moving the hydrophobic groups from the terminus to the middle of the DNA strand did not significantly affect the micelle shape, size, or CMC. An alternative approach to modulating hydrophobic:hydrophilic ratio is to incorporate an organic spacer between the DNA and polymer segments. Kokkoli and coworkers found that DPCs having hydrophilic spacers formed micelles while DPCs having hydrophobic spacers assembled into bilayer nanotapes.[28]

The size and sequence of the DNA portion of amphiphilic monomers can also be modulated in order to control assembly. Zauscher and coworkers investigated DNA amphiphiles having BODIPY as the hydrophobic portion and reported a combined theoretical and experimental approach to investigating the size and aggregation number of amphiphiles having 300-900 nucleotide DNA strands.[41] As the length of the DNA increased from 300 to 600 nucleotides, the N_{agg} decreased from 9 to 5 monomers, but for DNA lengths above 600 nucleotides, N_{agg} remained constant. Ionic strength was also found to influence the size of the DNA corona, with corona size increasing as ionic strength decreases. This occurs because at low ionic strength, fewer cations are available to shield the negative charge of the DNA, which leads to an increase in interstrand DNA repulsion. While these conjugates are not technically DPCs, the

results of this study would be expected to be applicable to a variety of DNA amphiphiles. For a vesicular DPC assembly, the diameter was found to be dependent upon DNA sequence, with increasing G content leading to an increase in vesicle diameter.[42] Assembly morphology can also be influenced by the conformation of the sugar of the nucleotide bound to the polymer. Changing the sugar conformation from syn to anti by heating to 35 °C resulted in an irreversible change in morphology from twisted micellar superstructures to aligned filaments.[37]

Stimuli-responsive changes in assembly

Engineering DPCs to enable stimuli-responsive control of assembly and disassembly has potential to enhance their functionality in applications such as drug delivery and biosensing. Alexander and coworkers have reported DPCs composed of two complementary DNA strands that are each functionalized with pTriEGMA such that upon hybridization, there is one polymer attached to each end of the duplex (Figure 1.4).[17] These amphiphilic duplexes can assemble into micellar structures, and this assembly process can be directed using three different types of stimuli. First, due to the thermoresponsive nature of pTriEGMA, the micelles dissociate when the solution temperature is reduced below the LCST. Second, the structure of the micelles can be altered by invading the DNA duplex with a longer complementary strand. Third, the polymer is attached to the DNA using a disulfide bond, which can be cleaved under reducing conditions, resulting in destruction of the micelle assembly.

Specific stimuli can also be utilized to alter the morphology of DPC

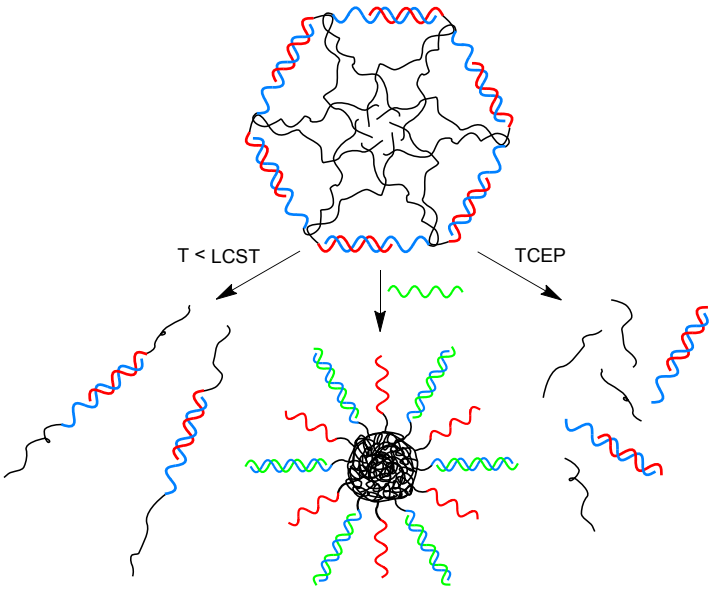

Figure 1.4. DPCs are capable of disassembly or morphology change in response to reducing temperature below the LCST of the thermoresponsive polymer, re-hybridizing one of the DNA strands to a complementary nucleic acid, or cleaving the disulfide bonds connecting the DNA to the polymer.

assemblies. Gianneschi and coworkers have explored the use of stimuli-responsive changes to the DNA portion of the DPC as a means to control monomer shape, and thus assembly morphology (Figure 1.5a).[43] Starting with conical shaped DPCs having a branched DNA structure and a linear polymer, a spherical assembly is formed. Enzymatic cleavage of the DNA brushes results in a decrease of curvature, causing the assemblies to switch to a tubular morphology. However, addition of a complementary DNA strand increases rigidity and electrostatic repulsion, enabling the assemblies to switch back to a spherical morphology. While the initial enzymatic cleavage step is irreversible, the tube-to-sphere transition can be reversibly controlled by adding or removing the complementary DNA strand. DNA hybridization can also be used to

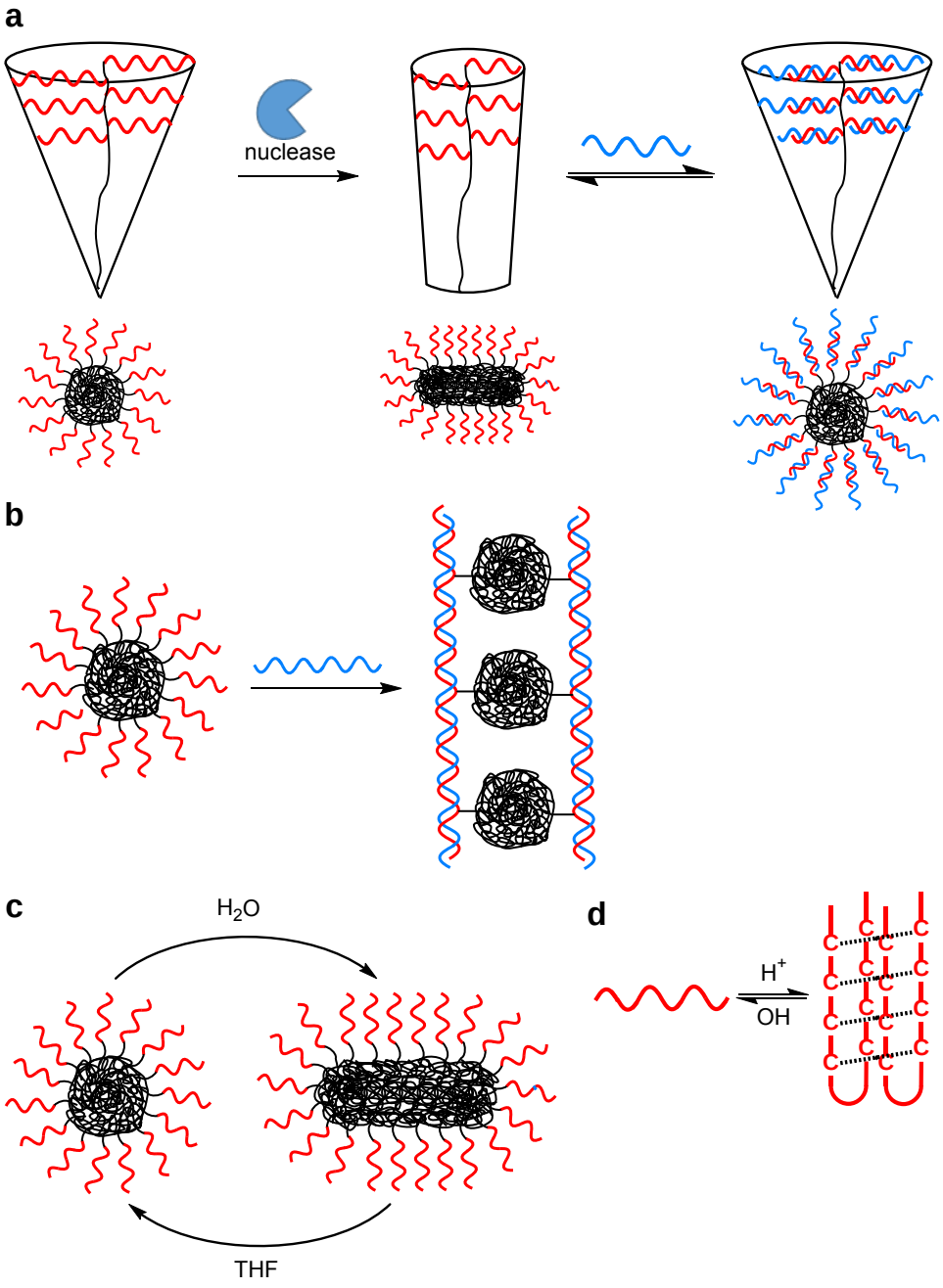

Figure 1.5. Stimuli-responsive changes to assembly morphology. (a) Enzymatic cleavage and addition of a complementary DNA strand enables switching between micelles and tubes (adapted with permission from Wiley); (b) Addition of a long complementary DNA strand transforms micelles into ladder structures (adapted with permission from Wiley); (c) Changing solvent polarity enables switching between micelles and tubes; (d) pH-dependent formation of an i-motif.

assemble micelles into higher order structures. For example, Herrmann and coworkers have shown that the addition of long DNA sequences capable of hybridizing to multiple DPC strands can shift assembly from micelles to ladder-like structures (Figure 1.5b).[44]

In addition to altering the chemical composition of the DPCs, changes in environmental conditions can be used to control assembly morphology. For example, DPCs can be designed to only assemble in the presence of ions such as Mg^{2+}.[27] In another example, Liu and coworkers showed that DPCs having a Fréchet-type dendrimer as the polymer unit form tubular structures in water, but can be switched to form micelles upon addition of 10% tetrahydrofuran (THF) (Figure 1.5c).[45] This transition could be reversed using dialysis to change the solvent conditions. X-ray diffraction (XRD) revealed that π-stacking in the dendrimer core contributed to stabilization of the tube formation, and presumably these interactions are strengthened in pure water. While switching assembly morphology using dialysis is effective, it can require long time scales. Thus, alternative methods such as changing pH offer some advantages. Liu and coworkers also investigated DPCs having cytosine-rich sequences, as these can form bimolecular i-motif structures at pH values below 6.3 (Figure 1.5d).[46] Under basic conditions, the cytosine-rich DNA is linear. But, as acidity increases, the cytosines become protonated, enabling them to base-pair with each other to form an i-motif. Interestingly, conjugation of the cytosine-rich DNA to poly(propylene oxide) (PPO) stabilizes the i-motif, increasing dissociation temperature by 30 °C compared to unconjugated DNA strands. At high pH, the DPCs composed of cytosine-rich DNA conjugated to PPO have a linear structure and thus form

micelles. However, upon lowering pH, the DNA transitions from linear to a bimolecular quadruplex structure, triggering the micelles to reassemble into tubes. Control DPCs that are not capable of forming the i-motif do not display this pH-dependent switching behavior.

Unique Properties of DNA-Polymer Conjugates

To take advantage of the information-rich nature of the DNA in DPCs, it is critical that the DNA retain its native function, such as the ability to hybridize to complementary nucleic acids with Watson-Crick specificity. Fortuitously, it has been found that some of the properties of DNA, including mismatch discrimination, duplex stability, and nuclease resistance, are actually enhanced upon polymer conjugation. These effects are hypothesized to predominantly arise from the close packing of DNA strands upon DPC assembly.

Duplex formation and stability

Circular dichroism studies reveal that the attachment of and identity of the polymer do not appear to effect the ability of DNA to adopt a canonical B-form structure.[42] Additionally, conjugating a polymer to a DNA strand does not prevent it from hybridizing to its complementary strand.[19,47] To further assess the ability of DNA to form duplexes while in DPC aggregates, the intercalating dye SYBR Green I was used in conjunction with polyacrylamide gel electrophoresis (PAGE).[18] SYBR Green I is specific for double-stranded DNA, enabling it to serve as a reporter of hybridization efficiency. No significant difference in hybridization efficiency was observed for free duplexes compared with those conjugated to a

hydrophobic polymer. As reported by others,[48] a slight increase in micelle radius upon DNA hybridization was observed, possibly due to transition of random-coil DNA into a rigid B-form duplex structure. One study has reported that the diameter of DPC aggregates in fact decreased upon hybridization of a complementary DNA strand. However, this can potentially be explained by a decrease in N_{agg} upon hybridization.[39] The cooperativity of hybridization has also been investigated for DNA assembled into DPC micelles compared with DNA that is free in solution. To observe thermal denaturation of the DNA duplexes, the DPC micelles were hybridized to gold nanoparticles (AuNPs). When the DNA is hybridized, the AuNPs aggregate and thus display a purple color. Upon thermal duplex melting, the AuNPs separate, turning the solution red. The DPCs showed a sharper melting transition than the free DNA, which is indicative of greater cooperativity in the hybridization process.[49] This cooperativity can be attributed to the close packing of DNA in DPC micelles, as these strands can interact with one another and share a cation cloud.[50]

Assembly of DPCs can also influence the effect of sequence mismatches on structure. For example, DPC micelles composed of DNA-PNIPAAm aggregate at high salt concentrations when hybridized with a fully complementary DNA strand. However, a single base pair mismatch at the terminus of the duplex prevents this aggregation (Figure 1.6a). This is hypothesized to arise from the increased entropy of the mismatched duplex, as fraying increases the flexibility of the duplex ends.[51] This study demonstrates that small modifications such as a single base pair mismatch can be sufficient for stabilizing DPC micelle structures in applications requiring high ionic strengths.

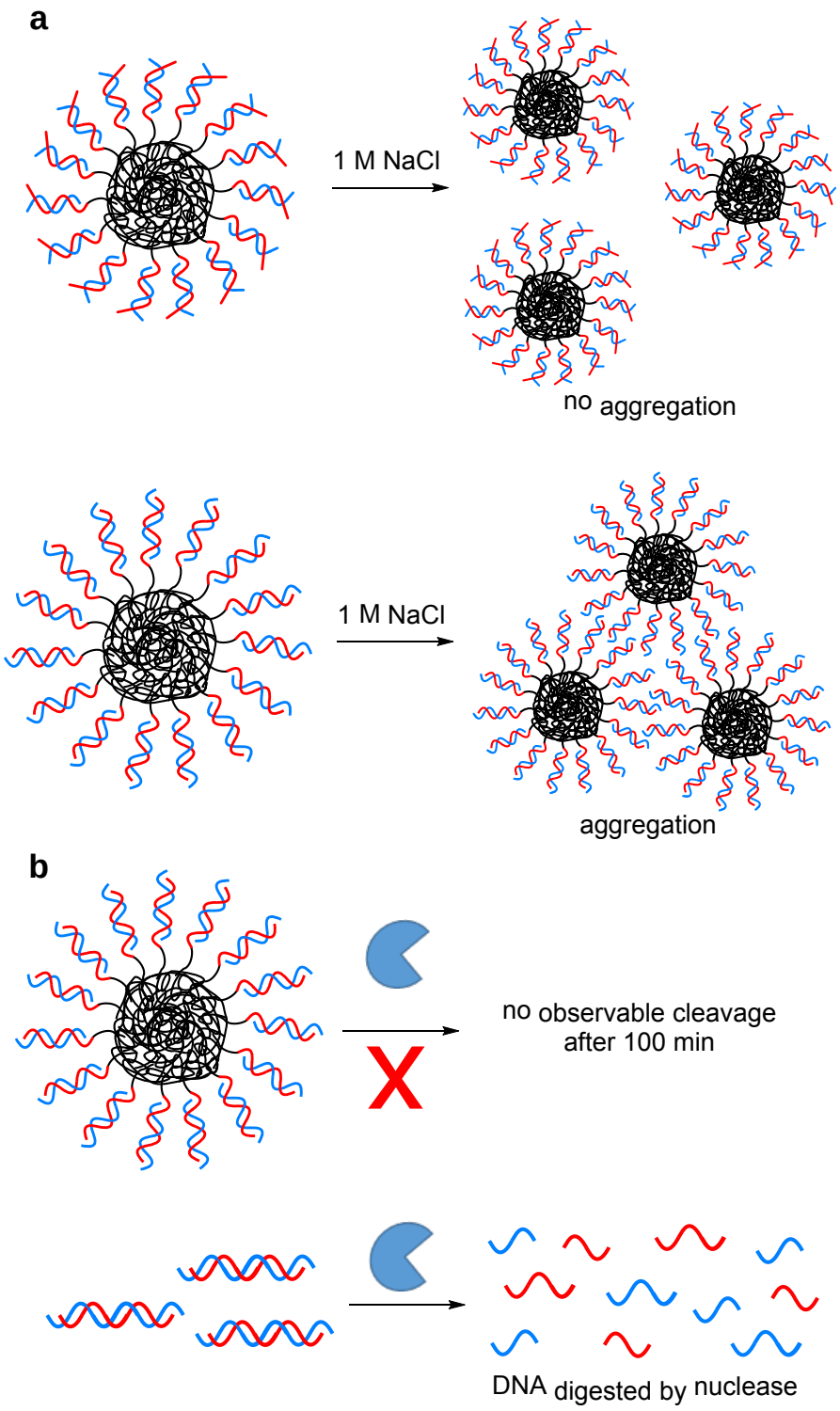

Figure 1.6. DNA properties can be altered by assembly into DPCs. (a) Terminal mismatches prevent aggregation at high ionic strength; (b) DPC assembly hinders cleavage of DNA by nucleases.

Nuclease resistance

A critical challenge for the use of DPCs and other nucleic acid-based technologies *in vivo* is degradation of the DNA by nucleases. Mirkin and coworkers have observed that nuclease degradation of DNA is slowed when the DNA is densely assembled onto the surface of AuNP.[52] It is hypothesized that the close packing of the DNA strands introduces steric hindrance and generates a dense cation cloud, both of which limit access of nucleases to the DNA. Considering that DPCs can have a similar high-density packing of DNA, it was anticipated that they might also benefit from increased resistance to nucleases. To test this hypothesis, Gianneschi and coworkers used Förster resonance energy transfer (FRET) experiments to quantify nuclease degradation of both single-stranded and double-stranded DNA when free in solution or assembled into DPC micelles.[26] Over the course of 100 min, the free DNA was cleaved, but the DNA assembled into DPC micelles showed no observable degradation (Figure 1.6b). This result demonstrates that polymer-driven assembly of DNA can impart the increased biostability necessary for *in vivo* applications.

Tissue and cell permeability

Tissue and cell permeability are also critical challenges for the use of nucleic acid technologies *in vivo*. DPC micelles often have diameters in the range of 10-100 nm, and it is hypothesized that this will enable them to accumulate in tumor tissues as a result of the enhanced permeability and retention (EPR) effect.[53] The ability of DPCs to cross the plasma membrane of cells has also been investigated. Tan and coworkers synthesized DPCs having diacyllipid tails,

and found that by varying DNA length, micelles having diameters of 8-36 nm could be formed.[54] Upon interacting with cell membranes, the micelles disassemble and undergo transferrin receptor-mediated endocytosis. Micelle size was found to impact cellular uptake, with smaller micelles showing more rapid endocytosis. These results in conjunction with studies of similar systems[55,56] led to the hypothesis that DPC monomers are capable of incorporating into cell membranes and endosomes. Importantly, even at monomer concentrations as high as 5 μM, no cytotoxicity was observed. In addition to assembly size, assembly morphology may also impact cell permeability. To investigate this effect, Herrmann and coworkers generated spherical micelles having a diameter of 5 nm and rod-like micelles having dimensions of 29 x 3 nm.[57] The rod-like micelles showed significantly higher cellular uptake as well as lower toxicity compared to their spherical counterparts.

Applications of DNA-Polymer Conjugates

Considering the high specificity of nucleic acid interactions combined with the biostability and cell permeability offered by DPCs, it is not surprising that these assemblies have found use in numerous biological and medical applications.[10] While DPCs do have many of the key properties required for *in vivo* use, further modifications have been required to enhance biocompatibility and functionality. In the sections below, we discuss these modifications, as well as applications of DPCs in therapeutics, medical imaging, and other areas including materials science and chemical synthesis.

Modifications for *in vivo* applications

The modifications made to DPCs to improve their function *in vivo* primarily fall into two categories: (1) passivation of the DPC surface to improve stability and reduce immunogenicity and (2) incorporation of targeting moieties to direct the DPCs to the desired site of action. Because these modifications are intended to influence the interactions of the DPCs with their surroundings, the modifications must be made at the surface of the DNA corona. Fortunately, modification at this site can be easily accomplished by either modifying the DNA used to generate the DPC architecture or by hybridizing the DPC to a complementary strand bearing the desired surface functionality.

PEG has been widely used to increase the biocompatibility of nanoparticles.[58,59] Passivation of nanoparticles using PEG increases circulation lifetime by reducing accumulation in the liver and kidneys, promotes accumulation in tumor regions via the EPR effect, and reduces immunogenicity. As described above, assembly of DPCs protects DNA from nuclease degradation,[26] but addition of PEG to the DPC surface contributes additional steric hindrance, further enhancing nuclease resistance.[60] However, the steric hindrance provided by PEG can also interfere with the intended function of the DPC assembly, and thus it is necessary to remove the PEG modification once the DPC reaches its desired target. If the PEG is conjugated to the DPC via hybridization, removal can be easily accomplished using a nucleic acid that is complementary to the PEG-DNA passivation strand (Figure 1.7). Using a similar hybridization approach, targeting moieties such as folate can be conjugated to the surface of the DPC assemblies, increasing their uptake by cancer cells

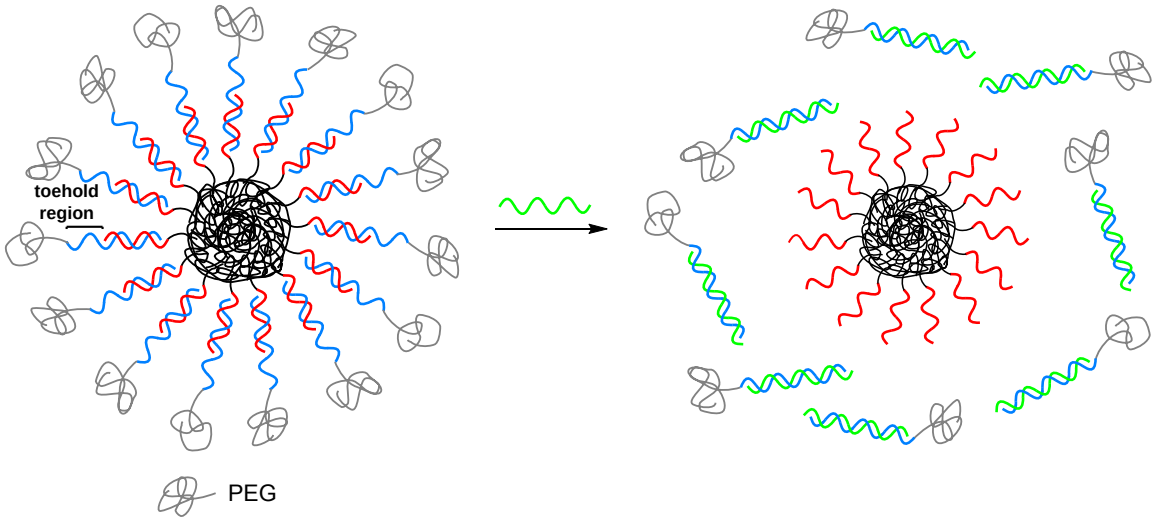

Figure 1.7. Hybridization of a PEG-modified DNA strand increases the biocompatibility of DPC assemblies. The PEG-modified strand can be removed by addition of a complementary nucleic acid.

overexpressing the folate receptor.[55]

Virus capsids can also be used to passivate the surface of DPC assemblies, as they form stable protein cage structures and have been naturally evolved to protect and deliver nucleic acid cargo. Herrmann and coworkers showed that DPCs could be assembled into micelles, loaded with hydrophobic guest molecules, then used to template the assembly of Cowpea Chlorotic Mottle Virus (CCMV) coat protein.[61] Assembly of the virus capsid protein on the surface of the DPC is driven by electrostatic interactions between the negatively charged nucleic acids and the positively charged interior surface of the protein, and thus occurs spontaneously. While not investigated in this study, it is anticipated that the virus capsid provides significant protection of the DPCs from nuclease degradation. Moreover, the DPCs aid in the retention of hydrophobic molecules within the interior of the capsid. Thus, the DPC assembly and virus capsid act

synergistically to create a stable vehicle with significant promise for use in drug delivery applications.

Therapeutics and drug delivery

DPCs can act as drug delivery vehicles in two distinct ways – the assembly can sequester hydrophobic drug molecules in the polymer interior, or the nucleic acids in the corona can be used directly as antisense therapeutics.[32] One of the first examples demonstrating the potential of DPC assemblies for use in drug delivery involved assembly of DNA-PPO DPCs in the presence of the anticancer drug doxorubicin (DOX). A folate-functionalized DNA strand was hybridized to the DPCs to aid in targeting of cancer cells. The DPC architectures were shown to be taken up by the cancer cells, resulting in cell death, presumably from release of the DOX payload into the cytosol.[55] Cellular delivery of DOX has also been accomplished using DPC vesicles.[62] In this case, the DNA strand hybridized to the DPCs was functionalized with the tLyp-1 peptide, which is known to enable targeting of breast cancer cells. Once assembled, the DPC vesicles were shown to be capable of sequestering DOX at a concentration of 3.5 μM. Binding of DOX to the vesicle was shown to be pH dependent, and drug release could be initiated by decreasing the solution pH below 6.5. This characteristic is especially useful for delivery of anticancer drugs, as tumor environments are known to have reduced pH.

As described in the section above on controlling assembly of DPCs, the assemblies can be designed such that disassembly occurs in the presence of specific chemical, biological, or environmental stimuli. Given this

programmability, the potential for use of these DPCs as selective drug delivery vehicles is clear. Herrmann and coworkers have reported DNA-PPO conjugates for which light can be used to trigger guest release.[63] The DPC monomers assemble into tightly packed vesicles, which are unable to release cargo molecules without the aid of synthetic channels or enzymes to disrupt the bilayer. However, the DNA segment of the DPC contains a sequence-specific photosensitizer that produces $^1O_2$ when activated with 530 nm light. This reactive oxygen species triggers release of bound guest molecules, likely due to oxidation of the PPO.

A method for specific stimuli-responsive guest release without disruption of the micelle structure has been reported by Barthélémy and coworkers (Figure 1.8).[64] In this study, DPCs having either two or three hydrophobic chains were assembled into micelles and loaded with the anticancer drug paclitaxel (PX). When the DNA segment of the DPC is single-stranded, the PX remains bound within the micelles. However, upon duplex formation with a complementary DNA strand, the PX is released into the surrounding environment. It is hypothesized that upon DNA duplex formation, the hydrophobic core of the micelle compacts, eliminating any available pockets for binding PX.

Given the cell permeability of DPCs, these architectures also hold significant promise for the delivery of nucleic acid therapeutics. Tan and coworkers have reported DPC micelles in which the DNA portion targets the c-raf-1 mRNA, which is a cancer biomarker. The DPCs induce apoptosis in A549 lung cancer cells, reducing viability to 25%. It is hypothesized that the DPCs act by binding to the target mRNA and activating RNase H for mRNA degradation.

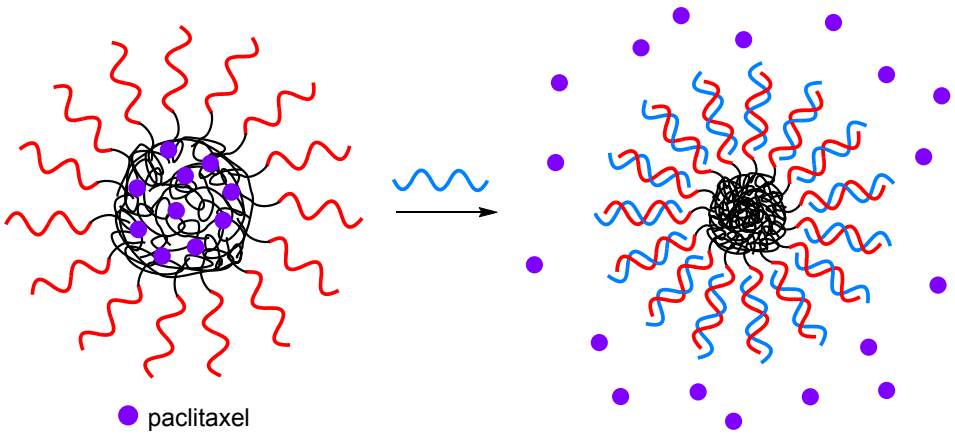

Figure 1.8. Addition of a complementary DNA strand compacts the hydrophobic core of the DPC, triggering release of paclitaxel.

Control experiments using unconjugated DNA molecular beacons or mismatched DPC micelles showed no significant cellular toxicity.[65]

Cellular imaging and theranostics

Imaging and biosensing applications generally require a molecular recognition event between the target molecule and a probe, followed by a transduction event that enables the probe to emit a detectible signal. For cellular imaging, fluorescence is among the most convenient types of output, as it is non-destructive to cells and can be easily detected and quantified using a fluorescence microscope[66] or flow cytometry.[65] In the case of DPCs, the DNA serves as an excellent recognition element, as it is able to bind with high fidelity to complementary nucleic acids. Additionally, nucleic acid sequences called aptamers can be generated by *in vitro* selection, and bind selectively to a wide variety of small-molecule, protein, and cellular targets.[67] In addition to the ability of DNA to bind to biological targets with high selectivity and affinity, DNA can

also be programmed to undergo a change in conformation upon binding, which in turn can be used to generate a fluorescence output via FRET.

In the DPCs targeting c-raf-1 mRNA reported by Tan and coworkers, the DNA portion is a molecular beacon, enabling fluorescence imaging of the target RNA (Figure 1.9a).[65] A molecular beacon is a hairpin structure which is functionalized with a fluorophore at one terminus and a quencher at the opposite terminus.[68] Upon hybridizing with the target mRNA sequence, the stem loop of the hairpin is disrupted, moving the fluorophore away from the quencher and thus increasing fluorescence emission. As described above, formation of the DNA:RNA duplex also initiates RNAse H activity, enabling the DPCs to trigger cell apoptosis. Thus, this DPC is an example of a theranostic, as it combines diagnostic imaging with a therapeutic effect. It is important to note that DNA molecular beacons have been widely used for cellular RNA imaging.[69] However, in this specific case, conjugation to a hydrophobic polymer provides the benefit of cell permeability, abrogating the need for transfection reagents that can interfere with fluorescence measurements.

Utilizing an aptamer as the DNA portion of the DPC significantly broadens the scope of molecules that can be imaged. Tan and coworkers constructed DPCs having an ATP-binding aptamer beacon (Figure 1.9b),[56] which functions similar to a molecular beacon, but changes conformation in response to the ATP target rather than a nucleic acid.[70] Importantly, the aptamer is selective for ATP over other nucleoside triphosphates. The DPCs were shown to undergo cellular uptake, and were successfully used to monitor changes in ATP concentration in HeLa cells. Aptamer DPCs have also been used for fluorescence-based

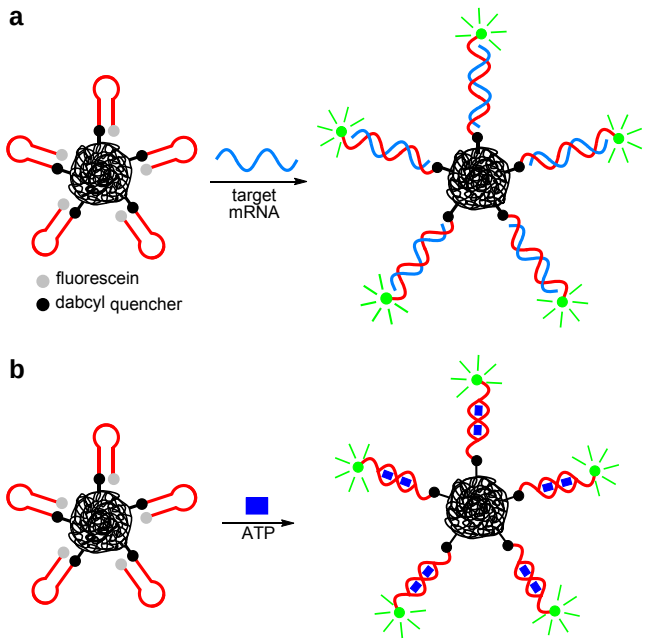

Figure 1.9. Cellular imaging using DPCs. (a) mRNA detection using molecular beacons; (b) ATP detection using aptamer beacons. In both DPC motifs, binding of the target moves the fluorophore away from the quencher, resulting in an increase in fluorescence emission.

detection of cancer cells. In this example, Yan and coworkers synthesized DPCs containing an aptamer that binds to nucleolin receptors, which are overexpressed on some cancer cells (Figure 1.10).[71] A separate set of micelles were also synthesized having a fluorescein dye. In both cases, the hydrophobic core was composed of the block copolymer hyperbranched poly [3-ethyl-3-oxetanemeth-anol)-*star*-poly(ethylene oxide)] (HBPO-*star*-PEO). The two types of micelles underwent co-assembly to form a larger structure, which was readily uptaken by MCF-7 cells, rendering them fluorescent. As an important control, incubation of the micelles with 3T3 cells which do not express the nucleolin receptor resulted in only minimal fluorescence, demonstrating the ability of the DPCs to selectively target the MCF-7 cancer cells.

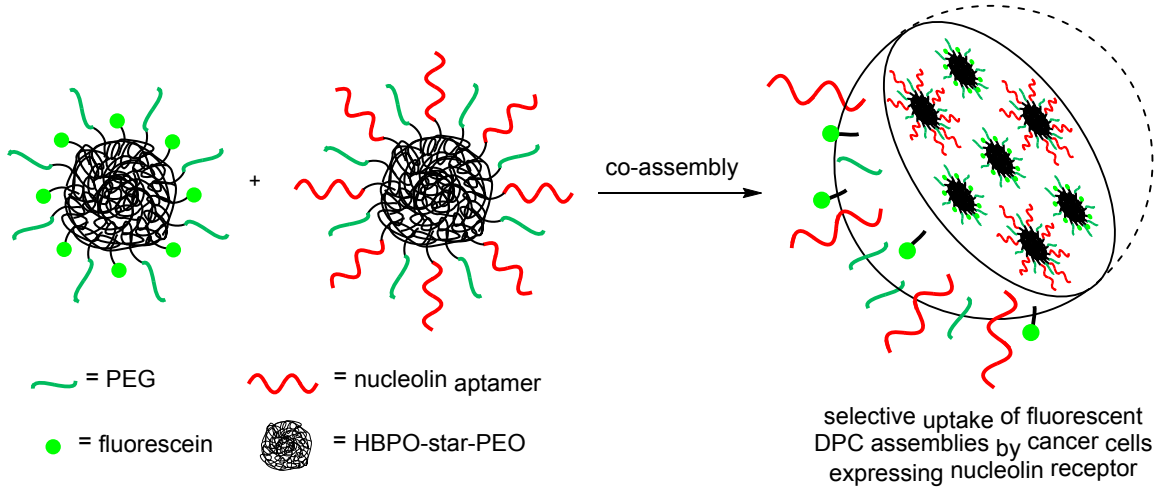

Figure 1.10. Co-assembly of FAM-labeled micelles with DPC micelles encoding the nucleolin aptamer enables selective uptake by and imaging of cancer cells (adapted with permission from Yu S, Dong R, Chen J, Chen F, Jiang W, Zhou Y, Zhu X, Yan D. *Biomacromolecules* **2014,** *15* (5), 1828-1836. Copyright 2014 American Chemical Society).

Other applications of DNA-polymer conjugates

While most applications of DPCs are focused on biology and medicine, there are a few that move beyond this scope into the fields of materials science and synthetic chemistry. For example, DPCs can be used to organize other materials, such as AuNPs.[45] DPCs having a mixed DNA/PEG corona and a hydrophobic PPO core are capable of binding to AuNP functionalized with a complementary DNA sequence, forming clusters of AuNPs surrounding the micelle.[47]

In addition to encapsulating hydrophobic organic drug molecules, DPCs can also encapsulate inorganic moieties such as magnetic nanoparticles. Park and coworkers synthesized DPCs containing a polystyrene polymer, and showed that dissolving the DPCs in DMF in the presence of iron oxide nanoparticles,

followed by addition of water and dialysis into buffer, resulted in micelles encapsulating the iron oxide nanoparticles.[72] These assemblies can be used for magnetic separation of DNA strands, and have potential for use in medical applications such as magnetic resonance imaging or magnetic hyperthermia treatment.

The close spatial arrangement of DNA strands in DPCs also enables them to serve as a scaffold to template organic reactions. DNA strands bearing reactive groups are hybridized to the DPC, bringing the reactants into close proximity and thus promoting a reaction. The reactants can be attached to either terminus of the free DNA strand, enabling the reactions to occur either in the interior of the micelle or at the solvent-exposed surface. Examples of reactions that can be carried out using this method include amide bond formation and Michael addition.[48] Another example using DPCs to control chemical reactions employs DPC vesicles to encapsulate an enzyme. The vesicle is initially impermeable to reactants, but upon addition of a pore-forming protein, the reagents can access the enzyme and undergo reaction.[42]

Conclusion and Dissertation Overview

In conclusion, DPCs provide a unique architecture which benefits from the information storage capacity of DNA and the ability of hydrophobic polymers to directly assemble in aqueous solution. A significant portion of structure space has been explored with regard to DPCs, and has revealed that modulating the properties of the DNA or polymer can lead to micelles having a wide range of assembly properties, as well as alternative assembly morphologies including

vesicles and tubes. However, the challenges associated with synthesis of some DPCs does still limit this exploration of structure-activity space. New techniques involving solid-phase addition of polymers to DNA appear promising for overcoming these challenges, as they avert many of the solubility issues experienced when trying to conjugate hydrophobic polymers to DNA in solution.

Critical to the use of DPCs in many applications, the DNA retains its ability to recognize complementary nucleic acids, as well as small molecules and proteins. And, in some cases, the properties of the DNA are actually enhanced by assembly into DPCs. Two notable examples of this are nuclease resistance and cell permeability. Interestingly, the use of non-native nucleic acids in DPCs remains relatively unexplored, and has potential to further improve biostability as well as provide new functions.

DPCs can be engineered to respond to chemical, biological, or environmental stimuli, enabling them to selectively release cargo molecules in response to these stimuli. This ability along with their cell permeability makes them well-suited for use in drug delivery applications. The DNA portion of the DPC can also be used as a recognition element to detect nucleic acids, proteins, and small molecules, making the DPCs useful in cellular imaging and theranostic applications. To date, examples of drug delivery and imaging using DPCs primarily use cells in culture. However, given the biostability of the DPCs, combined with efforts to increase biocompatibility through passivation, it is anticipated that DPCs will find use in multiple *in vivo* applications in the near future.

In order to develop DPC micelles for use in these applications, this

dissertation explores the use of DNA hybridization as a means to introduce noncovalent crosslinks throughout the micelle corona in order to stabilize the micelle and guest encapsulation. For these studies, the monomers consist of a DPC unit containing dendrimer DNA attached to a tocopherol unit. During assembly characterization, we found that Nile Red was not capable of measuring the CMCs. Therefore, we evaluated the utility of using DiO to measure the CMCs for a range of surfactants and found that it gave consistent, accurate values. Further studies investigated the function of free, aptameric DNA in the presence of surfactants, in which we showed that the binding ability of aptamers is preserved in the presence of micelles. Finally, PNA-DNA-AuNP conjugates were investigated. Like micelles, these structures require electrostatic tuning to maintain monodispersity, which is essential for maintaining nucleic acid assembly and hybridization properties.

References

(1) Church, G. M.; Gao, Y.; Kosuri, S. Next-Generation Digital Information Storage in DNA. *Science* **2012**, *337*, 1628-1628.

(2) Seeman, N. C. DNA NANOTECHNOLOGY: Novel DNA Constructions. *Annu Rev Biophys. Biomol. Struct.* **1998**, *27*, 225-248.

(3) Liu, J.; Cao, Z.; Lu, Y. Functional nucleic acid sensors. *Chem. Rev.* **2009**, *109*, 1948-1998.

(4) Willner, I.; Shlyahovsky, B.; Zayats, M.; Willner, B. DNAzymes for sensing, nanobiotechnology and logic gate applications. *Chem. Soc. Rev.* **2008**, *37*, 1153-1165.

(5) Schnitzler, T.; Herrmann, A. DNA block copolymers: functional materials for nanoscience and biomedicine. *Acc. Chem. Res.* **2012**, *45*, 1419-1430.

(6) Lemaitre, M.; Bayard, B.; Lebleu, B. Specific antiviral activity of a poly(L-lysine)-conjugated oligodeoxyribonucleotide sequence complementary to vesicular stomatitis virus N protein mRNA initiation site. *Proc. Natl. Acad. Sci.* **1987**, *84*, 648-652.

(7) Umeno, D.; Maeda, M. Single stranded DNA-poly(N-isopropylacrylamide) conjugate for affinity precipitation separation of oligonucleotides. *Chem. Commun.* **1998**, 1433-1434.

(8) Gibbs, J. M.; Park, S.-J.; Anderson, D. R.; Watson, K. J.; Mirkin, C. A.; Nguyen, S. T. Polymer−DNA hybrids as Electrochemical Probes for the Detection of DNA. *J. Chem. Soc.* **2005**, *127*, 1170-1178.

(9) Jeong, J. H.; Kim, S. W.; Park, T. G. A new antisense oligonucleotide delivery system based on self-assembled ODN–PEG hybrid conjugate micelles. *J. Control. Release* **2003**, *93*, 183-191.

(10) Alemdaroglu, F. E.; Herrmann, A. DNA meets synthetic polymers--highly versatile hybrid materials. *Org. Biomol. Chem.* **2007**, *5*, 1311-1320.

(11) Edwardson, T. G.; Carneiro, K. M.; McLaughlin, C. K.; Serpell, C. J.; Sleiman, H. F. Site-specific positioning of dendritic alkyl chains on DNA cages enables their geometry-dependent self-assembly. *Nat. Chem.* **2013**, *5*, 868-875.

(12) Jeong, J. H.; Park, T. G. Novel Polymer−DNA hybrid polymeric micelles composed of hydrophobic poly(d,l-lactic-co-glycolic Acid) and hydrophilic oligonucleotides. *Bioconjugate Chem.* **2001**, *12*, 917-923.

(13) Wilks, T. R.; Pitto-Barry, A.; Kirby, N.; Stulz, E.; O'Reilly, R. K. Construction of DNA-polymer hybrids using intercalation interactions. *Chem. Commun.* **2014**, *50*, 1338-1340.

(14) Ikonen, S.; Macíčková-Cahová, H.; Pohl, R.; and, M.; Hocek, M. Synthesis of nucleoside and nucleotide conjugates of bile acids, and polymerase construction of bile acid-functionalized DNA. *Org. Biomol. Chem.* **2010**, *8*, 1194-1201.

(15) Averick, S. E.; Dey, S. K.; Grahacharya, D.; Matyjaszewski, K.; Das, S. R. Solid-phase incorporation of an ATRP initiator for polymer–DNA biohybrids. *Angew. Chem. Int. Ed.* **2014**, *53*, 2739-2744.

(16) McLaughlin, C. K.; Hamblin, G. D.; Hänni, K. D.; Conway, J. W.; Nayak, M. K.; Carneiro, K. M. M.; Bazzi, H. S.; Sleiman, H. F. Three-dimensional organization of block copolymers on “DNA-minimal” scaffolds. *J. Am. Chem. Soc.* **2012**, *134*, 4280-4286.

(17) Yaşayan, G.; Magnusson, J. P.; Sicilia, G.; Spain, S. G.; Allen, S.; Davies, M. C.; Alexander, C. Multi-modal switching in responsive DNA block co-polymer conjugates. *Phys. Chem. Chem. Phys.* **2013**, 16263-16274.

(18) Anaya, M.; Kwak, M.; Musser, A. J.; Mullen, K.; Herrmann, A. Tunable hydrophobicity in DNA micelles: design, synthesis, and characterization of a new family of DNA amphiphiles. *Chemistry* **2010**, *16*, 12852-12859.

(19) Talom, R. M.; Fuks, G.; Kaps, L.; Oberdisse, J.; Cerclier, C.; Gaillard, C.; Mingotaud, C.; Gauffre, F. DNA–Polymer Micelles as Nanoparticles with Recognition Ability. *Chem. – Eur. J.l* **2011**, *17*, 13495-13501.

(20) Pan, P.; Fujita, M.; Ooi, W.-Y.; Sudesh, K.; Takarada, T.; Goto, A.; Maeda, M. DNA-functionalized thermoresponsive bioconjugates synthesized via ATRP and click chemistry. *Polymer* **2011**, *52*, 895-900.

(21) Isoda, K.; Kanayama, N.; Miyamoto, D.; Takarada, T.; Maeda, M. RAFT-generated poly(N-isopropylacrylamide)–DNA block copolymers for temperature-responsive formation of polymer micelles. *React. Funct. Polym.* **2011**, *71*, 367-371.

(22) Mayap Talom, R.; Fuks, G.; Mingotaud, C.; Gineste, S.; Gauffre, F. Investigation of the reversibility of the unimer-to-aggregate transition in block copolymers by surface tension-measurements. *J. Colloid Interf. Sci.* **2012**, *387*, 180-186.

(23) Besanceney-Webler, C.; Jiang, H.; Zheng, T.; Feng, L.; Soriano del Amo, D.; Wang, W.; Klivansky, L. M.; Marlow, F. L.; Liu, Y.; Wu, P. Increasing the

efficacy of bioorthogonal click reactions for bioconjugation: a comparative study. *Angew. Chem. Int. Ed.* **2011**, *50*, 8051-8056.

(24) Cavalieri, F.; Postma, A.; Lee, L.; Caruso, F. Assembly and functionalization of DNA−polymer microcapsules. *ACS Nano* **2009**, *3*, 234-240.

(25) Storhoff, J. J.; Elghanian, R.; Mucic, R. C.; Mirkin, C. A.; Letsinger, R. L. One-pot colorimetric differentiation of polynucleotides with single base imperfections using gold nanoparticle probes. *J. Am. Chem. Soc.* **1998**, *120*, 1959-1964.

(26) Rush, A. M.; Thompson, M. P.; Tatro, E. T.; Gianneschi, N. C. Nuclease-resistant DNA via high-density packing in polymeric micellar nanoparticle coronas. *ACS Nano* **2013**, *7*, 1379-1387.

(27) Edwardson, T. G.; Carneiro, K. M.; Serpell, C. J.; Sleiman, H. F. An efficient and modular route to sequence-defined polymers appended to DNA. *Angew. Chem. Int. Ed.* **2014**, *53*, 4567-4571.

(28) Pearce, T. R.; Waybrant, B.; Kokkoli, E. The role of spacers on the self-assembly of DNA aptamer-amphiphiles into micelles and nanotapes. *Chem. Commun.* **2014**, *50*, 210-212.

(29) Alemdaroglu, F. E.; Zhuang, W.; Zophel, L.; Wang, J.; Berger, R.; Rabe, J. P.; Herrmann, A. Generation of multiblock copolymers by PCR: synthesis, visualization and nanomechanical properties. *Nano Letters* **2009**, *9*, 3658-3662.

(30) Alemdaroglu, F. E.; Wang, J.; Borsch, M.; Berger, R.; Herrmann, A. Enzymatic control of the size of DNA block copolymer nanoparticles. *Angew. Chem. Int. Ed.* **2008**, *47*, 974-976.

(31) Ayaz, M. S.; Kwak, M.; Alemdaroglu, F. E.; Wang, J.; Berger, R.; Herrmann, A. Synthesis of DNA block copolymers with extended nucleic acid segments by enzymatic ligation: cut and paste large hybrid architectures. *Chem. Commun.* **2011**, *47*, 2243-2245.

(32) Kedracki, D.; Maroni, P.; Schlaad, H.; Vebert-Nardin, C. Polymer–aptamer hybrid emulsion templating yields bioresponsive nanocapsules. *Adv. Funct. Mater.* **2014**, *24*, 1133-1139.

(33) Teixeira Jr, F.; Rigler, P.; Vebert-Nardin, C. Nucleo-copolymers: oligonucleotide-based amphiphilic diblock copolymers. *Chem. Commun.* **2007**, 1130-1132.

(34) Schade, M.; Berti, D.; Huster, D.; Herrmann, A.; Arbuzova, A. Lipophilic nucleic acids--a flexible construction kit for organization and

functionalization of surfaces. *Adv. Colloid Interfac.* **2014**, *208*, 235-251.

(35) Discher, D. E.; Eisenberg, A. Polymer vesicles. *Science* **2002**, *297*, 967-973.

(36) Nagarajan, R. Molecular packing parameter and surfactant self-assembly: the neglected role of the surfactant tail. *Langmuir* **2001**, *18*, 31-38.

(37) Baldelli Bombelli, F.; Berti, D.; Milani, S.; Lagi, M.; Barbaro, P.; Karlsson, G.; Brandt, A.; Baglioni, P. Collective headgroup conformational transition in twisted micellar superstructures. *Soft Matter* **2008**, *4*, 1102-1113.

(38) Fuller, J. M.; Raghupathi, K. R.; Ramireddy, R. R.; Subrahmanyam, A. V.; Yesilyurt, V.; Thayumanavan, S. Temperature-sensitive transitions below LCST in amphiphilic dendritic assemblies: host–guest implications. *J. Am. Chem. Soc.* **2013**, *135*, 8947-8954.

(39) Ooi, W.-Y.; Fujita, M.; Pan, P.; Tang, H.-Y.; Sudesh, K.; Ito, K.; Kanayama, N.; Takarada, T.; Maeda, M. Structural characterization of nanoparticles from thermoresponsive poly(N-isopropylacrylamide)-DNA conjugate. *J. Colloid Interf. Sci.* **2012**, *374*, 315-320.

(40) Pan, P.; Fujita, M.; Ooi, W.-Y.; Sudesh, K.; Takarada, T.; Goto, A.; Maeda, M. Thermoresponsive micellization and micellar stability of poly(n-isopropylacrylamide)-b-DNA diblock and miktoarm star polymers. *Langmuir* **2012**, *28*, 14347-14356.

(41) Tang, L.; Tjong, V.; Li, N.; Yingling, Y. G.; Chilkoti, A.; Zauscher, S. Enzymatic polymerization of high molecular weight DNA amphiphiles that self-assemble into star-like micelles. *Adv. Mater.* **2014**, *26*, 3050-3054.

(42) Cottenye, N.; Syga, M.-I.; Nosov, S.; Muller, A. H. E.; Ploux, L.; Vebert-Nardin, C. Biological-like vesicular structures self-assembled from DNA-block copolymers. *Chem. Commun.* **2012**, *48*, 2615-2617.

(43) Chien, M.-P.; Rush, A. M.; Thompson, M. P.; Gianneschi, N. C. Programmable shape-shifting micelles. *Angew. Chem. Int. Ed.* **2010**, *49*, 5076-5080.

(44) Ding, K.; Alemdaroglu, F. E.; Börsch, M.; Berger, R.; Herrmann, A. Engineering the structural properties of DNA block copolymer micelles by molecular recognition. *Angew. Chem. Int. Ed.* **2007**, *46*, 1172-1175.

(45) Wang, L.; Feng, Y.; Yang, Z.; He, Y.-M.; Fan, Q.-H.; Liu, D. Reversibly controlled morphology transformation of an amphiphilic DNA-dendron hybrid. *Chem. Commun.* **2012**, *48*, 3715-3717.

(46) Zhao, Z.; Wang, L.; Liu, Y.; Yang, Z.; He, Y.-M.; Li, Z.; Fan, Q.-H.; Liu, D. pH-induced morphology-shifting of DNA-b-poly(propylene oxide) assemblies. *Chem. Commun.* **2012**, *48*, 9753-9755.

(47) Kwak, M.; Musser, A. J.; Lee, J.; Herrmann, A. DNA-functionalised blend micelles: mix and fix polymeric hybrid nanostructures. *Chem. Commun.* **2010**, *46*, 4935-4937.

(48) Alemdaroglu, F. E.; Ding, K.; Berger, R.; Herrmann, A. DNA-templated synthesis in three dimensions: introducing a micellar scaffold for organic reactions. *Angew. Chem. Int. Ed.* **2006**, *45*, 4206-4210.

(49) Li, Z.; Zhang, Y.; Fullhart, P.; Mirkin, C. A. Reversible and chemically programmable micelle assembly with DNA block-copolymer amphiphiles. *Nano Lett.* **2004**, *4*, 1055-1058.

(50) Gibbs-Davis, J. M.; Schatz, G. C.; Nguyen, S. T. Sharp melting transitions in DNA hybrids without aggregate dissolution: proof of neighboring-duplex cooperativity. *J. Am. Chem. Soc.* **2007**, *129*, 15535-15540.

(51) Isoda, K.; Kanayama, N.; Fujita, M.; Takarada, T.; Maeda, M. DNA terminal mismatch-induced stabilization of polymer micelles from RAFT-generated poly(N-isopropylacrylamide)-DNA block copolymers. *Chem.-Asian J.l* **2013**, *8*, 3079-3084.

(52) Rosi, N. L.; Giljohann, D. A.; Thaxton, C. S.; Lytton-Jean, A. K. R.; Han, M. S.; Mirkin, C. A. Oligonucleotide-modified gold nanoparticles for intracellular gene regulation. *Science* **2006**, *312*, 1027-1030.

(53) Maeda, H.; Wu, J.; Sawa, T.; Matsumura, Y.; Hori, K. Tumor vascular permeability and the EPR effect in macromolecular therapeutics: a review. *J. Control. Release* **2000**, *65*, 271-284.

(54) Liu, H.; Zhu, Z.; Kang, H.; Wu, Y.; Sefan, K.; Tan, W. DNA-based micelles: synthesis, micellar properties and size-dependent cell permeability. *Chemistry* **2010**, *16*, 3791-3797.

(55) Alemdaroglu, F. E.; Alemdaroglu, N. C.; Langguth, P.; Herrmann, A. DNA Block Copolymer Micelles – A Combinatorial Tool for Cancer Nanotechnology. *Adv. Mater.* **2008**, *20*, 899-902.

(56) Wu, C.; Chen, T.; Han, D.; You, M.; Peng, L.; Cansiz, S.; Zhu, G.; Li, C.; Xiong, X.; Jimenez, E.; Yang, C. J.; Tan, W. Engineering of switchable aptamer micelle flares for molecular imaging in living cells. *ACS Nano* **2013**, *7*, 5724-5731.

(57) Alemdaroglu, F. E.; Alemdaroglu, N. C.; Langguth, P.; Herrmann, A. Cellular

uptake of DNA block copolymer micelles with different shapes. *Macromol. Rapid Comm.* **2008**, *29*, 326-329.

(58) Ikeda, Y.; Nagasaki, Y. Impacts of PEGylation on the gene and oligonucleotide delivery system. *J. Appl. Polym. Sci.* **2014**, *131*.

(59) Amoozgar, Z.; Yeo, Y. Recent advances in stealth coating of nanoparticle drug delivery systems. *WIREs: Nanomed. Nanobiotechnol.* **2012**, *4*, 219-233.

(60) Magnusson, J. P.; Fernandez-Trillo, F.; Sicilia, G.; Spain, S. G.; Alexander, C. Programmed assembly of polymer-DNA conjugate nanoparticles with optical readout and sequence-specific activation of biorecognition. *Nanoscale* **2014**, *6*, 2368-2374.

(61) Kwak, M.; Minten, I. J.; Anaya, D.-M.; Musser, A. J.; Brasch, M.; Nolte, R. J. M.; Müllen, K.; Cornelissen, J. J. L. M.; Herrmann, A. Virus-like particles templated by DNA micelles: a general method for loading virus nanocarriers. *J. Am. Chem. Soc.* **2010**, *132*, 7834-7835.

(62) Choi, K. M.; Kwon, I. C.; Ahn, H. J. Self-assembled amphiphilic DNA-cholesterol/DNA-peptide hybrid duplexes with liposome-like structure for doxorubicin delivery. *Biomaterials* **2013**, *34*, 4183-4190.

(63) Rodríguez-Pulido, A.; Kondrachuk, A. I.; Prusty, D. K.; Gao, J.; Loi, M. A.; Herrmann, A. Light-Triggered Sequence-Specific Cargo Release from DNA Block Copolymer–Lipid Vesicles. *Angew. Chem. Int. Ed.* **2013**, *52*, 1008-1012.

(64) Pokholenko, O.; Gissot, A.; Vialet, B.; Bathany, K.; Thiery, A.; Barthelemy, P. Lipid oligonucleotide conjugates as responsive nanomaterials for drug delivery. *J. Mater. Chem. B* **2013**, *1*, 5329-5334.

(65) Chen, T.; Wu, C. S.; Jimenez, E.; Zhu, Z.; Dajac, J. G.; You, M.; Han, D.; Zhang, X.; Tan, W. DNA Micelle Flares for Intracellular mRNA Imaging and Gene Therapy. *Angew. Chem. Int. Ed.* **2013**, *52*, 2012-2016.

(66) Stephens, D. J.; Allan, V. J. Light Microscopy Techniques for Live Cell Imaging. *Science* **2003**, *300*, 82-86.

(67) Klussman, S.: *The Aptamer Handbook. Functional Oligonucleotides and Their Applications*; WILEY-VCH Verlag GmbH & Co: Weinheim, 2006.

(68) Tyagi, S.; Kramer, F. R. Molecular beacons: probes that fluoresce upon hybridization. *Nat. Biotechnolol.* **1996**, *14*, 303-308.

(69) Tyagi, S. Imaging intracellular RNA distribution and dynamics in living cells. *Nat. Methods* **2009**, *6*, 331-338.

(70) Tang, Z.; Mallikaratchy, P.; Yang, R.; Kim, Y.; Zhu, Z.; Wang, H.; Tan, W. Aptamer switch probe based on intramolecular displacement. *J. Am. Chem. Soc.* **2008**, *130*, 11268-11269.

(71) Yu, S.; Dong, R.; Chen, J.; Chen, F.; Jiang, W.; Zhou, Y.; Zhu, X.; Yan, D. Synthesis and self-assembly of amphiphilic aptamer-functionalized hyperbranched multiarm copolymers for targeted cancer imaging. *Biomacromolecules* **2014**, *15*, 1828-1836.

(72) Chen, X.-J.; Sanchez-Gaytan, B. L.; Hayik, S. E. N.; Fryd, M.; Wayland, B. B.; Park, S.-J. Self-assembled hybrid structures of DNA block-copolymers and nanoparticles with enhanced DNA binding properties. *Small* **2010**, *6*, 2256-2260.

CHAPTER 2

DNA CROSS-LINKED MICELLES AS PROGRAMMABLE MATERIALS

Introduction

Micelles form when amphiphilic monomers self-assemble to minimize unfavorable interactions between hydrophobic and hydrophilic surfaces. This assembly only occurs above what is known as the critical micelle concentration (CMC).[1] Since one of the major applications of micelles is drug delivery,[2] proper design and optimization must be performed to ensure that the micelles remain intact and the guest molecules encapsulated until a trigger is present. Keeping the micelle-drug complex intact can be a great challenge because the monomer concentration is drastically lowered as the complex disperses into a patient's blood stream. Therefore, if the CMC of the micelles is not low enough, disassembly will occur, releasing the drug molecule. In order to avoid this, the CMC must be low enough to withstand dilution into the bloodstream. However, if the micelle is still intact, the problem remains that guest molecules are at equilibrium with the surrounding solution.[3] Without further stabilization, as the micelles move through the body, they will leak their cargo. Many researchers have explored creating cross-links between the monomers, forming a micelle in

order to stabilize the structure.[4,5] Cross-links physically hold the structure together and create a steric barrier that prevents molecules from leaving the micelle. In these studies, it has been found that as cross-linking density increases, micellar stability increases, and guest molecule leakage decreases.[6] By designing the micelles to react with a condition-specific stimulus, targeted drug release can be achieved. Many approaches have been used to introduce stimuli responsiveness into micelles such that they react to changes in conditions such as temperature, pH, or redox potential.[7] These conditions are often based on distinct conditions present at the desired therapeutic site.

As many studies have explored incorporating negatively charged DNA into DNA polymer conjugate (DPC) monomers capable of forming micelles,[8,9] we proposed that using monomers having complementary DNA strands would enable duplex formation between monomers, creating noncovalent cross-links throughout the DNA corona (Figure 2.1). Although not covalent bonds, Watson-Crick base pairing between DNA strands is very strong, so we hypothesize they will behave similarly, stabilizing the micellar assembly and therefore lowering the CMC. Additionally, if DNA cross-links function similarly to other cross-linking

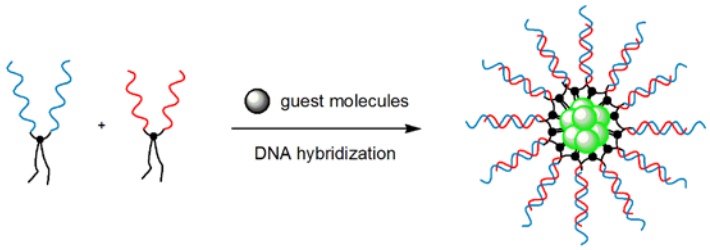

Figure 2.1. Monomers using complementary DNA sequences to create cross-links for micelle stabilization and to prevent the release of guest molecules.

methods, guest molecules would be stably encapsulated. Typically, stimuli-responsiveness in micelles is programmed by changes in temperature, pH, or redox potential. Alternatively, DNA has the ability to respond to many other stimuli, providing a versatile, programmable corona. Aptamers are short DNA strands that selectively bind a range of targets such as small molecules, proteins, or cells.[10-12] Some, such as the cocaine or L-tyrosinamide aptamers, function in the presence of a displacement strand (Figure 2.2).[13,14] In the absence of target, the strands are hybridized together; however, when the target is introduced, the aptamer preferentially binds the target, displacing the complement. Such a biosensor could be used to create a responsive micelle to a particular target. The duplex could also use its native function to bind a complementary sequence or be degraded by a restriction endonuclease, which targets specific sequences. Therefore, using DNA to facilitate cross-linking would allow the micelle to selectively respond to a target molecule, a complementary sequence, and/or enzymatic degradation (Figure 2.3).

In order to maximize the benefits of DNA cross-links, these interactions should occur throughout the entire corona of the micelle. In our design, this was achieved by incorporating multiple DNA strands within each monomer. If only two

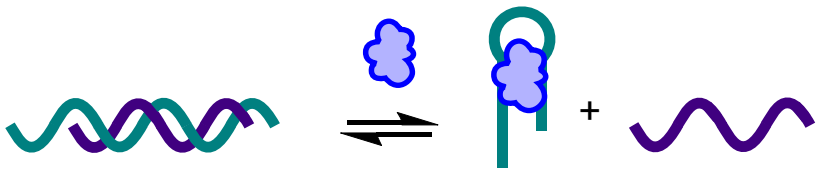

Figure 2.2. Structure-switching biosensor. The aptamer has a complementary strand, which is displaced in the presence of the target.

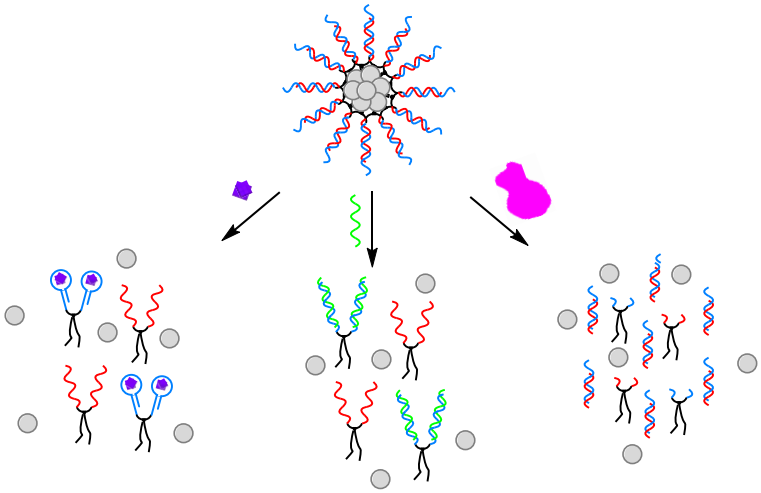

Figure 2.3. DNA cross-linked micelles could respond to a variety of stimuli such as a molecular target, a target nucleic acid, or enzymatic degradation.

DNA strands are incorporated within a monomer unit, the formation of dimers between two adjacent monomers is very likely, thus providing little to no stabilization for the overall micellar structure (Figure 2.4a). We hypothesize that if additional DNA strands are attached to each monomer unit, it would be sterically improbable to form a dimer using all of these strands, therefore enabling cross-linking between additional monomers (Figure 2.4b). We explored the use of an α-tocopherol (vitamin E) hydrophobic group, where a series of three or four tocopherol units were incorporated in an effort to tune dynamics through hydrophobicity. If the hydrophobic driving force is too strong, any changes within the hydrophilic corona have less of an effect. However, if there is not enough hydrophobicity to drive micelle formation, the polar groups may have too much of an effect, therefore solubilizing the monomer and increasing the CMC. The tocopherol units were attached to the DNA via a dendrimeric construct. One of these utilized a trebler DNA attachment where three equivalent DNA strands

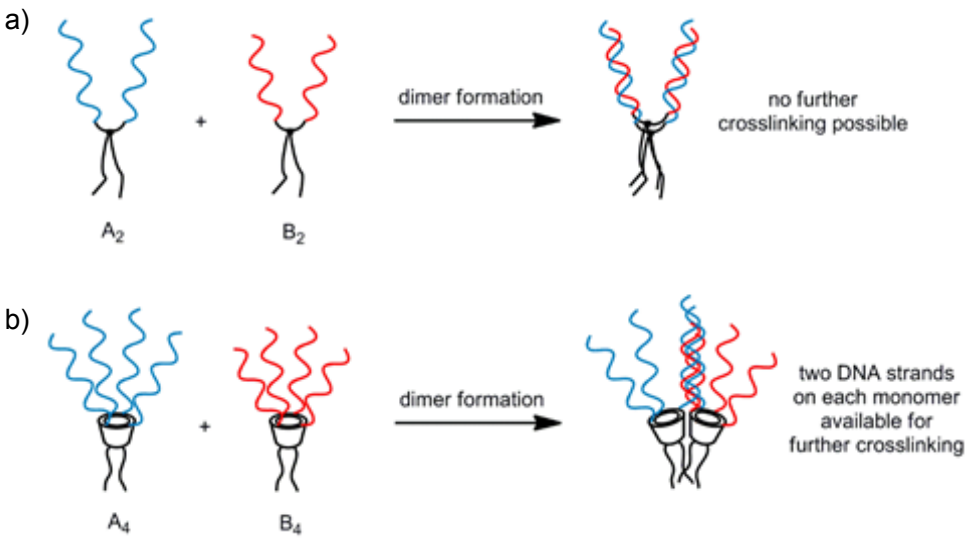

Figure 2.4. Monomer assembly (a) if a monomer has only two DNA strands, dimer formation is possible; (b) by incorporating more strands, duplexes form between multiple monomers, enabling cross-linking across the entire micelle formation.

branch off the multiplier. For our other construct, we used two doubler monomers in succession to enable attachment of four parallel DNA strands (Figure 2.5). By using two different constructs, we could compare to see if hybridization had a greater effect based on the number of incorporated strands.

Results and Discussion

Synthesis of DNA amphiphiles

The constructs explored herein were generated using solid-phase DNA synthesis. As shown in Table 2.1, we synthesized monomers using tocopherol and DNA strands to provide amphiphilic molecules capable of self-assembly to form micelles. During synthesis, the tocopherol amidites are added first, followed by the dendrimer unit(s). Therefore, in order to accommodate antiparallel DNA

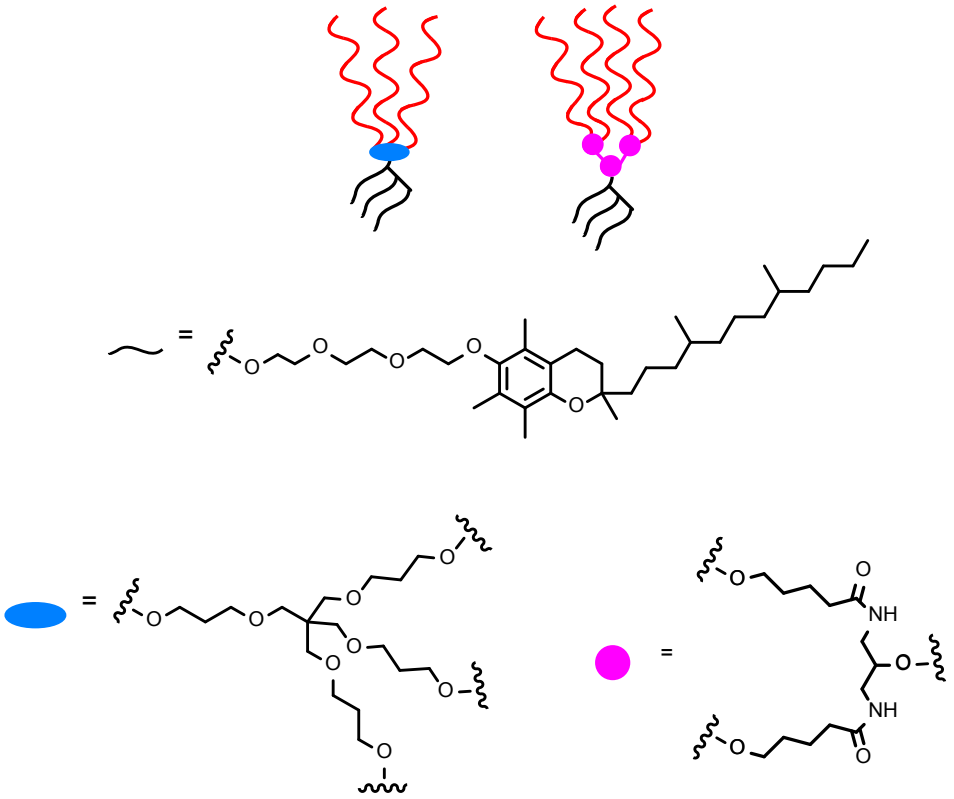

Figure 2.5. The structure of the monomer units. The waved line represents the hydrophobic tocopherol unit used. In order to synthesize multiple DNA strands within a single monomer, either a trebler (oval) was used to give three DNA strands or a series of two doublers (circle) was incorporated to give a total of four strands.

Table 2.1. The sequences for the monomers in this study. The sequences reported 5' -> 3' were synthesized using standard phosphoramidites while the 3' -> 5' strands are formed from reverse amidites. The green bases represent the mutated bases in the mismatched sequence. The red bases represent the EcoRI cleavage site.

Study	Strand Name	Sequence
Preliminary	PFT3	5' GCACGTCTAGCAGTA trebler-spacer9-toco$_3$
	PRT3	3' CGTGCAGATCGTCAT trebler-spacer9-toco$_3$
	PFT4	5' GCACGTCTAGCAGTA trebler-spacer9-toco$_4$
	PRT4	3' CGTGCAGATCGTCAT trebler-spacer9-toco$_4$
Main	TMT3	5' ACCGGCATGGAATTCTGTA trebler-spacer9-toco$_3$
	TFT3	5' ACAGGCACGGAATTCAGTA trebler-spacer9-toco$_3$
	TRT3	3' CGTGCCTTAAGTCAT trebler-spacer9-toco$_3$
	TFCT3	5' AATTCA GTA trebler-spacer9-toco$_3$
	TRCT3	3' GTCAT trebler-spacer9-toco$_3$
	DMT3	5' ACCGGCATGGAATTCTGTA doubler$_2$-spacer9-toco$_3$
	DFT3	5' ACAGGCACGGAATTCAGTA doubler$_2$-spacer9-toco$_3$
	DRT3	3' CGTGCCTTAAGTCAT doubler$_2$-spacer9-toco$_3$
	DFCT3	5' AATTCAGTA doubler$_2$-spacer9-toco$_3$
	DRCT3	3' GTCAT doubler$_2$-spacer9-toco$_3$
Doubler Series	DS1T3	5'GTC TCC C-C3-C3-toco$_3$
	DS1T2	5'GTC TCC C-C3-C3-toco$_2$
	DS2T3	5'GTC TCC C-doubler-C3-toco$_3$
	DS2T2	5'GTC TCC C-doubler-C3-toco$_2$
	DS4T3	5'GTC TCC C-doubler-doubler-toco$_3$
	DS4T2	5'GTC TCC C-doubler-doubler-toco$_2$

hybridization, the complementary DNA strands were synthesized using reverse-protected amidites to allow for 5' to 3' synthesis.

Assembly characterization

Preliminary DLS studies were performed using monomers that contained three or four tocopherol units. These were done to ensure that assembly occurred to form a monodisperse population. The diameters for the micelles are below 50 nm as shown in Table 2.2. Using DLS we were able to verify that the monomers mix to form a single population. For the four tocopherol series, we found that the micelles from monomers using the PFT4 (5'->3' amidites) were 48.8 ± 1.4 nm while the PRT4 (3' -> 5' amidites) were smaller at 28.7 ± 5.1 nm. This is likely caused by the different packing and configurations due to flipping the orientation of the chiral ribose-phosphate backbone. The difference in sizes made it easy to determine if they were making a single population upon mixing.

Table 2.2. The DLS averages, polydispersity index (PDI), and zeta potentials for the initial monomer studies. The error is an average of three trials.

Monomer(s)	Diameter (nm)	PDI	Zeta (mV)
PRT4	28.7 ± 5.1	0.265 ± 0.013	-
PFT4	48.8 ± 1.4	0.431 ± 0.010	-75.9 ± 0.3
PRT3	19.3 ± 1.9	0.275 ± 0.039	-78.6
PFT3	17.4 ± 8.8	0.332 ± 0.129	-63.2 ± 0.4
PRT4 + PFT4	26.1 ± 1.3	0.384 ± 0.009	-74.5 ± 2.1

Following mixing and heating-cooling the monomers, we found that they formed a single population at 26.1 ± 1.3 nm, similar in dimension to the reverse amidite monomers. This shows that the different monomers are indeed able to incorporate and form a single population. Additionally, the DLS data confirmed that the structures disassemble at low monomer concentrations (Figure 2.6). The zeta potentials were also measured to determine particle stability against agglomeration. As expected, due to the negative backbone, the zeta potentials were highly negative (Table 2.2). As such, they have strong repulsion between assemblies, preventing the particles from agglomerating. TEM was also employed to examine the structure and polydispersity of these structures. The TEM images suggest that micelles with defined structures were formed (Figure 2.7). Since both the monomers with three and four tocopherol units were able to form stable assemblies, we used three tocopherol units in our future studies in order to maximize any changes within the DNA corona.

CMC characterization

Initially we anticipated that the CMC and guest release could be controlled using DNA hybridization or DNA length. We hypothesized that the CMC could be lowered by creating DNA duplexes between monomer units to stabilize the micelle structure. Additionally, we anticipated that decreasing the length of the DNA strand would reduce the hydrophilic portion of the monomer, which should consequently increase the CMC. To accomplish this, we introduced an EcoRI recognition site into our DNA sequences. In the presence of the matched DNA

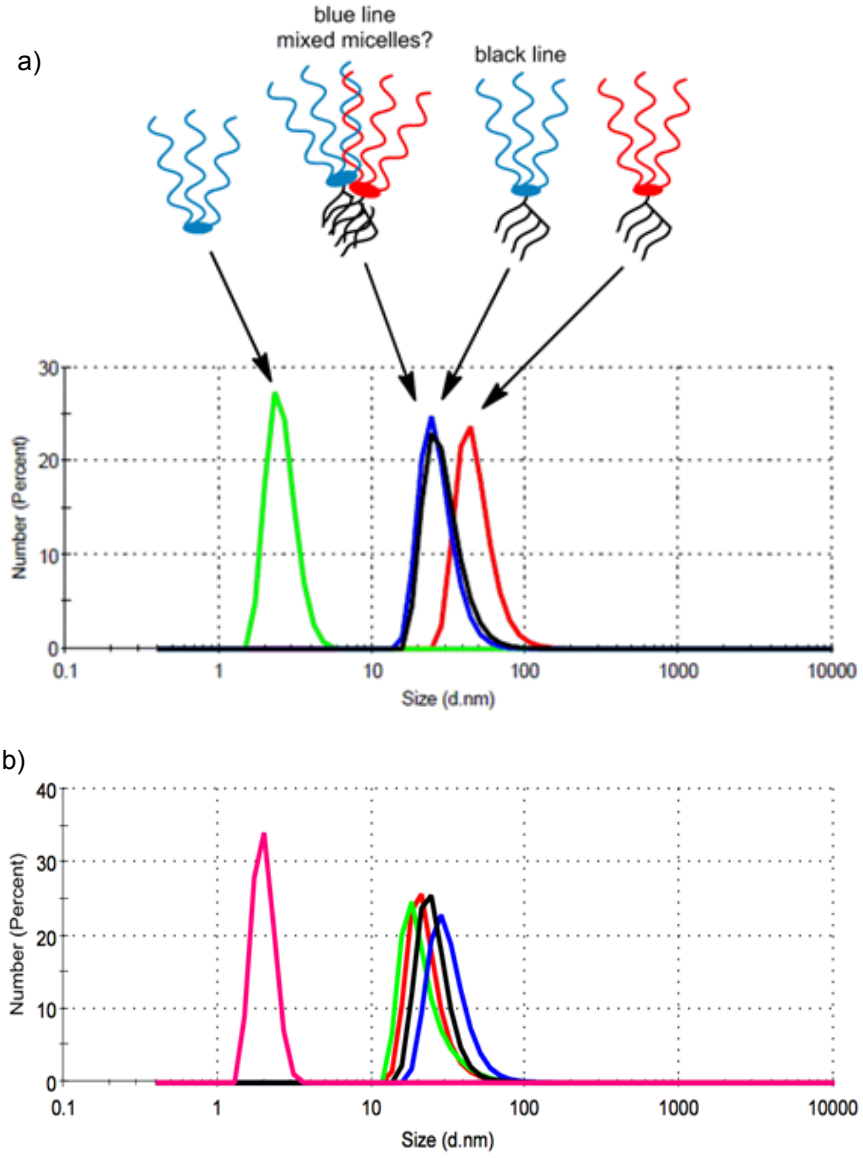

Figure 2.6. The DLS data for (a) the complementary PRT4 and PFT4 monomers form two distinct peaks; however, when combined, they form a single population; (b) as the concentration of the PRT4 monomer decreases, the radius stays the same. Below the CMC, the monomers dissociate.

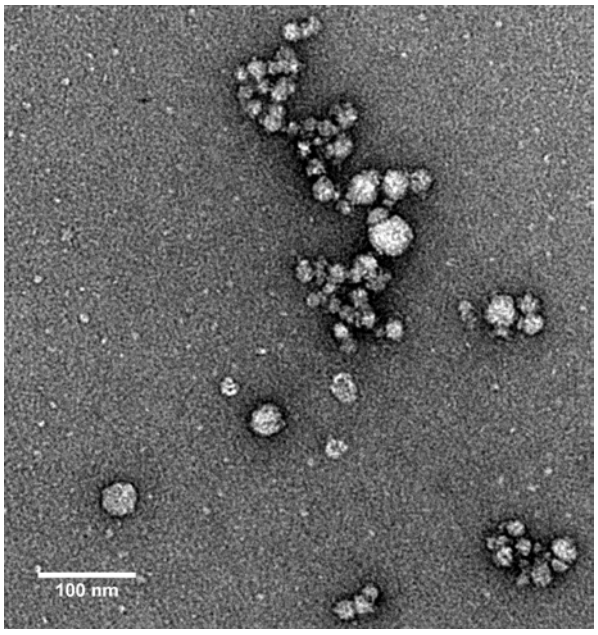

Figure 2.7. TEM image for PFT3. The image shows that distinct spherical structures are present.

duplex, EcoRI will cleave the DNA strands. We anticipated that this would initiate micelle dissociation if the monomer concentration is above the CMC for the full-length strand but below that of the cleaved product. Knowledge of the CMC is not only important for micelle dissociation control but also for the proper design of experiments such as those to quantify guest exchange kinetics. This is due to the fact that below the CMC, there are no micelles present, invalidating any experiments.

To test our hypotheses for tuning the critical micelle concentration (CMC) by introducing noncovalent cross-links or modulating DNA length, we first attempted to determine the CMCs of our micelles using pyrene as a fluorescent probe. When pyrene is excited at 332 nm, it has multiple emission peaks, including one at 373 nm (I_1) and one at 384 nm (I_3). (Figure 2.8). In a polar

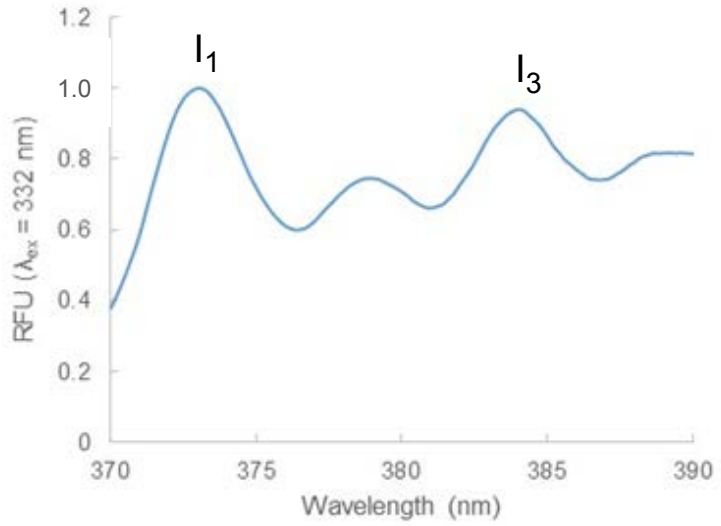

Figure 2.8. The emission spectrum of pyrene contains multiple bands. The emission peak at 373 nm is known as the I_1 band while the 384 peak is referred to as the I_3 band.

environment, the peak at 373 nm is larger than the 384 nm peak.[15] As the hydrophobicity of pyrene's environment increases, the peak at 384 nm increases relative to the 373 nm peak. By plotting the 384:373 nm ratio versus the monomer concentration, two distinct dependencies are observed. One line results from data below the CMC. This ratio increases gradually due to a greater number of hydrophobic groups available to interact with the pyrene. However, once micelles begin to form, pyrene is incorporated into the hydrophobic core, greatly changing the polarity of the environment where pyrene is located. As a result, the slope of the second trend increases at a sharper rate. After graphing the trends, the CMC is determined by using the calculated linear regression of the two lines to determine the concentration at which the two lines intersect (Figure 2.9).[16]

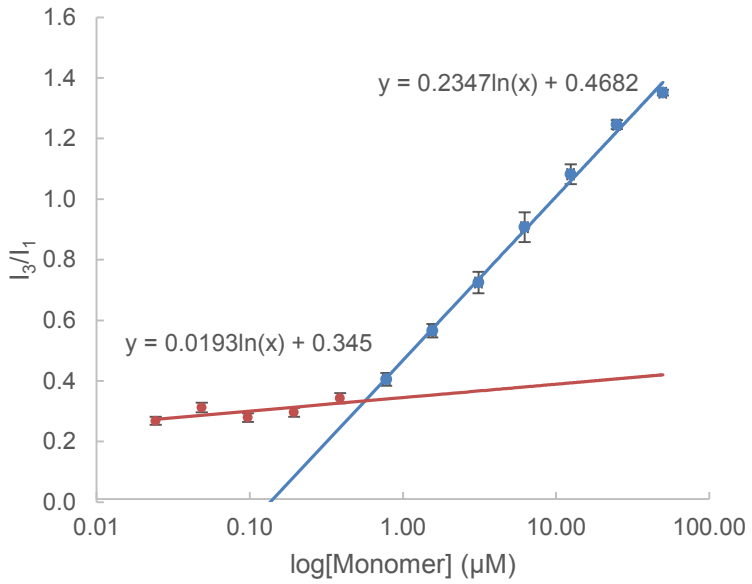

Figure 2.9. Example pyrene data for the matched micelle TFT3 and TRT3 in 20% EtOH. The CMC is determined by finding the intersection between the upper and lower regions.

In measuring the CMC values of the monomers, we found that the presence of DNA duplexes does slightly lower the CMC compared to the mismatched micelle, but it did not do so to a significant degree (Table 2.3). We also included what would be the product following digestion to allow testing this hypothesis (Table 2.1, cleaved sequences TFCT3 and DFCT3). We found that these truncated sequences did not significantly raise CMCs compared to their respective full-length sequences. We hypothesize that the presence of DNA duplexes or enzymatic degradation provides insignificant improvement in CMC due to the strong hydrophobic force from the tocopherol groups. Since micelles form due to a balance of hydrophobicity and hydrophilicity, if the hydrophobic forces are too strong, changes in the hydrophilic corona would not have as significant of an impact on the micelle formation. However, these CMC values

Table 2.3. The CMC values calculated using pyrene.

Sequences		CMC (nM)
Doublers	Matched DFT3 and DRT3	210
	Mismatched DFT3 and DMT3	300
	Digest DFCT3 and DRCT3	370
Trebler	Matched TFT3 and TRT3	470
	Mismatched TFT3 and TMT3	590
	Digest TFCT3 and TRCT3	630

are comparable to CMC values for drug delivery systems, which are typically in the range of 10^{-6} -10^{-7} M.[17] Following the CMC measurements, other characterization studies were done at concentrations 3-fold higher than the CMC.

In order to test the hypothesis that the hydrophobic force was overshadowing the driving forces from the DNA, we decided to measure the CMC values in a solution containing 10 or 20% ethanol in PBS. By adding ethanol, the polarity of the solvent is decreased, lowering the energy gained by hydrophobic assembly of the tocopherol units in micelle formation. We tested this using the trebler sequences having matched (TFT3 and TRT3) and mismatched (TFT3 and TMT3) DNA sequences. Interestingly, the CMC was not significantly affected by the presence of EtOH (Table 2.4). The difference between the CMC values of matched and mismatched micelles increases slightly but not by a clinically relevant amount. Since the driving forces for micelle formation are very

Table 2.4. CMC values calculated using the trebler monomers in 10 or 20% ethanol

Conditions		CMC (nM)
10% EtOH	Matched TFT3 and TRT3	630
	Mismatched TFT3 and TMT3	840
20% EtOH	Matched TFT3 and TRT3	610
	Mismatched TFT3 and TMT3	1320

strong using these monomers, changing the tocopherol to a less polar group may increase the impact that DNA alterations have on the CMC values.

The size and monodispersity of these structures were examined using DLS. As in the previous DLS studies, the monomers are assembling to form monodisperse structures with a diameter below 50 nm (Table 2.5)

EcoRI digestion

Some studies within the literature show that assembly of DNA into nanoparticles slows the enzymatic degradation of the DNA.[18] We therefore decided to monitor the kinetics for EcoRI digestion of the DNA in our micelles. In order to do this, we decided to use FRET to monitor the EcoRI digestion by labeling the complementary DNA sequences with a FRET pair (FAM and Cy3). When the strands are intact and hybridized, the FAM and Cy3 modifications are within FRET range. As the strands are digested, the ends of the strands with FAM and Cy3 are released and no longer have sufficient affinity to hybridize to

Table 2.5. DLS data for the EcoRI strands.

	Sequence	Diameter (nm)	PDI
Trebler	TRT3	28.26 ± 2.49	0.317 ± 0.042
	TFT3	39.46 ± 4.92	0.354 ± 0.048
	TMT3	49.95 ± 1.83	0.410 ± 0.014
Doublers	DRT3	44.36 ± 3.53	0.390 ± 0.019
	DFT3	34.89 ± 2.13	0.527 ± 0.010
	DMT3	47.62 ± 5.98	0.520 ± 0.024
Trebler Cleaved	TRCT3	17.45 ± 4.38	0.323 ± 0.005
	TFCT3	13.99 ± 2.48	0.295 ± 0.003
Doublers Cleaved	DRCT3	17.58 ± 0.98	0.286 ± 0.026
	DFCT3	16.57 ± 2.85	0.278 ± 0.012
Trebler Mix	TRT3 & TFT3	19.66 ± 8.88	0.288 ± 0.010
Doublers Mix	DRT3 & DFT3	33.48 ± 2.85	0.339 ± 0.066

one another, turning off FRET (Figure 2.10). We conducted an EcoRI digestion using the matched micelle TFT3 (FAM labelled) and TRT3 (Cy3 labelled). EcoRI digestion of these micelles was compared to the digestion of a free DNA duplex (no dendrimer or tocopherol) and the mismatched micelle formed from the strands TRT3 and TMT3 (FAM labelled). Assembly into micelles does appear to slightly slow the digestion compared to the free strand, but not significantly. As expected, our control containing mismatched monomers did not show digestion since they are not able to form a duplex (Figure 2.11).

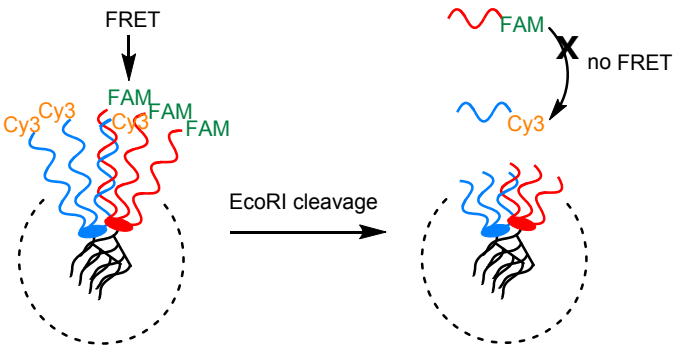

Figure 2.10. EcoRI digestion monitored by the disappearance of the Cy3 signal.

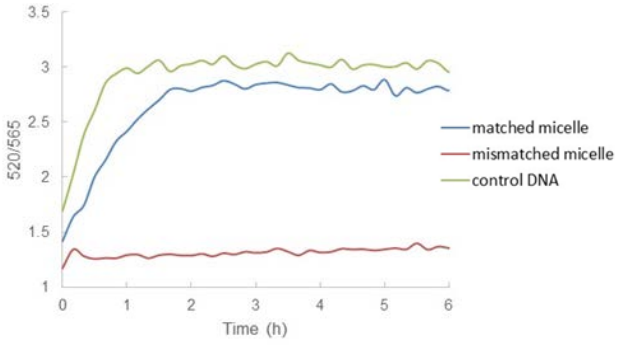

Figure 2.11. The progression of EcoRI digestion as monitored by FRET. The matched micelle sequences (blue) show slightly slowed kinetics compared to that of free DNA (green). The mismatched micelle sequences (red) did not show degradation.

Guest exchange

To probe the stability of guest molecule binding within our micelles, we used the FRET method developed by the Thayumanavan group using DiO (donor, λ_{em} = 510 nm) and DiI (acceptor, λ_{em} = 570 nm) as a FRET pair.[19] Due to their hydrophobic nature, these dyes are readily sequestered within the hydrophobic core of micelles, and the stability of this binding event can be determined by monitoring the exchange of guest molecules measured using FRET. In this method, two micelle populations are prepared, one containing DiO and the other containing DiI. Upon mixing the two populations, two possible outcomes may occur. If the micelles stably bind the guest molecules, no exchange occurs and the dyes remain sequestered apart from one another. However, in leaky micelles, the development of an emission signal around 570 nm can be observed from the acceptor dye coming into close proximity to the donor dye (Figure 2.12). The more stable binding is, the slower the exchange occurs. In the case of very leaky micelles such as Tween80 or SDS, this exchange occurs instantly (Figure 2.13). However, we found that the presence of the negative DNA slows this exchange. This is likely because the cationic molecules must cross through the highly charged DNA corona. By monitoring the ratio of the donor and acceptor peaks using Eq 1-5, we found that the exchange followed first-order kinetics (Figure 2.14). Using both the trebler and doubler units, we observed similar exchange rates between hybridized and unhybridized micelles. Next, we measured the differences between the full sequences and the EcoRI digests. Again, we observed that the exchange rate did not significantly

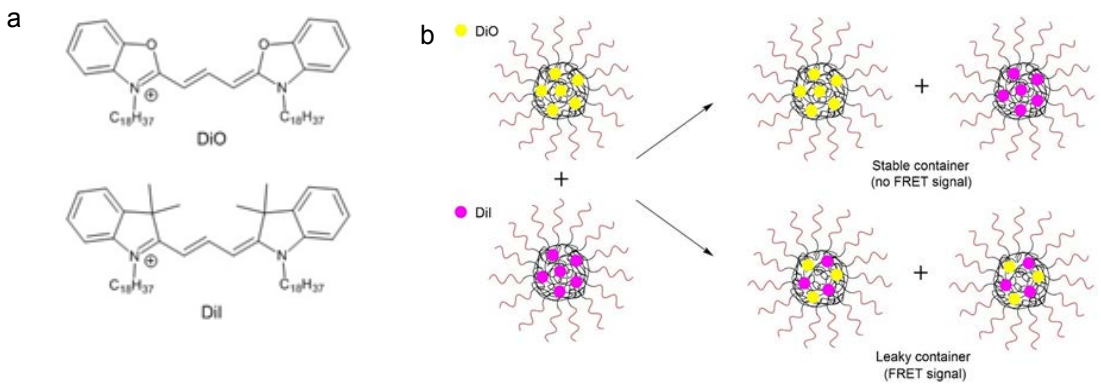

Figure 2.12. Guest molecule stability was monitored using the exchange of a FRET pair including (a) DiI and DiO; (b) There are two possible outcomes upon mixing a population containing DiI and one containing DiO. If the micelles stabilize the guest molecules, no exchange occurs and FRET is not observed (top). If the micelles are leaky, dye exchange occurs, initiating the FRET signal (bottom).

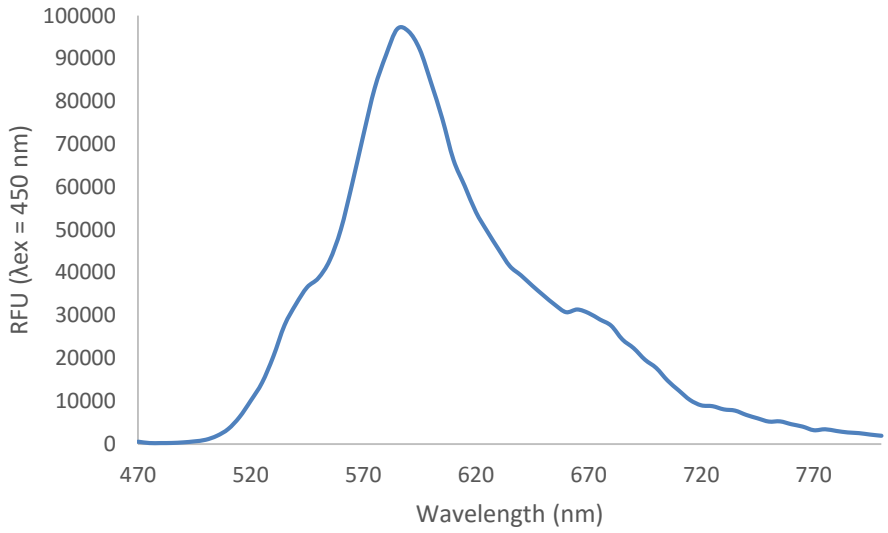

Figure 2.13. Upon mixing populations of SDS containing DiI and DiO, dye exchange occurs immediately, with the main emission peak being the acceptor peak at 580 nm. This shows that SDS is a leaky micelle.

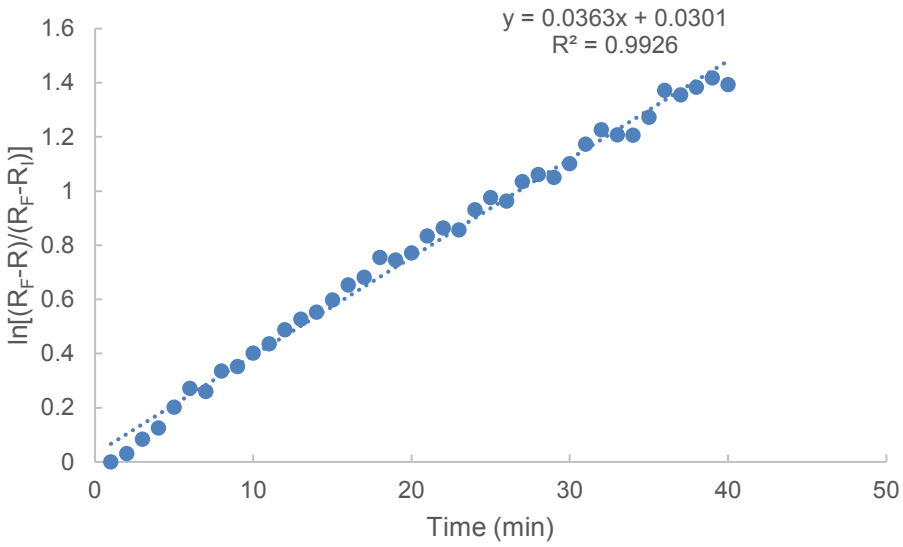

Figure 2.14. Dye exchange follows a first order rate equation (TFT3). The rate is given by determining the slope of the line.

change based on DNA length.

Doubler series

Since the presence of the DNA slowed the guest molecule exchange relative to traditional surfactants, we decided to see if the number of strands present in the monomer unit showed a difference in the exchange rate. Rather than compare the rates between three and four strands, we decided to explore a wider range, so we synthesized sequences containing one, two, and four DNA strands. In order to keep the length of the monomers the same, we included spacers to replace the missing dendrimer units. We also decided to try units with

two and three tocopherol monomers to investigate whether decreasing the hydrophobic driving force would allow changes in the DNA shell to have a larger effect on micelle formation. We again used pyrene to measure the CMCs for the monomers. The results are shown in Table 2.6. CMC values were obtained for monomers containing a single DNA strand. Our results for these monomers were inconsistent, likely due to the inability of these monomers to form stable micelles. While the CMC values were similar for the series using two and three tocopherol units, there was a slight deviation in the measurement depending on the number of DNA strands. Increasing the quantity of strands from two to four for the monomers containing three tocopherol units slightly stabilized the assembly. On the other hand, the units containing two tocopherol units appear to be slightly destabilized by increasing the number of DNA strands. Additional tests would need to be performed to confirm this trend. While the data are noisy, the number of DNA strands does not appear to significantly affect the exchange rate, so further testing was not performed on these monomers (Figure 2.15).

Conclusion

We hypothesized that DNA could be used to introduce cross-links for the stabilization of micelles in order to prevent guest molecule escape and decrease the CMC. Additionally, the incorporation of DNA introduces a potentially stimuli-responsive group into the micelle. In order to test this hypothesis, we surveyed a range of monomers containing different combinations of dendrimer DNA attached to tocopherol units where the amphiphilic nature drives assembly formation. We

Table 2.6. CMC values for the doubler series. *These monomers did not give consistent results and it is likely they are not forming micelles.

# DNA Strands	Sequence	CMC (nM)
1	DS1T3	1,800*
	DS1T2	2,100*
2	DS2T3	1,100
	DS2T2	930
4	DS4T3	540
	DS4T2	1,800

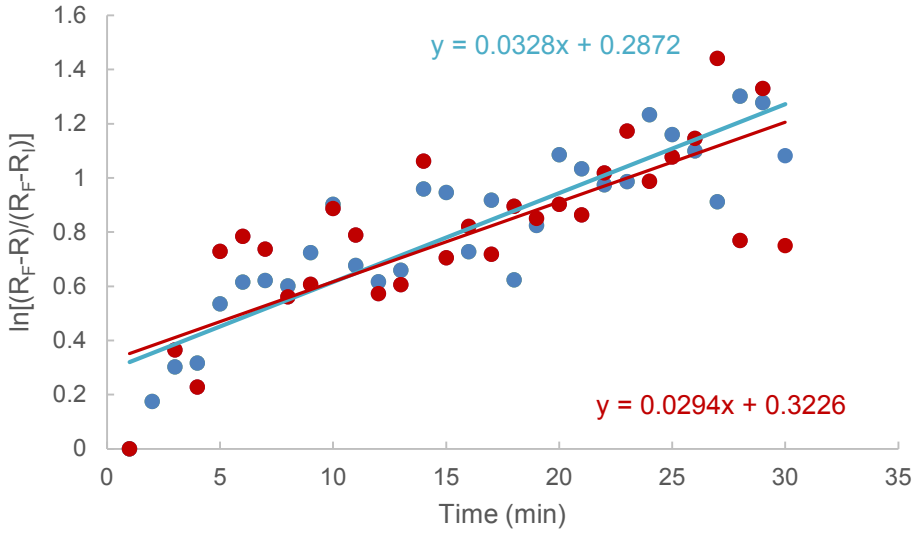

Figure 2.15. Exchange trend lines for DS2T3 (blue line) and DS4T3 (red line). Though the data are noisy, the exchange appears to occur at approximately the same rate.

characterized the resulting structures using DLS, TEM, and pyrene. We found using DLS and TEM that these sequences produce distinct structures that are under 50 nm in diameter. We also found that the complementary sequences are able to combine to form a single population, presumably having noncovalent crosslinks between the DNA strands. However, CMC analysis using pyrene did not show the differences that we were anticipating between cross-linked and noncross-linked micelles. Further, we tested the effects of hybridization and sequence truncation that would result from EcoRI cleavage. While the sequence length and hybridization had a slight effect on the CMC, these changes were not significant and would not provide adequate control over monomer assembly. We confirmed that the sequences were able to hybridize, as was evidenced by their ability to undergo EcoRI digestion. While the hybridization did not significantly affect the CMC, we wanted to determine if the hybridization was able to slow guest release. We were not able to observe a consistent, significant change in the exchange of guest molecules as analyzed using FRET to monitor the exchange of DiO and DiI molecules.

Experimental Section

General methods

All DNA was purchased from the University of Utah DNA/Peptide Synthesis Core Facility, where it was synthesized using phosphoramidites and CPG cartridges from Glen Research (Table 2.1). All other materials were purchased from commercial suppliers without further purification unless

otherwise noted. Absorbance and most fluorescence measurements were recorded using a Biotek Synergy Mx microplate reader.

For micelle preparation, the monomers were dissolved in phosphate-buffered saline (PBS) pH = 7.4. They were then heated to 95 °C and slowly cooled.

CMC measurements

For the pyrene studies, the fluorescence was measured using a Hitachi F-7000 spectrophotometer. DNA stock solutions were made concentrations (X) in 1 μM pyrene solution. Serial dilutions were then made in 1 μM pyrene in PBS and the solutions were incubated at 25 °C for 3 h. The samples were then excited at 332 nm, and the emission was scanned from 365 to 390 at a rate of 240 nm/min with an excitation bandpass of 5.0 nm and an emission bandpass of 2.5 nm. The ratio of fluorescence of the 384 and 373 wavelengths were graphed as a function of concentration. The CMC was then calculated by calculating the intersection of the two resulting lines.

Dynamic light scattering and zeta potentials

Prior to dynamic light scattering (DLS) measurements, all samples were filtered through a 200 nm filter and allowed to equilibrate at 25 °C overnight. DLS was carried out using a Malvern Zetasizer. All measurements were acquired at 25 °C. The DLS was measured at a 173° scattering angle. Zeta potentials were measured using a Smoluchowski model.

Transmission electron microscopy

For Transmission electron microscopy (TEM) visualization, formvar-coated copper grid with 200 mesh was used. The grid was arc discharged from 30 s to 4 min. The sample was dropped on the mesh and allowed to sit for 1 min. It was then wicked off, and replaced with uranyl acetate for 30 s. This was again removed and the grid was dipped in water for 5 sec, and the liquid wicked off. The grid was allowed to dry at room temperature and imaged at 120 kV using a FEI Technai T12 instrument.

EcoRI digestion

EcoRI digestion was monitored via FRET by labeling the TFT3 and TMT3 strands with FAM and the TRT3 with Cy3. The samples were equilibrated to 37 °C. EcoRI was then added to the samples to give 1 Unit/μL, and the fluorescence was excited at 440 nm and the emission was monitored at 520 and 565 nm, maintaining a temperature of 37 °C.

Guest exchange

Stock solutions were prepared at a concentration of six times the CMC for a given monomer and contained either 3,3’-dioctadecyloxacarbocyanine perchlorate (DiO) or 1,1'-dioctadecyl-3,3,3'3'-tetramethylindocarbocyanine perchlorate (DiI). This was done in one of two ways. In the first method, stock solutions of the dye were prepared in DMSO at 900 μM. This was added to the monomers to give a final dye concentration of 15 μM. The solutions were then sonicated and al-

lowed to equilibrate for 5 h. In the second method, 20 µL 15 µM dye was dissolved in 500 µL acetone. The DNA was added to the solution, and the acetone was evaporated. The solution was then resuspended in 10 µL PBS and sonicated for 30 min. The solutions were allowed to equilibrate at 25 °C for at least 3 hours. A control was prepared to quantify the final FRET signal. This was done by creating an equimolar solution of DiO and DiI before incubation with the monomers.

The solutions were then mixed and scanned using the fluorescence plate reader. The FRET signal was monitored using λ_{ex} = 450 nm and λ_{em} = 510 and 570 nm. The ratio of the emission wavelengths was then used to monitor exchange progression. In order to calculate the FRET ratio Eq 1 was used:

$$R = \frac{I_A}{I_A + I_D} \tag{1}$$

in which R is the normalized fluoresence ratio, I_A is the fluoresence of DiO, and I_D is the fluorescence of DiI. In order to monitor the kinetics of the exchange Eq 2 was used:

$$Ratio = \frac{R - R_I}{R_F - R_I} \tag{2}$$

where R_I is R at time = 0, R_F is the final ratio measured using the premixed dyes, and R is the value at the timepoint of interest. Using the integrated rate laws, it was determined that exchange follows first-order kinetics, giving Eq 3:

$$Ratio(t) = 1 - e^{-kt} \tag{3}$$

where t is time and k is is the rate constant. This can then be solved to give Eq 4:

$$\frac{R_F - R}{R_F - R_I} = e^{-kt} \tag{4}$$

and the rate can be determined by graphing the relationship

$$ln\left(\frac{R_F - R}{R_F - R_I}\right) = -kt \tag{5}$$

References

(1) Neugebauer, J. M.: [18] Detergents: An overview. In *Methods in Enzymology*; Murray, P. D., Ed.; Academic Press, 1990; Vol. 182; pp 239-253.

(2) Alemdaroglu, F. E.; Alemdaroglu, N. C.; Langguth, P.; Herrmann, A. DNA Block Copolymer Micelles – A Combinatorial Tool for Cancer Nanotechnology. *Adv. Mater.* **2008**, *20*, 899-902.

(3) Deng, C.; Jiang, Y.; Cheng, R.; Meng, F.; Zhong, Z. Biodegradable polymeric micelles for targeted and controlled anticancer drug delivery: Promises, progress and prospects. *Nano Today* **2012**, *7*, 467-480.

(4) Jiang, J.; Qi, B.; Lepage, M.; Zhao, Y. Polymer Micelles Stabilization on Demand through Reversible Photo-Cross-Linking. *Macromolecules* **2007**, *40*, 790-792.

(5) Shuai, X.; Merdan, T.; Schaper, A. K.; Xi, F.; Kissel, T. Core-Cross-Linked Polymeric Micelles as Paclitaxel Carriers. *Bioconjugate Chem.* **2004**, *15*, 441-448.

(6) O'Reilly, R. K.; Hawker, C. J.; Wooley, K. L. Cross-linked block copolymer micelles: functional nanostructures of great potential and versatility. *Chem. Soc. Rev.* **2006**, *35*, 1068-1083.

(7) Klaikherd, A.; Nagamani, C.; Thayumanavan, S. Multi-Stimuli Sensitive Amphiphilic Block Copolymer Assemblies. *J. Am. Chem. Soc.* **2009**, *131*, 4830-4838.

(8) Jeong, J. H.; Park, T. G. Novel Polymer−DNA Hybrid Polymeric Micelles Composed of Hydrophobic Poly(d,l-lactic-co-glycolic Acid) and Hydrophilic Oligonucleotides. *Bioconjugate Chem.* **2001**, *12*, 917-923.

(9) Li, Z.; Zhang, Y.; Fullhart, P.; Mirkin, C. A. Reversible and Chemically Programmable Micelle Assembly with DNA Block-Copolymer Amphiphiles. *Nano Lett.* **2004**, *4*, 1055-1058.

(10) Tuerk, C.; Gold, L. Systematic evolution of ligands by exponential enrichment: RNA ligands to bacteriophage T4 DNA polymerase. *Science* **1990**, *249*, 505-510.

(11) Robertson, D. L.; Joyce, G. F. Selection in vitro of an RNA enzyme that specifically cleaves single-stranded DNA. *Nature* **1990**, *344*, 467-468.

(12) Ellington, A. D.; Szostak, J. W. In vitro selection of RNA molecules that bind specific ligands. *Nature* **1990**, *346*, 818-822.

(13) Zhu, Z.; Schmidt, T.; Mahrous, M.; Guieu, V.; Perrier, S.; Ravelet, C.; Peyrin, E. Optimization of the structure-switching aptamer-based fluorescence polarization assay for the sensitive tyrosinamide sensing. *Anal. Chim. Acta* **2011**, *707*, 191-196.

(14) Liu, J.; Lu, Y. Fast Colorimetric Sensing of Adenosine and Cocaine Based on a General Sensor Design Involving Aptamers and Nanoparticles. *Angew. Chem. Int. Ed.* **2006**, *45*, 90-94.

(15) Kalyanasundaram, K.; Thomas, J. K. Environmental effects on vibronic band intensities in pyrene monomer fluorescence and their application in studies of micellar systems. *J. Am. Chem. Soc.* **1977**, *99*, 2039-2044.

(16) Khan, A. M.; Shah, S. S. Determination of Critical Micelle Concentration (Cmc) of Sodium Dodecyl Sulfate (SDS) and the Effect of Low Concentration of Pyrene on its Cmc Using ORIGIN Software. *J. Chem. Soc. Pak.* **2008**, *30*, 186-191.

(17) Oerlemans, C.; Bult, W.; Bos, M.; Storm, G.; Nijsen, J. F. W.; Hennink, W. E. Polymeric Micelles in Anticancer Therapy: Targeting, Imaging and Triggered Release. *Pharmaceut. Res*. **2010**, 27, 2569-2589

(18) Kabir, M. S.; Morjan, R. E.; Nerushev, O. A.; Lundgren, P.; Bengtsson, S.; Enokson, P.; Campbell, E. E. B.. Plasma-enhanced chemical vapour deposition growth of carbon nanotubes on different metal underlayers. *Nanotechnology* **2005**, *16*, 458.

(19) Jiwpanich, S.; Ryu, J.-H.; Bickerton, S.; Thayumanavan, S. Non-covalent Encapsulation Stabilities in Supramolecular Nanoassemblies. *J. Am. Chem. Soc.* **2010**, *132*, 10683-10685.

CHAPTER 3

3,3'-DIOCTADECYLOXACARBOCYANINE PERCHLORATE (DiO) AS A FLUOROGENIC PROBE FOR MEASUREMENT OF CRITICAL MICELLE CONCENTRATION

Introduction

Amphiphilic molecules, generally referred to as surfactants, can undergo phase-driven assembly to form higher order structures such as vesicles, bilayers, and micelles. Of these structures, micelles are the most common.[1] In aqueous environments, the micelle structure is solvated by the hydrophilic portion of the amphiphile to minimize unfavorable interactions between the hydrophobic region and the polar solvent. Because of their ability to sequester hydrophobic guest molecules, micelles have shown significant utility in applications including drug delivery, separations, and reaction catalysis.[2-6] In order to utilize micelles in these applications, their assembly must be well-characterized. Micelle assembly is a concentration-dependent process that is characterized by a sharp transition at the critical micelle concentration (CMC). Below this concentration, the surfactant

[1] Reprinted with permission from Peterson, A. M.; Tan, Z.; Kimbrough, E. M.; Heemstra, J. M. 3,3'-Dioctadecyloxacarbocyanine Perchlorate (DiO) as a Fluorogenic Probe for Measurement of Critical Micelle Concentration. *Anal. Methods*. **2015**, 7, 6877-6882. Copyright 2015 The Royal Society of Chemistry

molecules can be free in solution or form a monolayer at the air-solvent interface. However, as the surfactant concentration increases above the CMC, the molecules assemble to form micelles. While the CMC is largely dictated by the chemical properties of the surfactant, it is also dependent on environmental conditions such as pH, temperature, or ionic strength.[7]

CMC values have been measured using a variety of methods including tensiometry,[8] conductivity,[9] dynamic light scattering (DLS),[10] fluorescence polarization,[11] and capillary electrophoresis.[12] However, these procedures require specialized equipment and are not well suited for all surfactants. For example, conductivity requires a charged state, and thus is not capable of measuring the CMC values of nonionic surfactants. In contrast, a number of methods utilize fluorogenic probe molecules that undergo a change in fluorescence intensity or emission wavelength upon sequestration in the hydrophobic core of a micelle. The key benefit of this approach is that analysis is carried out using a fluorimeter or fluorescence plate reader, which is more commonly available in research labs. A number of fluorogenic probes have been reported, including coumarin, curcumin, 1,6-diphenyl-1,3,5-hexatriene (DPH), pyrene, and Nile Red (NR).[13-15] Of these probes, pyrene and NR are used most commonly in CMC studies using DPC monomers. In the presence of micelles, pyrene undergoes a change in the relative intensity of emission at 373 and 384 nm.[16,17] Though useful, resolving these two wavelengths requires a more sophisticated fluorimeter, and we have found that a standard fluorescence plate reader does not provide sufficient resolution to enable CMC measurement using pyrene. In contrast, with NR (Figure 3.1a), the fluorescence intensity increases in the presence of micelles

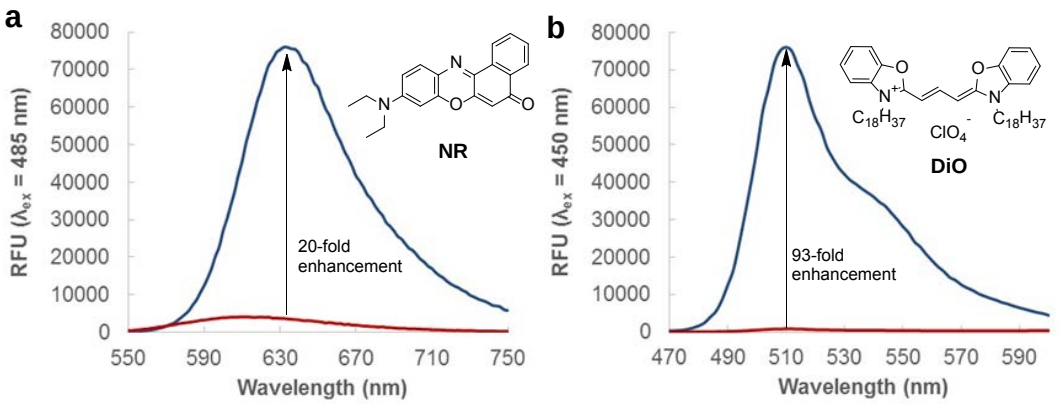

Figure 3.1. Chemical structure and emission spectra for (a) NR and (b) DiO in DMSO (blue) and water (red). RFU = relative fluorescence intensity.

and often undergoes a blue shift in emission wavelength. These changes are of sufficient magnitude to enable CMC measurement using a standard fluorescence plate reader.[18,19] However, instances have been reported in which the emission wavelength of NR instead undergoes a red shift as surfactant concentration increases.[20,21] In these cases, the authors hypothesize that this anomalous behavior may be the result of dye aggregation. This is consistent with a recent report by Mohr and coworkers describing aggregation of NR to form nonemissive dimers via π-π stacking interactions.[22] This behavior creates a significant challenge for CMC measurement, as aggregation results in a hydrophobic environment similar to the core of a micelle, producing misleading results.

In our attempt to measure the CMC of our DPC micelles, we observed many inconsistencies using NR. These inconsistent results coupled with our observation of NR aggregation in our own lab caused us to seek an alternative fluorogenic dye that could offer greater reliability while remaining suitable for measuring CMC values using a standard fluorescence plate reader. We found

that 3,3'-dioctadecyloxacarbocyanine perchlorate (DiO, Figure 3.1b) shows similar fluorogenic properties to NR, and has been previously used for lipophilic staining[23] and monitoring guest exchange dynamics in micelles and nanogels.[24] Upon transitioning from water to DMSO, DiO undergoes a dramatic increase in fluorescence intensity, with an emission maximum at 510 nm. Impressively, DiO shows a 93-fold fluorescence enhancement upon transition from water to DMSO, compared to only 20-fold enhancement observed for NR (Figure 3.1).

Herein, we evaluate the utility of DiO for fluorescence-based CMC measurement and directly compare its performance to that of NR. We find that DiO is compatible with a variety of surfactant types, and while NR and DiO both provide CMC measurements that agree with literature values, DiO did not suffer from failed measurements, as NR often did. Additionally, DiO was easier to handle than NR, as solubility and aggregation problems were not observed with DiO, but were frequent with NR. Therefore, DiO provides an accurate and reliable method for measuring CMC values without the need for specialized equipment.

Results and Discussion

To test the feasibility of using DiO as a fluorogenic dye for CMC measurement, we first employed the widely used nonionic surfactant Triton X-100. As shown in Figure 3.2, increasing the surfactant concentration produces an increase in fluorescence intensity with a λ_{max} of 510 nm. This increase mirrors the change in fluorescence intensity observed when DiO is transferred from aqueous to organic solvent, strongly suggesting that DiO is being sequestered to

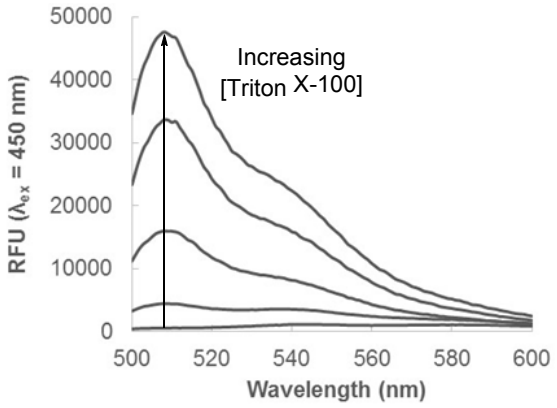

Figure 3.2. DiO shows increasing fluorescence intensity with increasing concentrations of Triton X-100 surfactant.

the hydrophobic core of the Triton X-100 micelles.

Having established that DiO displays a dramatic fluorescence enhancement in the presence of Triton X-100, we set out to evaluate the accuracy and versatility of DiO for CMC measurement. We selected a set of 12 commonly used surfactants that included examples from each of the four ionic states and spanned a wide range of CMC values. For each surfactant, we carried out parallel experiments using DiO and NR to compare the accuracy and consistency of each probe. We initially used a dye concentration of 2 μM, as this is typical for NR studies.[19] While this dye concentration provided accurate CMC values for most surfactants, we observed atypical results in some cases, and found that increasing the dye concentration to 10 μM produced consistent results for all surfactants. Thus, unless otherwise noted, all reported data were collected using DiO or NR concentrations of 10 μM. In CMC measurements using fluorogenic dyes, an incubation time is required to allow equilibration of the dyes binding in the micelles. We found that for all surfactants, accurate CMC values

could be measured after 5 hours of incubation, and for some surfactants, DiO provided accurate results with only 2 hours of incubation. This allows for fast screening of CMC values compared to some NR protocols that suggest overnight incubation.[25]

The λ_{max} values for DiO and NR show small variations based on surfactant structure, but at concentrations near or above the CMC of the surfactants, the emission maxima for DiO and NR were found to be centered upon 510 and 636 nm, respectively. Thus, these wavelengths were used in all CMC calculations. For each dye, plotting the fluorescence intensity as a function of surfactant concentration yields a sigmoidal curve, if a wide enough concentration range is used. In the region far below the CMC, fluorescence intensity is constant or increases slightly. Upon approaching the CMC, fluorescence intensity increases sharply as micelles form and sequester the dye molecules. Then, this trend levels off as all of the dye molecules become bound in micelles. Typically, the transition is sufficiently gradual to allow linear fits of the lower and middle regions of the sigmoid, and the intersection point of these two lines provides the CMC value (Figure 3.3a).[1,11] In some cases, the transition is too sharp to provide a linear fit for the transition region. In these cases, the entire curve can be fit to a sigmoid, and the CMC value calculated by finding the maximum of the second derivative. This value represents the lower transition point, which is analogous to the intersection of the two lines in the former approach (Figure 3.3b).

The data in Table 3.1 show the CMC values obtained using DiO and NR with each of the twelve surfactants tested. Both dyes show good accuracy, giving

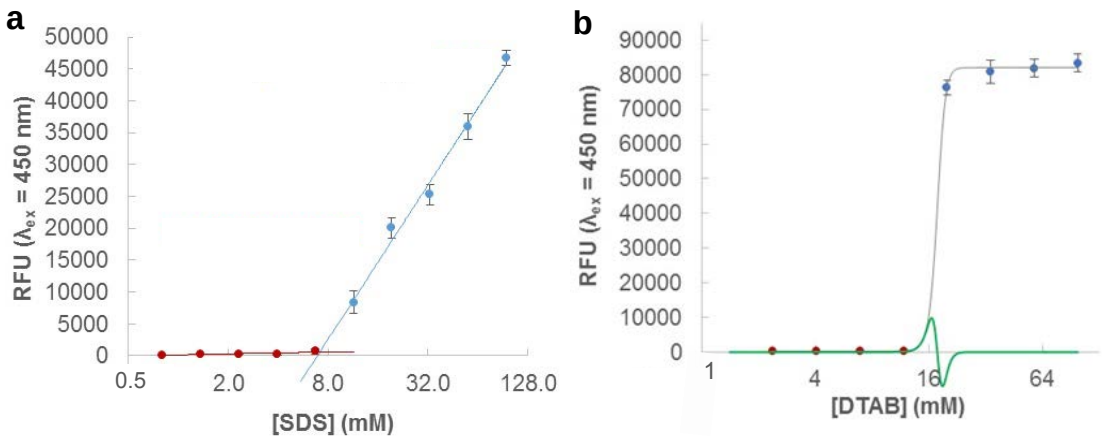

Figure 3.3. Representative fluorescence data for CMC calculation. (a) If three or more data points can be obtained for the transition region, the CMC value can be calculated using the two-line method. (b) If the slope of the transition region is too steep to enable a linear fit, the second derivative method is used.

CMC values comparable to those reported in the literature.[7,8,26-28] However, DiO provided overall greater precision, as some measurements using NR gave inconsistent data, leading to higher standard deviations. This is especially pronounced in the cases of Triton X-100, Brij 58, and Zwittergent 3-14. Figure 3.4 shows data collected for Triton X-100 using both DiO and NR. The first NR trial gave two distinct lines, while the subsequent two trials resulted in noisy data that were more difficult to fit. On the other hand, each of the three DiO trials provided consistent data. It is also important to note that in the case of DiO, the change in slope between the two lines is much greater than that observed for NR. This made the assignment of data points to their respective regions easier when working with DiO, further demonstrating its superior accuracy and precision.

We also found that DiO consistently provided usable data, whereas many trials using NR provided data that could not be used to calculate a CMC value (Figure 3.5). These failures on the part of NR are not directly reflected in the

Table 3.1. CMC values obtained at 25 ± 0.2 °C using DiO and Nile Red compared to those reported in the literature. Most CMC values were calculated using the two-line method. CMC values calculated using a sigmoidal fit are noted with an asterisk. The error represents the average of at least three trials.

†The CMC value for Tween20 was obtained using 1.25 μM NR.

Charge State	Surfactant	CMC (lit)	CMC (DiO)	CMC (NR)	Ref.
Nonionic	Triton X-100	240 μM	195 ± 2 μM	271 ± 19 μM	7, 25
	Tween 20	60-80 μM	66.5 ± 0.5 μM	79.9 ± 1.5† μM	7, 8, 25
	Tween 80	12 μM	13.0 ± 0.2 μM	11.4 ± 1.6 μM	7, 8, 25
	Brij 58	24-77 μM	32.4 ± 2.4 μM	36.7 ± 7.3 μM	8, 25
Anionic	SDS	8.2 mM	7.11 ± 0.77 mM	8.37 ± 0.45* mM	7
	NaGC	4-14 mM	14.2 ± 0.1 mM	9.12 ± 0.34 mM	24
	NaTC	6-11 mM	14.3 ± 0.5 mM	6.10 ± 0.18 mM	7, 23
Cationic	DTAB	14-16 mM	12.7± 0.8* mM	14.1 ± 1.0* mM	7
	CTAB	0.9-1.0 mM	2.65 ± 0.14 mM	0.780 ± 0.135* mM	7, 25
Zwitterionic	CHAPS	6-10 mM	8.25 ± 0.20 mM	8.46 ± 2.13 mM	7, 25
	EMPIGEN BB	1.6-2.1 mM	1.95 ± 0.04 mM	1.38 ± 0.07 mM	7
	Zwittergent 3-14	100-400 μM	268 ± 14 μM	259 ± 26 μM	25

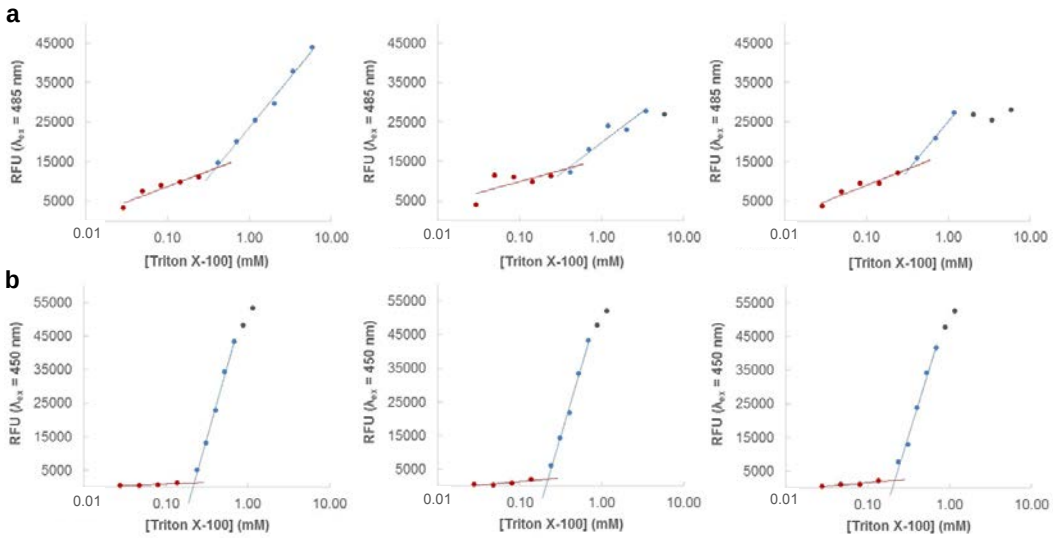

Figure 3.4. CMC curves collected for Triton X-100 using (a) NR and (b) DiO. DiO shows superior consistency as well as greater change in slope upon micelle formation.

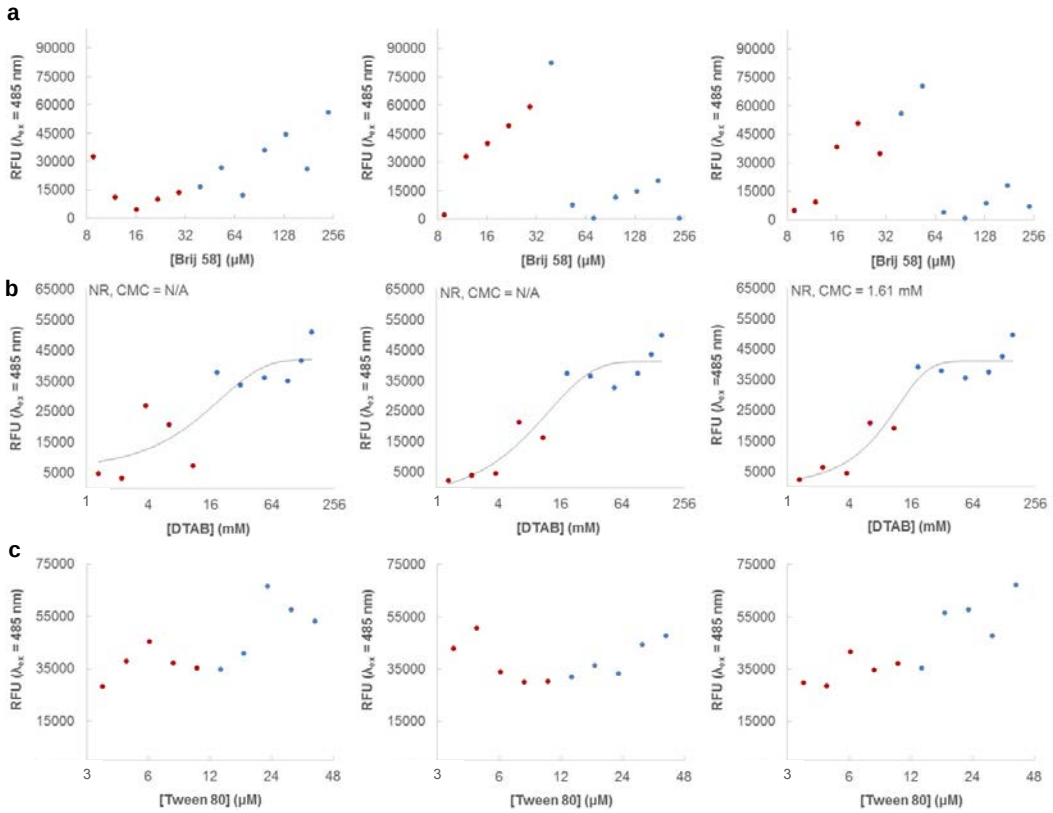

Figure 3.5. Examples of failed trials with NR: (a) Brij 58 (b) DTAB. The sigmoidal fit produced a CMC for one of the trials. (c) Tween 80. In each graph, the red and blue points represent concentrations below and above the literature CMC value, respectively.

data, as we repeated these experiments numerous times to obtain at least three usable data sets with NR that were then utilized to generate the CMC values reported in Table 3.1. This highlights the fact that CMC measurement using NR generally required greater time and resources compared to DiO, further convincing us of the superiority of DiO.

In addition to lower precision and success rate, we found that NR often showed a problematic shift in λ_{max} as a function of surfactant concentration, while the λ_{max} values for DiO remained consistent across surfactant concentrations. For example, in the case of NaGC, DiO maintains a λ_{max} value of 508-510 nm across all surfactant concentrations. In contrast, the λ_{max} for NR undergoes a gradual increase, followed by a sharp decrease, as surfactant concentration decreases (Table 3.2). While working with both of the dyes in our lab, we found that DiO consistently showed excellent solubility at 10 μM concentration, while NR often left a ring of dye adhered to the side of the microcentrifuge tube (Figure 3.6). This observation is worrisome, as it indicates that the actual concentration of NR in the solutions is not necessarily reproducible, which may be the source of many

Table 3.2. λ_{max} for DiO and NR emission in the presence of NaGC. White boxes indicate data above the CMC and shaded boxes indicate data below the CMC.

[NaGC] (mM)	DiO (nm)	NR (nm)
51.0	508	638
26.0	508	638
18.0	508	642
6.47	510	650
2.24	508	654
0.77	510	620

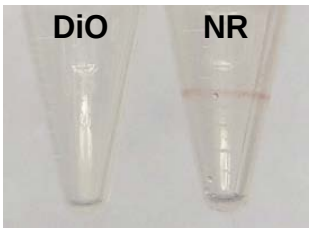

Figure 3.6. NR often left a visible ring of aggregated dye (right) while DiO did not (left).

of the issues discussed above. It also accounts for the inconsistencies observed in λ_{max} value, as the NR is likely aggregating in solution, leading to a change in local environment and thus emission wavelength.

Among the four classes of surfactants, we found that the cationic surfactants CTAB and DTAB proved to be the most challenging for measuring CMC values using either DiO or NR. Despite surveying very narrow intervals of surfactant concentration, we were typically unable to acquire a sufficient number of data points in the transition region to calculate CMC using the two-line method. Thus, in the analysis of DTAB using either DiO or NR and the analysis of CTAB using NR, we instead employed the second derivative method. Despite using a different analysis method, CMC values in line with reported values were still obtained (Table 3.1). In the case of CTAB analysis using DiO, we observed an interesting and reproducible peak in fluorescence intensity at approximately 0.6 μM surfactant (Figure 3.7a). While the source of this peak is unclear, we did observe the expected transition as surfactant concentration was increased, and were able to measure the CMC of CTAB by using data points at concentrations above this anomalous signal (Figure 3.7b). Our calculated CMC value using this

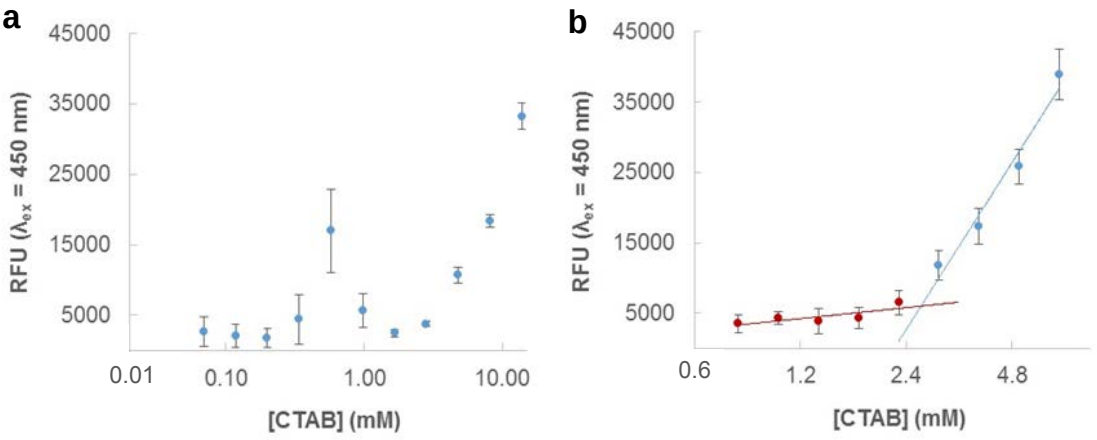

Figure 3.7. CMC measurements for CTAB (a) The emission intensity of DiO temporarily spikes at approximately 0.6 μM CTAB. (b) However, the CMC can be calculated for CTAB using a smaller concentration interval range.

method is slightly higher than the previously reported values, demonstrating that for this surfactant, NR does provide greater accuracy than DiO. However, it is important to note that cationic surfactants represent only about 5% of all commercially available surfactants,[29] and thus this limitation associated with DiO is relatively minor.

Conclusion

The data presented here demonstrate that DiO is a promising alternative to NR for the measurement of surfactant CMC values. We find that both DiO and NR provide CMC values that are consistent with those previously reported in the literature. However, DiO provides superior precision and reproducibility. We hypothesize that the inconsistency of results obtained using NR largely stems from its propensity to aggregate in aqueous solution, especially in the presence of low surfactant concentrations. In our hands, this led to difficulties in sample

handling as well as multiple instances of failed experiments. Thus, we find that DiO is generally a more user-friendly and reliable fluorogenic dye for the measurement of surfactant CMC values.

Experimental Section

All chemicals were purchased from commercial sources and used without further purification. NR and DiO stock solutions were prepared by dissolving the dye in DMSO to a concentration of 900 μM. Concentrated stock solutions of each surfactant were prepared in water (MilliQ), then combined with dye solution and additional water (MilliQ) to provide the appropriate final concentrations. The solutions were sonicated for 30 min at 35 °C then incubated at 25 °C for 5 hours. Following incubation, the solutions were transferred to a 96- or 384-well microplate, centrifuged, and allowed to equilibrate at 25 °C for 10 minutes.

All fluorescence measurements were carried out using a Biotek Synergy MX plate reader at 25 ± 0.5 ^{o}C. Excitation/emission wavelengths of 450/510 nm (DiO) and 485/636 nm (NR) were used, with a bandwidth of ±9 nm. Fluorescence intensity was plotted as a function of surfactant concentration, and each CMC value was calculated by one of two methods: (1) If the data formed two distinct lines, the concentration at which these lines intersect was calculated and determined to be the CMC. (2) If the transition was too sharp to provide a second intersecting line, the data were fit to a sigmoid function using Origin Pro 9.0. The second derivative was then used to determine the surfactant concentration at the lower inflection point, which is analogous to the intersection of the two lines, and thus represents the CMC.[1,30]

References

(1) Khan, A. M.; Shah, S. S. Determination of critical micelle concentration (CMC) of sodium dodecyl sulfate (SDS) and the effect of low concentration of pyrene on its CMC using origin software. *J. Chem. Soc. Pak.* **2008**, *30*, 186-191.

(2) Ding, J.; Chen, L.; Xiao, C.; Chen, L.; Zhuang, X.; Chen, X. Noncovalent interaction-assisted polymeric micelles for controlled drug delivery. *Chem. Comm.* **2014**, *50*, 11274-11290.

(3) Peterson, A. M.; Heemstra, J. M. Controlling self-assembly of DNA-polymer conjugates for applications in imaging and drug delivery. *WIREs Nanomed. Nanobiotechnol.* **2014**, 282-297.

(4) Paleologos, E. K.; Giokas, D. L.; Karayannis, M. I. Micelle-mediated separation and cloud-point extraction. *Trends Anal. Chem.* **2005**, *24*, 426-436.

(5) Moss, R. A.; Talkowski, C. J.; Reger, D. W.; Powell, C. E. Micellar control of stereochemistry and kinetics in the nitrous acid deamination reaction. *J. Am. Chem. Soc.* **1973**, *95*, 5215-5224.

(6) Turro, N. J.; Grätzel, M.; Braun, A. M. Photophysical and photochemical processes in micellar systems. *Angew. Chem. Int. Ed. Engl.* **1980**, *19*, 675-696.

(7) Neugebauer, J. M.: [18] Detergents: An overview. In *Methods in Enzymology*; Murray, P. D., Ed.; Academic Press, 1990; Vol. 182; pp 239-253.

(8) Suradkar, Y. R.; Bhagwat, S. S. CMC Determination of an Odd Carbon Chain Surfactant (C13E20) Mixed with Other Surfactants Using a Spectrophotometric Technique. *J. Chem. Eng. Data* **2006**, *51*, 2026-2031.

(9) Dominguez, A.; Fernandez, A.; Gonzalez, N.; Iglesias, E.; Montenegro, L. Determination of Critical Micelle Concentration of Some Surfactants by Three Techniques. *J. Chem. Educ.* **1997**, *74*, 1227-1231.

(10) Topel, Ö.; Çakır, B. A.; Budama, L.; Hoda, N. Determination of critical micelle concentration of polybutadiene-block-poly(ethyleneoxide) diblock copolymer by fluorescence spectroscopy and dynamic light scattering. *J. Mol. Liq.* **2013**, *177*, 40-43.

(11) Held, P.: *Rapid Critical Micelle Concentration (CMC) Determination Using Fluorescence Polarization*; Biotek Application Note, 2013.

(12) Cifuentes, A.; Bernal, J. L.; Diez-Masa, J. C. Determination of Critical Micelle Concentration Values Using Capillary Electrophoresis Instrumentation. *Anal. Chem.* **1997**, *69*, 4271-4274.

(13) Prazeres, T. J. V.; Beija, M.; Fernandes, F. V.; Marcelino, P. G. A.; Farinha, J. P. S.; Martinho, J. M. G. Determination of the critical micelle concentration of surfactants and amphiphilic block copolymers using coumarin 153. *Inorg. Chim. Acta* **2012**, *381*, 181-187.

(14) Mondal, S.; Ghosh, S. Role of curcumin on the determination of the critical micellar concentration by absorbance, fluorescence and fluorescence anisotropy techniques. *J. Photochem. Photobiol., B* **2012**, *115*, 9-15.

(15) Chattopadhyay, A.; London, E. Fluorimetric determination of critical micelle concentration avoiding interference from detergent charge. *Anal. Biochem.* **1984**, *139*, 408-412.

(16) Kalyanasundaram, K.; Thomas, J. K. Environmental effects on vibronic band intensities in pyrene monomer fluorescence and their application in studies of micellar systems. *J. Am. Chem. Soc.* **1977**, *99*, 2039-2044.

(17) Aguiar, J.; Carpena, P.; Molina-Bolívar, J. A.; Carnero Ruiz, C. On the determination of the critical micelle concentration by the pyrene 1:3 ratio method. *J. Colloid Interface Sci.* **2003**, *258*, 116-122.

(18) Deye, J. F.; Berger, T. A.; Anderson, A. G. Nile Red as a solvatochromic dye for measuring solvent strength in normal liquids and mixtures of normal liquids with supercritical and near critical fluids. *Anal. Chem.* **1990**, *62*, 615-622.

(19) Stuart, M. C. A.; van de Pas, J. C.; Engberts, J. B. F. N. The use of Nile Red to monitor the aggregation behavior in ternary surfactant–water–organic solvent systems. *J. Phys. Org. Chem.* **2005**, *18*, 929-934.

(20) Nizri, G.; Magdassi, S. Solubilization of hydrophobic molecules in nanoparticles formed by polymer–surfactant interactions. *J. Colloid Interface Sci.* **2005**, *291*, 169-174.

(21) Daban, J.-R.; Samsó, M.; Bartolomé, S. Use of Nile red as a fluorescent probe for the study of the hydrophobic properties of protein-sodium dodecyl sulfate complexes in solution. *Anal. Biochem.* **1991**, *199*, 162-168.

(22) Kurniasih, I. N.; Liang, H.; Mohr, P. C.; Khot, G.; Rabe, J. P.; Mohr, A. Nile Red Dye in Aqueous Surfactant and Micellar Solution. *Langmuir* **2015**, *31*, 2639-2648.

(23) Gan, W.-B.; Grutzendler, J.; Wong, W. T.; Wong, R. O. L.; Lichtman, J. W. Multicolor “DiOlistic” Labeling of the Nervous System Using Lipophilic Dye Combinations. *Neuron* **2000**, *27*, 219-225.

(24) Jiwpanich, S.; Ryu, J.-H.; Bickerton, S.; Thayumanavan, S. Non-covalent Encapsulation Stabilities in Supramolecular Nanoassemblies. *J. Am. Chem. Soc.* **2010**, *132*, 10683-10685.

(25) Goodling, K.; Johnson, K.; Lefkowitz, L.; Williams, B. W. The Modern Student Laboratory: Luminescent Characterization of Sodium Dodecyl Sulfate Micellar Solution Properties. *J. Chem. Educ.* **1994**, *71*, A8-A12.

(26) Meyerhoffer, S. M.; McGown, L. B. Critical micelle concentration behavior of sodium taurocholate in water. *Langmuir* **1990**, *6*, 187-191.

(27) Reis, S.; Moutinho, C. G.; Matos, C.; de Castro, B.; Gameiro, P.; Lima, J. L. F. C. Noninvasive methods to determine the critical micelle concentration of some bile acid salts. *Anal. Biochem.* **2004**, *334*, 117-126.

(28) Bhairi, S. M.; Mohan, C.: *Detergents: A guide to the properties and uses of detergents in biology and biochemistry*; EMD Biosciences, 2007.

(29) Hung, Y. T.; Wang, L. K.; Shammas, N. K.: *Handbook of Environment and Waste Management: Air and Water Pollution Control*; World Scientific, 2012.

(30) Pérez-Rodríguez, M.; Prieto, G.; Rega, C.; Varela, L. M.; Sarmiento, F.; Mosquera, V. A Comparative Study of the Determination of the Critical Micelle Concentration by Conductivity and Dielectric Constant Measurements. *Langmuir* **1998**, *14*, 4422-4426.

CHAPTER 4

MODULATING THE SUBSTRATE SELECTIVITY OF DNA APTAMERS USING SURFACTANTS*

Introduction

Nucleic acid aptamers[1-3] hold significant promise for replacing antibodies in analytical applications, as aptamers are capable of binding to a wide variety of small-molecule and protein targets.[4-8] The most commonly cited benefits of aptamers relative to antibodies include their ability to retain function after thermal denaturation and the fact that they are chemically synthesized, which reduces both cost and batch-to-batch variation.[8,9] We were curious as to whether aptamers might also have the advantage of functioning in the presence of chemical denaturants such as surfactants, but we found no reports in the literature exploring this intriguing question. Antibodies and other proteins are readily denatured by surfactants, as the hydrophobic portion of the surfactant can interact with hydrophobic surfaces on the protein, reducing the enthalpic cost of protein unfolding in an aqueous medium.[10] However, unlike proteins, nucleic acids do not pos-

---

* Reprinted with permission from Peterson, A. M.; Jahnke, F. M.; Heemstra, J. M. Modulating the Substrate Selectivity of DNA Aptamers Using Surfactants. *Langmuir.* 2015, 11769–11773. Copyright 2015 American Chemical Society

sess large surfaces composed of aliphatic side chains, and thus we hypothesized that they would be less likely to be disrupted by surfactants. In addition to exploring the ability of aptamers to function in the presence of surfactants, we envisioned that the surfactants could provide a unique dimension of control over the substrate binding preferences of aptamers. At low concentrations, amphiphilic surfactant molecules are dispersed in solution and form a monolayer at the air-water interface. However, at concentrations above the critical micelle concentration (CMC) of the surfactant, self-assembly occurs to form micelles.[11] These spherical or ellipsoidal structures possess a hydrophobic core that is capable of sequestering nonpolar molecules. As a result, surfactants are commonly used for applications such as purification and reaction catalysis.[12,13] In the context of aptamer-target binding, we hypothesized that analytes would show variable partitioning into the micelle core depending upon their hydrophobicity, effectively increasing the selectivity of aptamers toward hydrophilic analytes. Substrate binding selectivity is critical to many applications of aptamers, and previous studies have explored approaches to modulating selectivity through sequence mutation, the incorporation of unnatural bases, or the addition of hydrophobic groups near the binding pocket of the aptamer.[14-17] Due to the nature of these chemical modifications, they typically increase the binding affinity for hydrophobic targets. Thus, the use of surfactants offers a complementary approach to modulating the substrate binding selectivity of aptamers.

To explore the effect of surfactants on aptamer function and the substrate binding preference, we used a series of structure-switching DNA aptamer biosensors previously reported by Stojanovic and co-workers that bind to steroid

targets (Figure 4.1).[18] Each structure-switching biosensor is composed of an aptamer and a short complementary strand, which are functionalized with a fluorophore and quencher, respectively. In the absence of the target molecule, the complementary strand binds to the aptamer and fluorescence is quenched. However, in the presence of a target that binds to the aptamer, the complementary strand is displaced, resulting in a dose-dependent increase in fluorescence signal. Here we show that the aptamers maintain their secondary structure and substrate binding capability in the presence of neutral and anionic surfactants, and that the presence of surfactant can be used to modulate the substrate binding preference to favor more hydrophilic ligands (Figure 4.2). The demonstrated ability of aptamers to function in the presence of surfactants is anticipated to expand their scope of potential applications. Additionally, the ability to

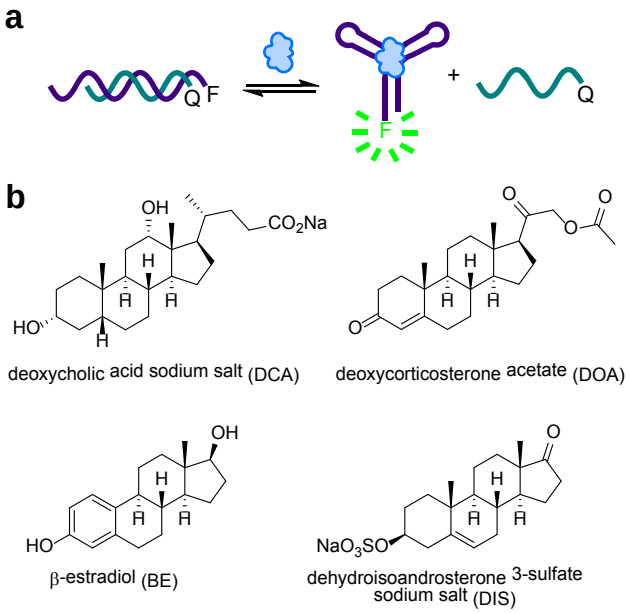

Figure 4.1. Experimental design for the steroid biosensors. (a) Structure-switching biosensors provide a dose-dependent fluorescence response to target analytes. (b) Chemical structures of steroid targets.

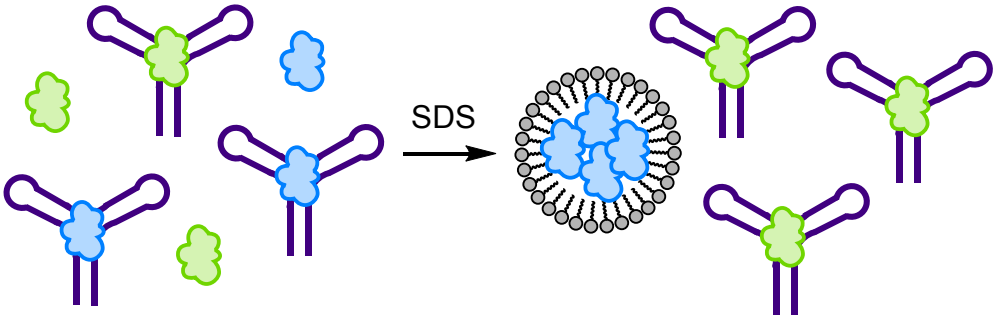

Figure 4.2. At surfactant concentrations above the CMC, the hydrophobic molecules are sequestered in the micelle. As a result, the biosensor selectively responds to the more hydrophilic molecules.

modulate the substrate binding preferences of aptamers using a simple additive provides a novel route to increasing the selectivity in analytical applications.

Results and Discussion

Choice of aptamer sequences

To investigate the effect of surfactants on aptamer-ligand recognition, we realized that it was necessary to use aptamers that bind to small-molecule, rather than protein, targets. This is because nearly all protein-binding aptamers have been selected to recognize folded proteins, and thus even if the aptamer retained its structure and function, the addition of surfactant would compromise the protein target in such a way as to preclude binding. We also strategically sought to utilize aptamers that had been reported in a structure-switching biosensor format,[19] as this enables convenient fluorescence-based monitoring of target binding. Thus, we chose three aptamer biosensors previously reported by Stojanovic and co-workers that bind to small-molecule steroid targets.[18] These aptamers were selected using the steroid targets DCA, DIS, and BE, and were

intentionally selected to have a broad substrate scope, with each aptamer sequence having an affinity for multiple steroid targets.

Exploring the effect of surfactant type

We chose the DIS aptamer as a model to survey the effect of varying surfactant types on substrate binding. Using five common surfactants that represent all four ionic states including cationic, anionic, nonionic, and zwitterionic, we measured the fluorescence response of the aptamer biosensor to DIS in the presence of 1% (w/v) of each surfactant. This concentration is above the CMC for each of the surfactants,[11] ensuring the formation of micelles. We were very encouraged to observe that in the presence of SDS, Tween 20, or Triton X-100, the biosensor shows only a slightly attenuated response compared to its behavior in pure buffer (Figure 4.3). However, the biosensor shows no detectible response in the presence of positively charged CTAB, and in zwitterionic CHAPS, the biosensor begins to show a response only at the highest DIS concentrations. This is not surprising, as surfactants having a positively charged functional group are more likely to interact with the negatively charged DNA backbone. In fact, a 2% CTAB solution is often used for DNA precipitation.[20] We decided to utilize SDS for all further studies, as the biosensor performed well in this surfactant, and SDS is frequently used for protein denaturation.

Structural analysis using CD spectroscopy

The ability of the DIS aptamer to bind its target molecule in the presence of 1% SDS suggests that this concentration of surfactant does not significantly

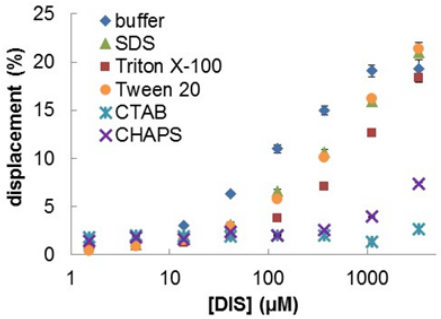

Figure 4.3. Response of the DIS biosensor to increasing concentrations of DIS ligand in the presence of 1% of various commonly used surfactants. The error bars represent the standard deviation of three independent trials.

disrupt DNA folding. To validate this idea and explore the tolerance of DNA folding to increased concentrations of SDS, we acquired CD spectra for each of the three aptamers in the presence of 0, 0.01, 1, and 4% SDS. These SDS concentrations were chosen as they allow a comparison of DNA secondary structure at SDS concentrations below (0 and 0.01%) and above (1 and 4%) the CMC. As a positive control to ensure that a change in the CD spectrum would be observed upon DNA unfolding, we also acquired spectra for each aptamer in the presence of 8 M urea, which is well established to denature the DNA secondary structure.[21]

As shown in Figure 4.4, the CD spectra for each aptamer remain constant as the SDS concentration is increased from 0 to 4%. However, in the presence of 8 M urea, the CD signal undergoes a noticeable bathochromic shift and a slight decrease in intensity. Together, these data suggest that the aptamers are able to maintain their secondary structure in the presence of up to 4% SDS, which is impressive given that this concentration of SDS leads to the denaturation of most

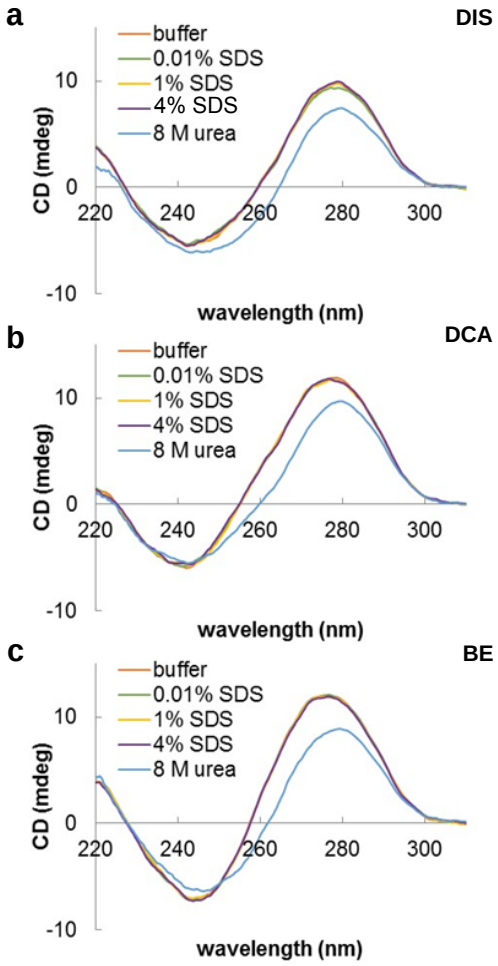

Figure 4.4. CD spectra for the (a) DIS, (b) BE, and (c) DCA aptamers in the presence of 0, 0.01, 1, and 4 % SDS, or 8 M urea.

proteins.[10] Additionally, we were encouraged by these results in which all three aptamers were likely to maintain their target-binding ability in the presence of up to 4% SDS.

Modulating target selectivity

To test our hypothesis that surfactant could be used to increase the selectivity for hydrophilic ligands, we investigated the response of the DIS

aptamer to both DIS and the more hydrophobic steroid, DOA (Table 4.1), in the presence of increasing concentrations of SDS (Figure 4.5). In buffer and 0.01% SDS, we observed that DOA binds to the DIS biosensor with a slightly higher affinity than the DIS ligand. In both of these solutions, the fluorescence signal from DOA unexpectedly decreases at high ligand concentrations, possibly due to aggregation of the hydrophobic steroid. Upon increasing the SDS concentration to 1 or 4%, we were excited to observe that the biosensor shows no response to even millimolar concentrations of DOA, but shows only a slightly attenuated binding to DIS. This switch in substrate binding preference presumably results from the sequestration of the hydrophobic DOA in the micelles, whereas the hydrophilic DIS remains solvated by the aqueous phase.

We also investigated the impact of increasing SDS concentration on the substrate specificity of the DCA and BE biosensors. As shown in Figure 4.6, the DCA biosensor binds DCA with a slightly higher affinity than it does DIS in buffer or 0.01% SDS. However, in the presence of micelles at 1 or 4% SDS, the binding to DCA is dramatically attenuated, switching the preferred ligand to DIS. We were initially surprised to observe such a dramatic reduction in DCA binding in the presence of micelles, as DCA has a charged carboxylate functional group, and thus would be expected to have some ability to remain solvated by the aqueous phase. However, DCA does possess an additional aliphatic chain relative to DIS, and the sulfate group of DIS contains a greater number of polar heteroatoms than the carboxylate of DCA. Thus, it is reasonable that the micelles sequester DCA, while leaving DIS free in solution.

In the case of the BE biosensor, the effect of SDS on substrate selectivity

Table 4.1. Partitioning coefficients (logD) estimated using the ChemAxon logD calculator. All values calculated for pH= 7.4.

Steroid	logD
DIS	1.04
DOA	3.77
DCA	1.15
BE	3.75

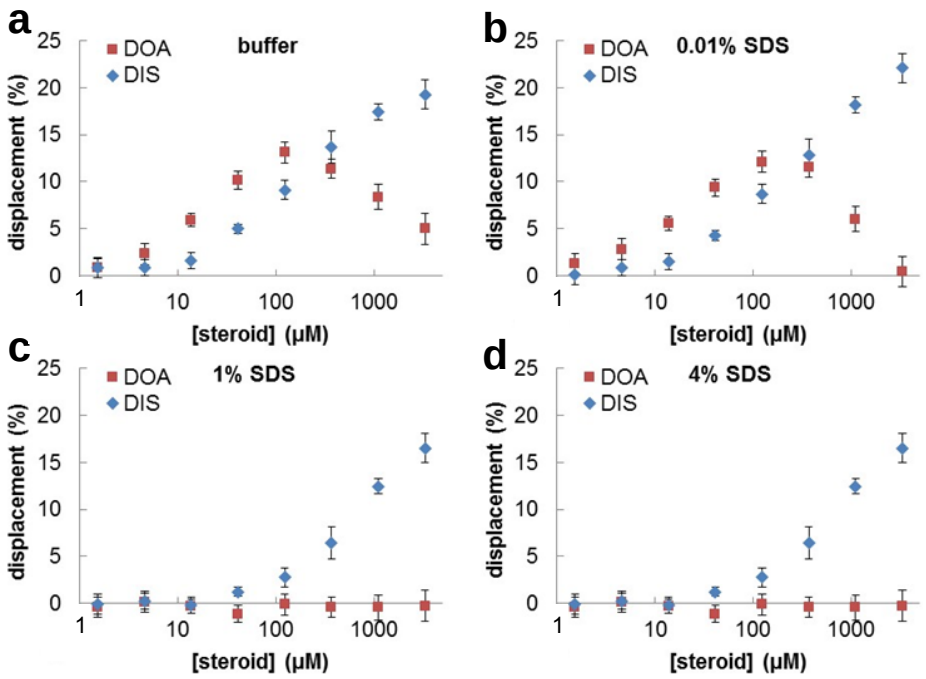

Figure 4.5. Fluorescence response of the DIS biosensor to DOA (red) or DIS (blue) in (a) buffer, (b) 0.01% SDS, (c) 1% SDS, and (d) 4% SDS. The error bars represent the standard deviation of three independent trials.

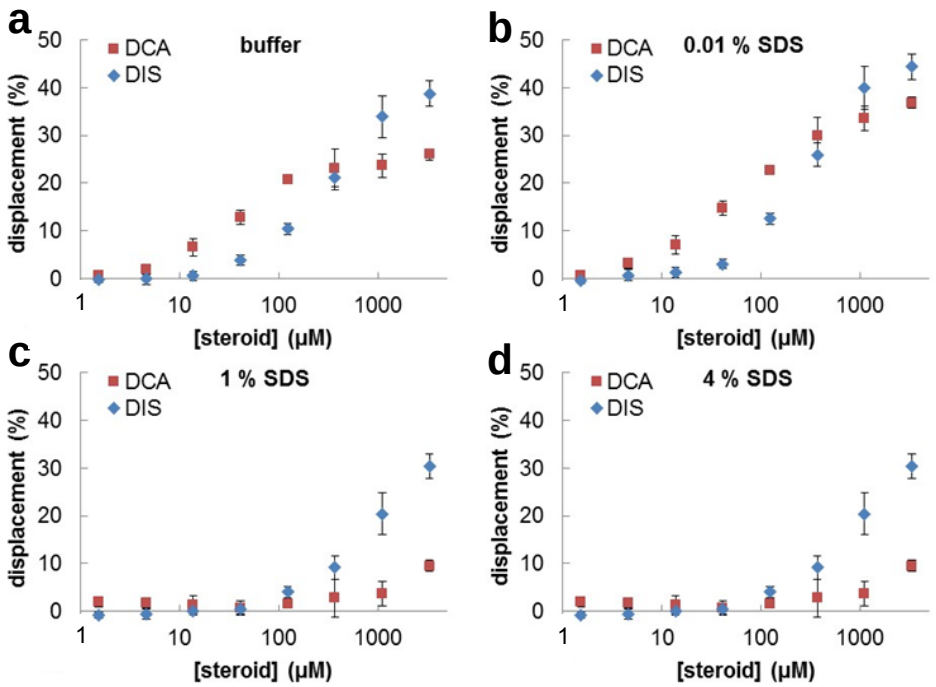

Figure 4.6. Fluorescence response of the DCA biosensor to DCA (red) or DIS (blue) in (a) buffer, (b) 0.01% SDS, (c) 1% SDS, and (d) 4% SDS. The error bars represent the standard deviation of three independent trials.

proved to be slightly more complex. At SDS concentrations below the CMC, the biosensor strongly favors BE, showing the highest affinity binding of all of the aptamer-ligand pairs (Figure 4.7 a,b). Above the CMC, the biosensor shows nearly equal binding to both DIS and BE (Figure 4.7 c,d). Increasing the concentration of SDS from 1 to 4% shows no appreciable effect on the binding, which is somewhat surprising, as we expected that BE would be strongly sequestered within the micelles due to its hydrophobicity. However, BE has been shown to bind to its cognate aptamer with a much higher affinity than any of the other aptamer-ligand pairs,[18] and the exchange of hydrophobic ligands between micelles is known to be a dynamic process.[22] Thus, we hypothesize that the anomalous behavior observed for BE reflects the ability of the aptamer to

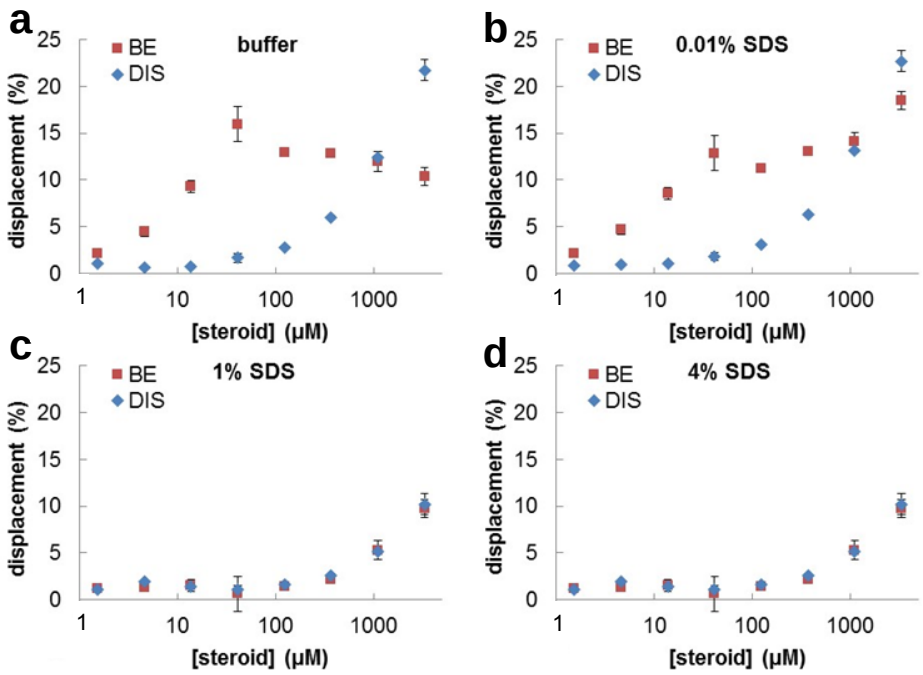

Figure 4.7. Fluorescence response of the BE biosensor to BE (red) or DIS (blue) in (a) buffer, (b) 0.01% SDS, (c) 1% SDS, and (d) 4% SDS. The error bars represent the standard deviation of three independent trials.

effectively compete with the micelles for binding to the BE that is transiently available in the solution. However, despite some unexpected results, we found that for each of the three biosensors, surfactant can be used to increase the relative affinity for hydrophilic over hydrophobic substrates.

Conclusions

Here we provide the first evidence that DNA aptamers can retain their secondary structure and substrate binding capability in the presence of up to 4% surfactant. We find that anionic and nonionic surfactants are well tolerated, whereas cationic and zwitterionic surfactants do compromise substrate binding, likely because the positively charged functional groups on the surfactant interact

with the negatively charged backbone of the DNA. However, SDS and Triton X-100 are among the most commonly used surfactants in biochemical applications, and SDS in particular is known to readily denature antibody reagents.[23] Thus, the ability of aptamers to maintain their function in the presence of both of these surfactants provides an additional competitive advantage relative to antibodies, and is likely to significantly increase the scope of analytical applications for which aptamers can be employed. We also investigated the hypothesis that surfactant micelles could be used to modulate the substrate binding preferences of aptamers by selectively encapsulating more hydrophobic ligands. For all three aptamers tested, we observe that the presence of SDS at concentrations above the CMC greatly diminishes or completely eliminates the biosensor response to the more hydrophobic substrate. However, the biosensor response to the hydrophilic substrate is only slightly attenuated. Thus, the studies reported here establish surfactant addition as a novel, facile, and effective method for increasing the substrate selectivity of DNA aptamers. We anticipate that this will enable the use of aptamers having nonideal substrate selectivity for analytical applications where minimizing the cross-reactivity is of critical importance.

Experimental Section

General methods

All DNA was purchased from the University of Utah DNA/Peptide Synthesis Core Facility, where it was synthesized using phosphoramidites and CPG cartridges from Glen Research (Table 4.2). All other materials were purchased from commercial suppliers and used without further purification.

Table 4.2. Sequences of DNA aptamers (Apt) and complementary strands (CS). FAM = fluorescein; BHQ1 = Black Hole quencher 1.

Name	Sequence (5'-3')
BE-Apt	FAM-CTCTCGGGACGACATGGATTTTCCATCAACGAAGTGCGTCCGTCCCG
BE-CS	GTCGTCCCGAGAG-BHQ1
DCA-Apt	FAM-CTCTCTCGGGACGCTGGGTTTTCCCAGGACGAAGTCCGTCCCGA
DCA-CS	CGTCCCGAGAGA-BHQ1
DIS-Apt	FAM-CTGCTCTCGGGACGTGGATTTTCCGCATACGAAGTTGTCCCGAG
DIS-CS	GTCCCGAGAGCA-BHQ1

Absorbance and fluorescence measurements were recorded using a Biotek Synergy Mx microplate reader.

Preparation of stock solutions

All samples were prepared in a buffer containing 20 mM Tris, and 150 mM NaCl, at pH 7.4. This salt concentration was chosen to avoid SDS precipitation. The aptamer and complementary strand were annealed by incubating at 90 °C for 5 min, followed by rapid cooling. The following DNA concentrations were used for each biosensor: DIS, 1 μM aptamer and 2 μM displacement strand; BE, 0.15 μM aptamer, and 0.30 μM displacement strand; DCA, 1 μM aptamer and 2 μM displacement strand. DNA structure-switching biosensors rely on competing equilibria to bind the aptamer to the displacement strand or the target. Thus, the DNA concentration impacts the response of the sensor to the target ligand. The DNA concentrations used in our experiments were chosen empirically to

maximize the signal-to-background ratio. Stock solutions of surfactants were prepared by dissolving sodium dodecyl sulfate (SDS), cetyltrimethylammonium bromide (CTAB), 3-[(3-cholamidopropyl)dimethylammonio]-1-propanesulfonate (CHAPS), Triton X-100, or Tween 20 in Tris buffer at 5 or 10% (w/v). Ligand solutions were prepared by dissolving each steroid in DMSO (DCA, BE, DIS) or 2:1 $CHCl_3$/DMSO (DOA) at 500 mM and then performing a 3-fold dilution series in DMSO to maintain the concentration of organic solvent in all samples constant at 2%.

Fluorescence measurements

For initial testing of the surfactant scope, solutions were prepared having 0 or 1% (w/v) surfactant. To monitor the effects of increasing SDS, solutions were prepared having 0, 0.01, 1, or 4% SDS. The DNA stock solution and surfactant were combined in Tris buffer and allowed to equilibrate for 5 min. The ligand was then added, and the solutions were incubated for 20 min at 25 °C. Fluorescence measurements were then acquired with λ_{ex} = 495 nm and λ_{em} = 525 nm at 25.0 ± 0.2 °C. The percent displacement (%D) for each biosensor was calculated using eq 1:

$$\%D = \left(\frac{F-F_0}{F_m-F_0}\right) * 100 \quad (1)$$

in which F is the measured fluorescence, F_0 is the fluorescence of the biosensor in the absence of ligand, and F_m is the fluorescence of the aptamer alone.[24]

Circular dichroism (CD) analysis

CD spectra were acquired using a Jasco J815 CD spectrometer. The CD spectra were collected using unlabeled aptamers (10 μM) prepared in Tris buffer containing 0, 0.01, 1, or 4% SDS. As a positive control for denaturation, we also acquired CD spectra for each aptamer in Tris buffer with 8 M urea. Following heating and cooling, the aptamer strands were incubated at 25 °C for 2 h. All CD spectra were recorded at 23 °C, scanning from 220 to 320 nm at 100 nm/min (cell path length = 2.00 mm). The final spectra are an average of six scans.

References

(1) Tuerk, C.; Gold, L. Systematic evolution of ligands by exponential enrichment: RNA ligands to bacteriophage T4 DNA polymerase. *Science* **1990**, *249*, 505-510.

(2) Robertson, D. L.; Joyce, G. F. Selection in vitro of an RNA enzyme that specifically cleaves single-stranded DNA. *Nature* **1990**, *344*, 467-468.

(3) Ellington, A. D.; Szostak, J. W. In vitro selection of RNA molecules that bind specific ligands. *Nature* **1990**, *346*, 818-822.

(4) O'Sullivan, C. K. Aptasensors--the future of biosensing? *Anal. Bioanal. Chem.* **2002**, *372*, 44-48.

(5) Famulok, M.; Hartig, J. S.; Mayer, G. Functional aptamers and aptazymes in biotechnology, diagnostics, and therapy. *Chem. Rev.* **2007**, *107*, 3715-3743.

(6) Cho, E. J.; Lee, J. W.; Ellington, A. D. Applications of aptamers as sensors. *Annu. Rev. Anal. Chem.* **2009**, *2*, 241-264.

(7) Mascini, M.; Palchetti, I.; Tombelli, S. Nucleic Acid and Peptide Aptamers: Fundamentals and Bioanalytical Aspects. *Angew. Chem. Int. Ed.* **2012**, *51*, 1316-1332.

(8) Liu, J.; Cao, Z.; Lu, Y. Functional nucleic acid sensors. *Chem. Rev.* **2009**, *109*, 1948-1998.

(9) Bradbury, A.; Pluckthun, A. Reproducibility: standardize antibodies used in research. *Nature* **2015**, *518*, 27-29.

(10) Otzen, D. Protein–surfactant interactions: A tale of many states. *BBA-Proteins Proteom.* **2011**, *1814*, 562-591.

(11) Neugebauer, J. M.: [18] Detergents: An overview. In *Methods in Enzymology*; Murray, P. D., Ed.; Academic Press, 1990; Vol. 182; pp 239-253.

(12) Fendler, J. H.; Fendler, E. J.: Chapter 7 - Micellar catalysis of miscellaneous ionic reactions. In *Catalysis in Micellar and Macromoleular Systems*; Academic Press, 1975; pp 230-253.

(13) Paleologos, E. K.; Giokas, D. L.; Karayannis, M. I. Micelle-mediated separation and cloud-point extraction. *Trends Anal. Chem.* **2005**, *24*, 426-436.

(14) Green, E.; Olah, M. J.; Abramova, T.; Williams, L. R.; Stefanovic, D.; Worgall, T.; Stojanovic, M. N. A rational approach to minimal high-resolution cross-reactive arrays. *J. Am. Chem. Soc.* **2006**, *128*, 15278-15282.

(15) Stojanović, M. N.; Green, E. G.; Semova, S.; Nikić, D. B.; Landry, D. W. Cross-reactive arrays based on three-way junctions. *J. Am. Chem. Soc.* **2003**, *125*, 6085-6089.

(16) Reinstein, O.; Neves, M. A.; Saad, M.; Boodram, S. N.; Lombardo, S.; Beckham, S. A.; Brouwer, J.; Audette, G. F.; Groves, P.; Wilce, M. C.; Johnson, P. E. Engineering a structure switching mechanism into a steroid-binding aptamer and hydrodynamic analysis of the ligand binding mechanism. *Biochemistry* **2011**, *50*, 9368-9376.

(17) Gold, L.; Ayers, D.; Bertino, J.; Bock, C.; Bock, A.; Brody, E. N.; Carter, J.; Dalby, A. B.; Eaton, B. E.; Fitzwater, T.; Flather, D.; Forbes, A.; Foreman, T.; Fowler, C.; Gawande, B.; Goss, M.; Gunn, M.; Gupta, S.; Halladay, D.; Heil, J.; Heilig, J.; Hicke, B.; Husar, G.; Janjic, N.; Jarvis, T.; Jennings, S.; Katilius, E.; Keeney, T. R.; Kim, N.; Koch, T. H.; Kraemer, S.; Kroiss, L.; Le, N.; Levine, D.; Lindsey, W.; Lollo, B.; Mayfield, W.; Mehan, M.; Mehler, R.; Nelson, S. K.; Nelson, M.; Nieuwlandt, D.; Nikrad, M.; Ochsner, U.; Ostroff, R. M.; Otis, M.; Parker, T.; Pietrasiewicz, S.; Resnicow, D. I.; Rohloff, J.; Sanders, G.; Sattin, S.; Schneider, D.; Singer, B.; Stanton, M.; Sterkel, A.; Stewart, A.; Stratford, S.; Vaught, J. D.; Vrkljan, M.; Walker, J. J.; Watrobka, M.; Waugh, S.; Weiss, A.; Wilcox, S. K.; Wolfson, A.; Wolk, S. K.; Zhang, C.; Zichi, D. Aptamer-based multiplexed proteomic technology for biomarker discovery. *PLoS ONE* **2010**, *5*, e15004.

(18) Yang, K.-A.; Pei, R.; Stefanovic, D.; Stojanovic, M. N. Optimizing cross-reactivity with evolutionary search for sensors. *J. Am. Chem. Soc.* **2012**, *134*, 1642-1647.

(19) Nutiu, R.; Li, Y. Structure-switching signaling aptamers. *J. Am. Chem. Soc* **2003**, *125*, 4771-4778.

(20) Del Sal, G.; Manfioletti, G.; Schneider, C. The CTAB-DNA precipitation method: a common mini-scale preparation of template DNA from phagemids, phages or plasmids suitable for sequencing. *Biotechniques* **1989**, *7*, 514-520.

(21) Albright, L. M.; Slatko, B. E. Denaturing polyacrylamide gel electrophoresis. *Curr. Protoc. Nucleic Acid Chem.* **2001**, Appendix 3.

(22) Jiwpanich, S.; Ryu, J.-H.; Bickerton, S.; Thayumanavan, S. Non-covalent encapsulation stabilities in supramolecular nanoassemblies. *J. Am. Chem. Soc.* **2010**, *132*, 10683-10685.

(23) Brown, D.; Lydon, J.; McLaughlin, M.; Stuart-Tilley, A.; Tyszkowski, R.; Alper, S. Antigen retrieval in cryostat tissue sections and cultured cells by treatment with sodium dodecyl sulfate (SDS). *Histochem. Cell Biol.* **1996**, *105*, 261-267.

(24) Feagin, T. A.; Olsen, D. P. V.; Headman, Z. C.; Heemstra, J. M. High-throughput enantiopurity analysis using enantiomeric dna-based sensors. *J. Am. Chem. Soc.* **2015**, *137*, 4198-4206.

CHAPTER 5

miRNA-221 DETECTION USING PNA-DNA-AuNP CONJUGATES

Introduction

Prostate cancer is a serious disease which accounts for approximately 3% of male deaths in the United States; however, nearly half of prostate cancer tumors pose little to no health threat if left untreated.[1] Consequently, many patients are overtreated, leaving them with unnecessary side effects in surrounding organs such as the colon and bladder. Since the risks of prostate cancer can vary so widely, the ability to properly diagnose and treat patients depends greatly on the ability to distinguish between aggressive and indolent prostate cancer. However, current methods for analysis are invasive, often requiring a transrectal biopsy.[2] Developing a noninvasive screening procedure would greatly aid in the diagnosis of aggressive cancers and help prevent the overtreatment of prostate cancer.

Accurate diagnosis for this and any other diseases requires the identification of a proper biomarker. Nucleic acids are excellent biomarkers for detecting gene-related diseases such as cancer due to the specificity of Watson-Crick base-pairing. Many studies have looked specifically at miRNA since these small

noncoding RNA sequences control gene expression and are misregulated in most cancers. In searching for prostate cancer biomarkers, researchers found that aggressive forms of prostate cancer have a 10-fold increase in the expression of miRNA-221 compared to the indolent forms, making it a good indicator for the aggressiveness of the tumor.[3,4]

While native nucleic acids such as DNA and RNA bind specific miRNA sequences, they risk degradation in the body. Therefore, many labs have employed nucleic acid mimics to increase oligonucleotide stability. Peptide nucleic acid (PNA) is one such mimic where, in place of the negatively charged phosphate groups, there is a neutral peptide-like aminoethylglycine backbone (Figure 5.1).[5] Due to this unique architecture, PNA is resistant to both proteases and nucleases.[6] Further, PNA is capable of forming Watson-Crick base pairs with native nucleic acids at greater stabilities than a native duplex. Due to its increased stability, PNA shows great promise in medicinal applications targeting a specific genetic sequence. However, it faces challenges for use within the body, as it has low cell permeability and rapid clearance through the kidneys. In mouse studies, intravenously delivered PNA was removed from circulation within half an hour.[7]

As native nucleic acids face similar challenges, many transfection agents have been developed to prevent renal clearance and enable cellular delivery. The Mirkin group has shown that gold nanoparticles (AuNPs) effectively deliver nucleic acids into cells when functionalized with thiolated DNA due to the high negative charge density. This charge density recruits positively charged chaperone proteins, which assist the DNA-AuNPs across the cell membrane.[8] Additionally, due to their increased size, AuNPs avoid removal by the kidneys, and the

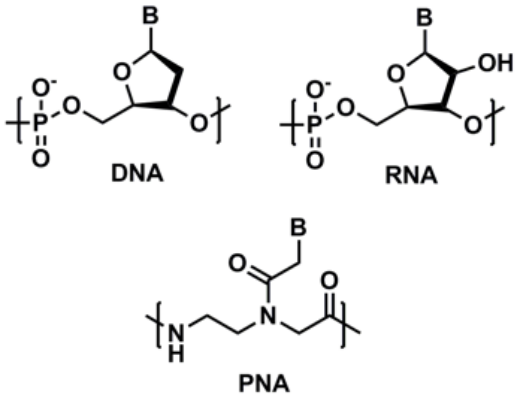

Figure 5.1. The chemical structures of DNA, RNA, and PNA

plasmonic properties efficiently quench fluorescence near the surface.[9] In one study, Mirkin and coworkers used fluorophore-labeled DNA to detect the mRNA sequence SKBR3. Compared to control cells, they measured a 3.8-fold fluorescence increase in cells containing SKBR3.[10]

While the Mirkin group found that the DNA-AuNP conjugates partially protect DNA from nucleases, degradation still occurs, limiting the detection accuracy. We hypothesize that, due to the resistance to degradation and higher target specificity of PNA, PNA-DNA-AuNP conjugates would achieve better efficiency and sequence flexibility than DNA-AuNPs for intracellular targeting. Due to their high surface area-to-volume ratio, nanoparticles inherently have high surface energies, which cause particle agglomeration. This is often prevented by placing charged molecules on the nanoparticle surface to cause repulsion. In the case of DNA-AuNPs, DNA provides the necessary repulsive forces to maintain monodispersity. However, since PNA has a neutral backbone, it does not create the repulsive forces necessary to maintain monodispersity when functionalized to AuNPs. Other studies use surfactants for PNA-AuNP stabilization, but these

cannot be used for biological purposes due to surfactant toxicity.[11] Also, the lack of a high negative charge density would prevent the particles from recruiting the proteins necessary for cell permeability. We hypothesize that DNA can be used to circumvent these challenges if the AuNP surface is covalently functionalized with DNA possessing a terminal thiol. Fluorophore-modified PNA can then be hybridized to the DNA-AuNP conjugates, resulting in attenuation of the signal due to quenching. Due to a toe-hold region on the PNA, the PNA will leave the DNA-AuNPs and hybridize the RNA target due to the increased number of base pairs, consequently restoring fluorescence in a dose-dependent manner (Figure 5.2).

We anticipate that by using a fluorescent PNA-DNA-AuNP detection platform, aggressive and indolent prostate cancers can be distinguished as a function of cellular miRNA-221 levels. We will target miRNA-221 using complementary fluorescently-labeled PNA hybridized to DNA-AuNP conjugates, wherein the AuNPs will quench the fluorescence until the PNA leaves in the presence of

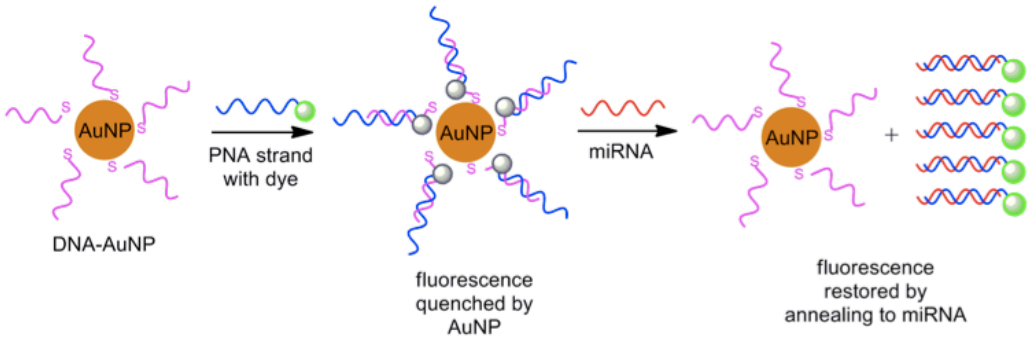

Figure 5.2. Thiolated DNA bonded to a gold nanoparticle then hybridized to a fluorophore-labeled PNA strand quenching fluorescence. Upon miRNA-221 addition, the PNA rehybridizes to the RNA and leaves the AuNP, restoring fluorescence.

miRNA-221. This study aimed to develop and characterize a PNA-DNA-AuNP detection platform, determine its ability to quantify miRNA-221, and perform initial studies into the cellular permeability of PNA-DNA-AuNP conjugates.

Results and Discussion

PNA-DNA-AuNP conjugates

As we started designing and characterizing our initial detection platform, we wanted to verify that PNA without a toehold region would not cause agglomeration by shielding the repulsive forces. We initially used the Nielsen 10-mer sequence of PNA (Table 5.1, PNA 5.1) since it has been well studied in previous research.[5] As is customary with PNA studies, a positively charged lysine monomer was added to the C-terminus in order to facilitate water solubility. While many of the properties have been optimized for DNA-AuNP systems, we tested some to verify if the same trends remain when PNA is hybridized to the conjugates. These properties include the number of bases between the AuNP and the hybridization region (spacer), the method for attaching the thiolated DNA, and the hybridization technique.[12-14] In order to test the spacer length required for maximum PNA hybridization, we tested DNA 5.1.NS with no spacer between the thiol and hybridization region, and two spacer types, poly(A) and poly(T) with 5 and 10 bases (DNA 5.1.A5, A10, T5, and T10). Similar to studies using DNA-DNA duplexes, the 10 base spacers gave the best hybridization, with T10 giving better hybridization than A (Table 5.2). Thus the studies described below all use a poly$(T)_{10}$ spacer.

AuNPs have unique optical properties that make it easy to detect agglome-

Table 5.1. DNA sequences used during the AuNP studies. The orange region shows the PNA-DNA hybridization region. For the miRNA-221 sequence, the blue region shows the binding footprint of PNA 5.2 to miRNA-221 and the underlined portion is the hybridization region for PNA 5.3.

Name	Sequence (5'-3')
DNA 5.1.NS	$^{5'}$-AGT GAT CTA C-S-$^{3'}$
DNA 5.1.A5	$^{5'}$-AGT GAT CTA CAA AAA-S-$^{3'}$
DNA 5.1.A10	$^{5'}$-AGT GAT CTA CAA AAA AAA AA-S-$^{3'}$
DNA 5.1.T5	$^{5'}$-AGT GAT CTA CTT TTT-S-$^{3'}$
DNA 5.1.T10	$^{5'}$-AGT GAT CTA CTT TTT TTT TT-S-$^{3'}$
PNA 5.1	^{C}-Lys^{+} TCA CTA GAT G-^{N}
DNA 5.2	$^{5'}$- TTG TCT GCT TTT TTT TTT-S-$^{3'}$
PNA 5.2	^{C}-Lys^{+} CGA TGT AAC AGA CGcf-^{N}
miRNA-221	$^{5'}$-A GCU ACA UUG UCU GCU GGG UUU C-$^{3'}$
DNA 5.3	$^{5'}$- CA TTG TCT GCT TTT TTT TTT-S-$^{3'}$
PNA 5.3	^{C}-Asp^{-} A TGT AAC AGA CGcf-^{N}

Table 5.2. The fluorescence increase upon addition of miRNA-221 to PNA-DNA-AuNP conjugates containing an A10 or T10 spacer.

[miRNA-221] (μM)	A10	T10
60	3.72	4.21
47	3.48	3.95
43	3.25	3.71
36	2.70	3.15
20	2.05	2.88
30	0.56	1.51

ration. Due to their plasmonic properties, 12 nm AuNPs are red and have a sharp extinction peak around 520 nm when they are monodisperse in solution. As the particles agglomerate, this peak broadens, the λ_{max} redshifts, and the solution becomes purple, eventually turning blue. While different approaches were employed for functionalization and hybridization, the results from each method were similar. During each step of the functionalization we monitored for agglomeration using UV analysis. As shown in Figure 5.3, after DNA functionalization the λ_{max} shifts only slightly while retaining its sharp peak. Upon PNA addition, λ_{max} remains the same, showing that the repulsive forces from the DNA are sufficient to stabilize the AuNPs despite the neutral charge shielding and positive charge due to Lys^{+}-PNA addition.

Next, we wanted to verify the functionality of the conjugates and ensure that the PNA was still able to leave the DNA-AuNPs. We did this using melting

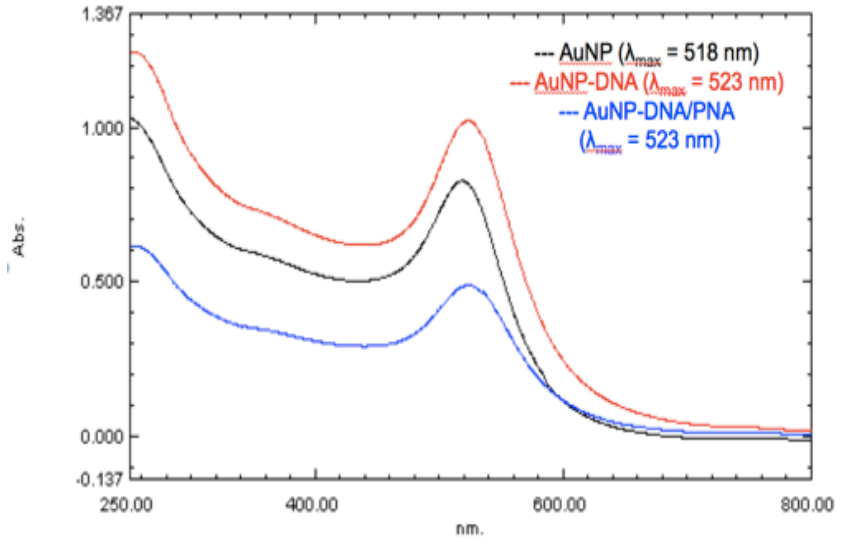

Figure 5.3. UV scans of AuNPs at various stages of functionalization. Black is citrate-AuNPs, red is DNA-AuNPs, and blue is PNA-DNA-AuNPs. The sharp peak and λ_{max} show that agglomeration did not occur.

behavior. The melting temperature was measured for both the free PNA-DNA duplex and the PNA-DNA-AuNP conjugates. The absorbance was graphed as a function of temperature and fit to a sigmoidal function using Origin 8.5.1 (Figure 5.4). The melting temperature was then calculated by using the first derivative to find the inflection point of the sigmoid. For our PNA-DNA-AuNP conjugates, the melting temperature was determined to be 44 ± 2 °C compared to the free duplex, which was measured at 50.3 ± 0.4 °C. Interestingly, this trend is the opposite of what is observed in DNA-AuNP studies. However, like DNA-AuNPs, the transition of the AuNP conjugates was sharper than the free duplex, suggesting cooperativity in the hybridization event.[15] The duplex dissociation demonstrates that the PNA can reversibly hybridize to the DNA-AuNPs.

miRNA-221 detection studies

After demonstrating that PNA successfully hybridizes to DNA-AuNPs without causing agglomeration, we moved forward to develop a conjugate using the miRNA-221 target, we extended PNA 5.2 beyond the DNA 5.2 terminus to give a toehold region for the miRNA (Table 5.1). As we knew nothing of the displacement kinetics or tolerance for the hydrophobic region, the initial length was experimental. The PNA was fluorescently labeled using carboxyfluorescein, which is quenched upon hybridization to the DNA-AuNPs. In these experiments, we used the “fast” salt method described by Mirkin and coworkers to functionalize the AuNPs with DNA.[13] Following DNA functionalization, PNA was hybridized to the conjugates. Unlike the previous study, PNA hybridization induced agglomeration, as demonstrated by the solution turning purple. The agglomeration was confirm-

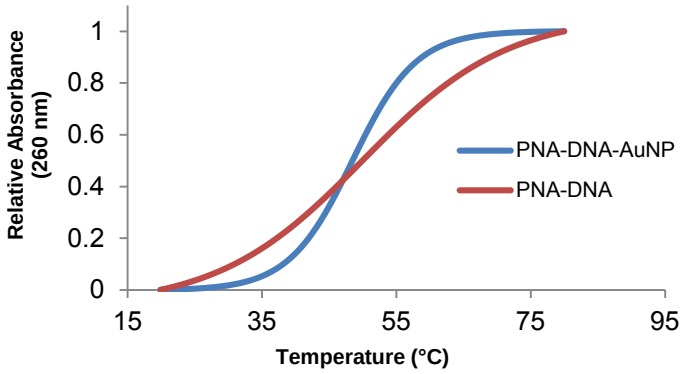

Figure 5.4. Melting curve for PNA-DNA-AuNPs and a PNA-DNA duplex. The inflection point represents the melting point.

ed using Dynamic Light Scattering (DLS), which showed a large population of agglomerates having hydrodynamic diameter around 150 nm (Figure 5.5).

We decided to proceed with the miRNA-221 addition to see if it could remove the PNA from the DNA-AuNPs, and if doing so would reverse agglomeration of the particles. (Figure 5.6). While we saw an increase in fluorescence, it did not correlate with the quantity of added miRNA-221. This is likely due to the agglomeration of the particles, which creates a heterogeneous solution. Additionally, rather than a smooth displacement, they showed a slower initial rate followed by a more rapid release. The change in rate likely occurs as the particles begin to separate, and all the PNA can be released from inside the agglomerated particles. Additionally, following the PNA displacement, the AuNPs returned to a red color, confirming that the agglomeration was due to the presence of the PNA on the particles.

After reflecting on these results, we determined that two factors likely caused the agglomeration upon PNA addition. First, we followed standard proto-

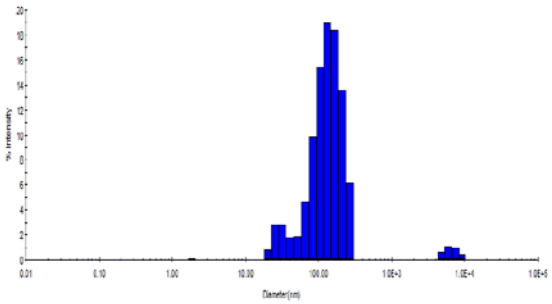

Figure 5.5. DLS of PNA-DNA-AuNP complex showing particle agglomeration.

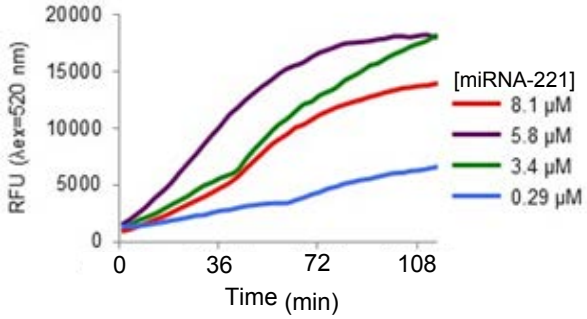

Figure 5.6. Fluorescence monitoring upon addition of miRNA-221 to PNA-DNA-AuNPs. The fluorescence increases as the PNA is displaced from the AuNPs.

col and synthesized the PNA with a positively charged lysine residue to enhance its solubility. Following PNA hybridization, the positive charge is on the outermost portion of the conjugate, allowing the lysine to interact with the negatively charged DNA on other particles. Also, as anticipated when developing our preliminary study, the toehold region extends the neutral PNA beyond the DNA shell. The neutral PNA can then form hydrophobic interactions with PNA on other particles. Our preliminary results show that PNA release occurred within a clinically desirable timeframe and could even be slowed without losing applicability. Rather than verifying if the agglomeration was due to one or both factors, we decided to reduce the toehold region and change to a negatively charged amino acid. In order to shorten the toehold, we removed some of the overhanging PNA bases and extended the DNA hybridization region, thus increasing the negative charge surrounding the particles. We also changed our amino acid from positively charged lysine to negatively charged aspartic acid, yielding strands PNA 5.3 and DNA 5.3 (Table 5.1).

Following functionalization and hybridization as previously described, DLS showed that the particles remained separate with a narrow size distribution (Figure 5.7). Since the particles had a good distribution after DNA functionalization and PNA hybridization, we were able to compare the sizes throughout the process. As expected, the hydrodynamic radius became larger with each step. The citrate-capped AuNPs have the smallest hydrodynamic radius at 18.5 ± 0.4 nm. Upon DNA functionalization, the size increases to 26 ± 1 nm, then 29 ± 1 nm following PNA hybridization. Again, the particles displayed a sharp melting point transition with a melting point of 42.1± 0.9 °C. This is above body temperature,

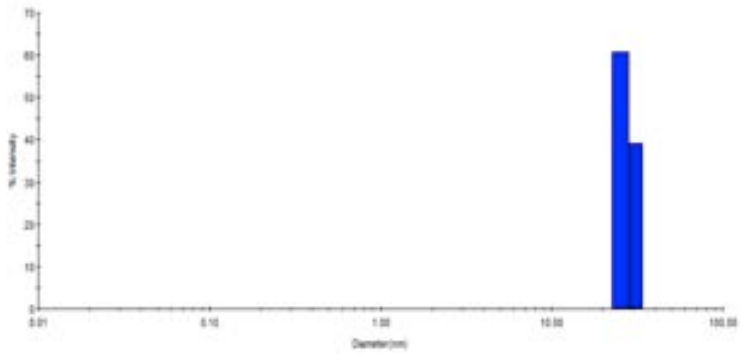

Figure 5.7. DLS data for the PNA-DNA-AuNPs after changing to aspartic acid and shortening the overhang region

so the PNA will remain on the nanoparticle in physiological conditions.

Since our particles were stable with the new DNA and PNA strands, we tested their ability to give consistent, dose-dependent fluorescence upon miRNA-221 addition. Following optimization, we were able to generate displacement curves that showed a good, logarithmic trend for both the increase after 20 min and the initial slope of the displacement (Figure 5.8).

Cell permeability study

Next, we wanted to test the ability of the nanoparticles to enter cells. We chose HeLa cells as our initial model since they are widely studied. Table 5.3 shows the raw data as well as the calculated number of particles per cell. As shown, it is likely that the DNA-AuNPs and DNA-PNA-AuNPs are able to enter HeLa cells without killing the cells. Further testing is needed to verify this conclusion. Once it is verified that the AuNP conjugates are able to enter HeLa cells, permeability studies will also be performed using prostate cancer cell lines.

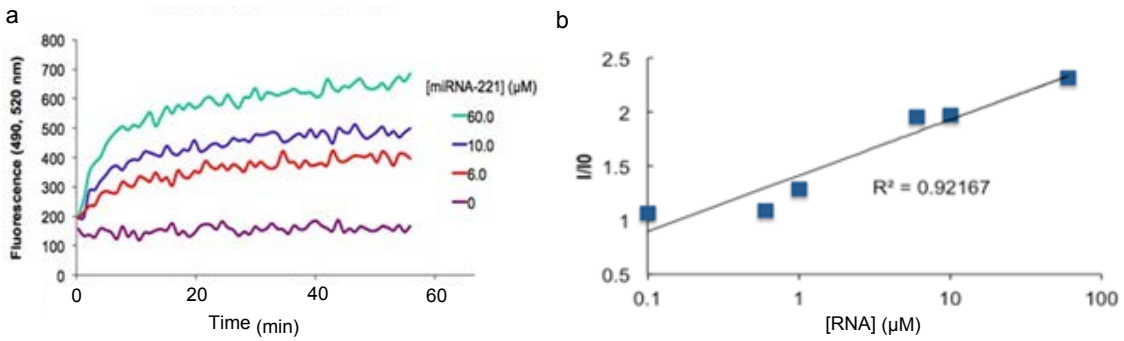

Figure 5.8. Dose-dependent PNA displacement with miRNA-221 addition. (a) Displacement curves of the modified PNA-DNA-AuNP conjugates (b) Fluorescence increase 20 min after miRNA-221 addition.

Table 5.3. The cell count and viability, gold found in the cells, and the calculated particles per cell. The PNA samples are two different PNA hybridization methods.

		Cells/mL	Viability	Au (ng)	Particles /Cell
Cells without AuNPs		4.02E+05	97	<0.1	-
		4.05E+05	96	<0.1	-
5 nM	DNA-AuNPs	2.25E+05	95	21.8	5.63E+11
10nM		2.21E+05	84	51.6	1.35E+12
5 nM	PNA-DNA-AuNPs 1	2.38E+05	89	7.0	1.70E+11
10nM		2.43E+05	71	11.7	2.79E+11
5 nM	PNA-DNA-AuNPs 2	2.40E+05	90	4.7	1.14E+11
10nM		2.61E+05	90	26.1	5.81E+11

Conclusions

By using negatively charged DNA as the repulsive force in AuNP conjugates, PNA can successfully hybridize to DNA-AuNPs without causing agglomeration. However, the electrostatics of the PNA also play a key role in maintaining particle dispersity. When designed with a toehold region, the length of the overhang region and the amino acid chosen for water solubility both affect particle stability and dispersity. Detection with this AuNP conjugate system is achieved using fluorescently labeled PNA where the fluorescence is quenched when hybridized to DNA-AuNPs. Signal can be subsequently restored upon PNA dissociation from the AuNPs during rehybridization to the target miRNA. In the presence of miRNA-221, the fluorescence increases in a dose-dependent manner and can therefore be used for measuring miRNA-221 concentration. Toward the goal of studying miRNA-221 levels in cells, preliminary studies suggest that PNA-DNA-AuNPs can enter HeLa cells. These results show potential for fluorescently detecting aggressive prostate cancer *in vivo*.

Experimental Section

General methods

For the studies reported here, we used 12 nm citrate-stabilized AuNPs from nanoComposix. DNA was purchased from the core facility at the University of Utah (Table 5.1). All absorbance and fluorescence readings were recorded using a Biotek Synergy Mx plate reader. All studies were done in phosphate-buffered saline (PBS) (pH = 7.2)

PNA synthesis

PNA was synthesized according to literature methods in a manual vessel or using a semiautomated Activotec P-14 Peptide Synthesizer.[16] The oligomers were synthesized using solid phase synthesis on TGR R resin (0.2 mmol/g). Following synthesis, the PNA was cleaved using TFA:triisopropylsilane:H2O (95:2.5:2.5) and precipitated using diethyl ether. Purification was carried out using RP-HPLC (Agilent ZORBAX 300SB-C18, 5 μM particle size, 9.4×250 mm) and analyzed using MALDI-TOF mass spectrometry (Waters Micromass MALDI Micro MX). [17] The samples were lyophilized and resuspended in MilliQ water prior to use. All experiments were performed in PBS (pH = 7) unless otherwise noted.

AuNP conjugate preparation

The thiol group on the DNA was activated by suspending the DNA in 0.1 M DTT in 0.18 M phosphate buffer (pH = 8.0). It was then allowed to incubate for 1 h at room temperature. The DNA was purified using a NAP-5 column and lyophilized. The DNA was then resuspended in MilliQ water. The DNA-AuNP conjugates were prepared using literature methods.[13] Briefly, DNA was incubated with AuNPs (1 OD DNA/1 mL AuNP) in 0.1 M phosphate buffer (pH = 8.0) and 0.01% SDS. The solution was sonicated for 10 s and allowed to incubate at room temperature for 20 min. NaCl solution was then increased to 0.1 M in 0.05 M then to 1 M in 0.1 increments, sonicating and incubating each time. Following the last addition, the particles were incubated at room temperature overnight. The particles washed by centrifuging at 4 °C at 13,000 rpm, removing the supernatant and resuspending in PBS. This was repeated three times.

After washing the particles, the PNA complement was hybridized to the DNA by adding PNA to the DNA-AuNPs (1 OD PNA/500 µL AuNP) and incubated overnight at room temperature. The particles were again washed via centrifugation until the supernatant was no longer fluorescent. All concentrated conjugates were stored at 4 °C until use and were resuspended prior to use.

Melting temperature analysis

Melting temperatures were acquired with a Shimadzu UV-1800 instrument with temperature control and a 10 mm path length. UV-Vis absorbance was recorded at 260 and 520 nm using the absorbance at 380 nm as a correction factor. The melting temperature was measured for both the PNA-DNA-AuNP conjugates and a free PNA-DNA duplex. The samples were heated at a rate of 1 °C/min from 20-80 °C. The samples were shaken every 5 minutes, and the data were recorded every 1 °C. Origin 8.5.1 was used to fit the data to a sigmoidal trend, and the melting temperature was calculated by determining the maximum value of the first derivative.

DLS measurements

Prior to DLS measurement, all samples were filtered through a 220 nm filter. DLS was done using a Malvern Zetasizer. All measurements were done at 25 °C using a 173° scattering angle.

miRNA-221 displacement

To measure the displacement of PNA using miRNA-221, 90 µL PNA-DNA-AuNP conjugates were placed in a white, nonstick, 384-well plate. The samples were equilibrated to 37 °C, and 10 µL miRNA-221 was added to give a final concentration from 0-8.1 µM. The fluorescence was monitored using λ_{ex}= 490 nm and λ_{em}= 520 nm every 1 min, slowly shaking between measurements to prevent particle agglomeration.

Cell permeability studies

HeLa cells were grown at 37 °C in 5% CO_2. For this study, we put 25,000 cells/well in a 96 well plate with MEM media supplemented with 10% heat-inactivated FBS and 1% penicillin/streptomycin. After 24 h, the media was removed and replaced with fresh media containing either 5 or 10 nM DNA-AuNPs or PNA-DNA-AuNPs. After 48 h, the cells were washed 3 times with PBS. Following trypsinization, the cells were counted and their viability measured using an Orflo Moxi Z cell counter, and they were digested using hot HCl and HNO_3. The quantity of gold present was then measured using ICP-MS.

References

(1) Dall'Era, M. A.; Cooperberg, M. R.; Chan, J. M.; Davies, B. J.; Albertsen, P. C.; Klotz, L. H.; Warlick, C. A.; Holmberg, L.; Bailey, D. E., Jr.; Wallace, M. E.; Kantoff, P. W.; Carroll, P. R. Active surveillance for early-stage prostate cancer: review of the current literature. *Cancer* **2008**, *112*, 1650-1659.

(2) Ciatto, S.; Zappa, M.; Bonardi, R.; Gervasi, G. Prostate cancer screening: the problem of overdiagnosis and lessons to be learned from breast cancer screening. *Eur. J. Cancer* **2000**, *36*, 1347-1350.

(3) Galardi, S.; Mercatelli, N.; Giorda, E.; Massalini, S.; Frajese, G. V.; Ciafre, S. A.; Farace, M. G. miR-221 and miR-222 expression affects the proliferation potential of human prostate carcinoma cell lines by targeting p27Kip1. *The J. Biol. Chem.* **2007**, *282*, 23716-23724.

(4) Sun, T.; Wang, Q.; Balk, S.; Brown, M.; Lee, G. S.; Kantoff, P. The role of microRNA-221 and microRNA-222 in androgen-independent prostate cancer cell lines. *Cancer Res.* **2009**, *69*, 3356-3363.

(5) Nielsen, P. E.; Egholm, M.; Berg, R. H.; Buchardt, O.: Sequence-selective recognition of DNA by strand displacement with a thymine-substituted polyamide. *Science*, **1991**, *254,* 1497-1500.

(6) Demidov, V. V.; Potaman, V. N.; Frank-Kamenetskil, M. D.; Egholm, M.; Buchard, O.; Sönnichsen, S. H.; Nlelsen, P. E. Stability of peptide nucleic acids in human serum and cellular extracts. *Biochem. Pharmacol.* **1994**, *48*, 1310-1313.

(7) Nielsen, P. E.: Addressing the challenges of cellular delivery and bioavailability of peptide nucleic acids (PNA). *Q Rev Biophys*. **2005**, *38*, 345-350.

(8) Giljohann, D. A.; Seferos, D. S.; Patel, P. C.; Millstone, J. E.; Rosi, N. L.; Mirkin, C. A. Oligonucleotide Loading Determines Cellular Uptake of DNA-Modified Gold Nanoparticles. *Nano Lett.* **2007**, *7*, 3818-3821.

(9) Dulkeith, E.; Ringler, M.; Klar, T. A.; Feldmann, J.; Muñoz Javier, A.; Parak, W. J. Gold Nanoparticles Quench Fluorescence by Phase Induced Radiative Rate Suppression. *Nano Lett.* **2005**, *5*, 585-589.

(10) Seferos, D. S.; Giljohann, D. A.; Hill, H. D.; Prigodich, A. E.; Mirkin, C. A. Nano-Flares: Probes for Transfection and mRNA Detection in Living Cells. *J. Am. Chem. Soc.* **2007**, *129*, 15477-15479.

(11) Duy, J.; Connell, L.; Eck, W.; Collins, S.; Smith, R. Preparation of surfactant-stabilized gold nanoparticle–peptide nucleic acid conjugates. *J. Nanopart. Res.* **2010**, *12*, 2363-2369.

(12) Storhoff, J. J.; Elghanian, R.; Mucic, R. C.; Mirkin, C. A.; Letsinger, R. L. One-Pot Colorimetric Differentiation of Polynucleotides with Single Base Imperfections Using Gold Nanoparticle Probes. *J. Am. Chem. Soc.* **1998**, *120*, 1959-1964.

(13) Hurst, S. J.; Lytton-Jean, A. K. R.; Mirkin, C. A. Maximizing DNA Loading on a Range of Gold Nanoparticle Sizes. *Anal. Chem.* **2006**, *78*, 8313-8318.

(14) Thaxton, C. S.; Mirkin, C. A.: DNA–Gold-Nanoparticle Conjugates. In *Nanobiotechnology*; Wiley-VCH Verlag GmbH & Co. KGaA, 2004; pp 288-307.

(15) Lytton-Jean, A. K. R.; Mirkin, C. A. A Thermodynamic Investigation into the Binding Properties of DNA Functionalized Gold Nanoparticle Probes and Molecular Fluorophore Probes. *J. Am. Chem. Soc.* **2005**, *127*, 12754-12755.

(16) Joshi, R.; Jha, D.; Su, W.; Engelmann, J. Facile synthesis of peptide nucleic acids and peptide nucleic acid-peptide conjugates on an automated peptide synthesizer. *J. Pept. Sci.* **2011**, *17*, 8-13.

(17) De Costa, N. T. S.; Heemstra, J. M. Evaluating the Effect of Ionic Strength on Duplex Stability for PNA Having Negatively or Positively Charged Side Chains. *PLoS ONE* **2013**, *8*, e58670.

CHAPTER 6

CONCLUSION AND FUTURE DIRECTIONS

Micellar Studies

The presence of cross-links in micelles has been shown to improve stability, prevent the release of guest molecules, and provide stimuli-responsiveness. We have incorporated nucleic acids by attaching them to a hydrophobic tail to form amphiphilic monomers capable of forming micelles. We hypothesized the DNA would provide a means of forming noncovalent cross-links to stabilize the micelles nonand prevent guest molecules from escaping. The DNA strand also allows for micelle response to a complementary target nucleic acid, enzyme, or small-molecule target. In order to encourage the formation of cross-links across the surface of the micelle rather than the formation of dimers, DNA was synthesized using a trebler or two sequential doubler modifications to introduce three or four DNA strands, respectively.

The studies reported here show the initial characterization of micelles formed using trebler or doubler DNA attached to a hydrophobic tocopherol tail. We found that these sequences did in fact form micellar structures. Additionally, multiple sequences can be combined to form a single population of micelles. Pyrene was used to measure the CMCs for our monomers by comparing the

emission bands at 373 and 384 nm to monitor micelle formation. Initially it was anticipated that the hybridization of the DNA would stabilize the micelles and decrease the CMC; however, it was found that this stabilization was minimal. It was shown that the micelles could undergo enzymatic degradation, which confirmed the presence of crosslinks. The stability of these micelles was also investigated using an exchange process monitoring the FRET after combining micelle populations containing DiO and DiI. We observed that the presence of DNA slowed the exchange; however, the exchange did not appear to be slowed by introduction of the cross-links.

We had previously hypothesized that EcoR1 cleavage of the micelles would initiate guest exchange. CMC measurements of the full-length sequences and the truncated sequences that would result from EcoR1 cleavage did not yield significantly different results. Additionally, we used FAM- and Cy3-labeled sequences to monitor EcoR1 cleavage of the duplexes via FRET. We observed that the digestion of the duplexes in the micelle was slightly slower than that of the free DNA duplex.

In conducting these experiments, we found that DiO was very responsive to changes in polarity and was easy to work with. These observations were extremely encouraging, since previous attempts to characterize our micelles using NR had proven frustrating and inconsistent. As a result, we tried to measure the CMC of micelles using DiO and found that this method gave accurate, consistent results. We show DiO gives better data by performing a side-by-side comparison with NR. This was done using multiple commonly used surfactants which encompass the four ionic states. We found that while both NR and DiO give

accurate results, DiO gives more reliable, precise data. Preliminary studies have been performed using the DiO method for our DNA amphiphiles, giving CMC values comparable to those found using pyrene. Conversely, NR failed to yield accurate results. Therefore, future characterization of our monomers will be performed using DiO.

Future studies for this system will continue looking for methods to change micelle stability and guest release due to changes in the DNA corona. Changing to a different hydrophobic group may affect these properties, since micelle formation represents a balance between hydrophobic and hydrophilic groups. In these studies, we have used trietyhleneglycol groups to connect the tocopherol to the DNA. It is probable that this linker has a role in monomer geometry, which in turn affects the packing capability and stability of the micelle structure. It may also interact with guest molecules that change the stability of the assembly. Therefore, exploring different lengths of PEG chain or the use of a carbon chain may improve the desired properties in assembly. It may also be possible to change the CMC and guest release kinetics by using a structure-switching aptamer in the corona. The monomers would be formed by attaching the displacement strand to the hydrophobic group. When the aptamer is hybridized to the monomer, it would increase the blockage of the micelle; however, when the aptamer is released upon target binding, we anticipate that it would then allow for increased guest exchange. Targeted drug delivery and sensing applications would become accessible upon control of guest release using DNA cross-linked micelles.

Aptamer Functionality in the Presence of Surfactants

Many affinity reagents, such as antibodies, are not stable in solutions containing surfactants and lose their ability to bind their target molecules. We hypothesized that DNA aptamers may be able to overcome this limitation. Aptamers are rising in their use as affinity reagents and, unlike antibodies, can be developed *in vitro* and produced with low batch-to-batch variability. Herein we demonstrated that aptamers retain their functionality in the presence of negative and neutral surfactants. Using CD spectroscopy, we were able to verify that aptamers retain their structure in the presence of up to 4% surfactant. We were also able to show that the presence of micelles modulates the binding of hydrophobic molecules to the biosensor likely due to encapsulation of these molecules. Importantly, the binding of hydrophilic molecules is only slightly affected.

Since we have determined that aptamers maintain their functionality in surfactants, we are currently working to select aptamers under such conditions. Specifically, we would like to be able to generate an aptamer that can bind to denatured proteins. Detecting new disease biomarkers is a great challenge because they are found in very low quantities and can be masked by high abundance proteins such as HSA. However, HSA cannot be simply removed from the plasma samples, because it frequently interacts with other proteins, causing the loss of potential biomarker proteins or peptides.[1] Therefore, we propose that all protein-protein interactions must be disrupted before removing the HSA. In order to do this, we will use SDS and a reducing agent such as DTT or tris(2-carboxyethyl)phosphine (TCEP) to eliminate disulfide bonds. Using the biosensor

for L-tyrosinamide,[2] we have shown that DTT only minimally affects target binding (Figure 6.1).

We have started employing a process known as the systematic evolution of ligands by exponential enrichment (SELEX) to generate an aptamer which can bind denatured HSA. SELEX is an iterative process to select for nucleic acid sequences that have affinity for a selected target. We are specifically using the procedure known as FluMag-SELEX, where the target is covalently attached to a magnetic bead (Figure 6.2).[3] This allows for separation of the bound sequences from the vast majority of nonbinding sequences and also allows for washing of the protein to remove weak or nonspecific binders. With each cycle, the bound fraction is amplified, consequently enriching the binding sequences in the next round of selection. Once the percent of strands that bind during selection plateaus, the enriched pool of nucleic acids can be sequenced and tested for binding affinity. Once an aptamer is selected, it will be tested for affinity and specificity, minimized, and will be used to deplete HSA within a sample.

PNA-DNA-AuNP Conjugates

Many labs use DNA-DNA-AuNP conjugates in order to deliver DNA into cells and monitor the increase in fluorescence to quantify a target nucleic acid sequence. While this approach provides increased stability to the DNA duplex, it is still susceptible to degradation. The use of an artificial nucleic acid, such as PNA, prevents any degradation from occurring. However, since PNA has a neutral backbone, it results in aggregation of the AuNP. By first attaching DNA to AuNP, PNA can be subsequently hybridized to AuNP for cellular delivery and detecting a

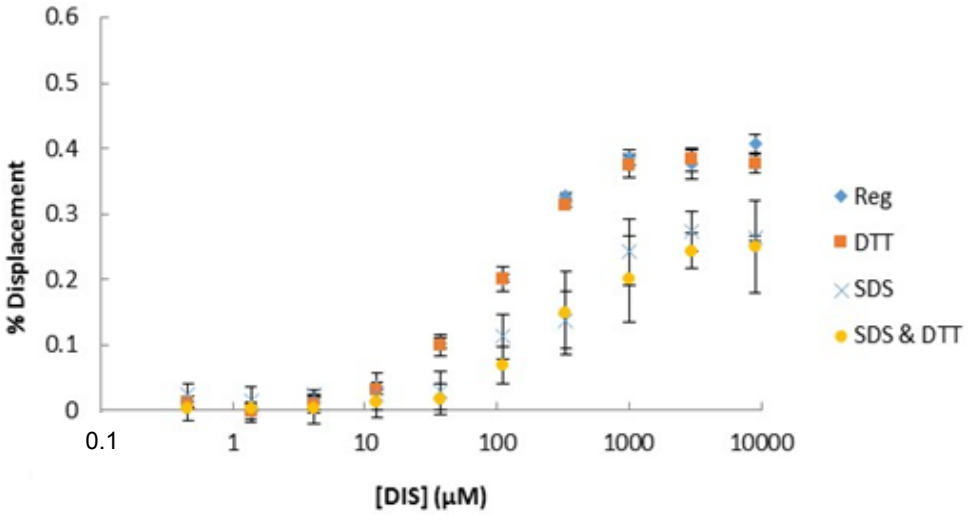

Figure 6.1. Binding of the L-tyrosinamide biosensor to its target in the presence of 4% SDS and 50 mM DTT.

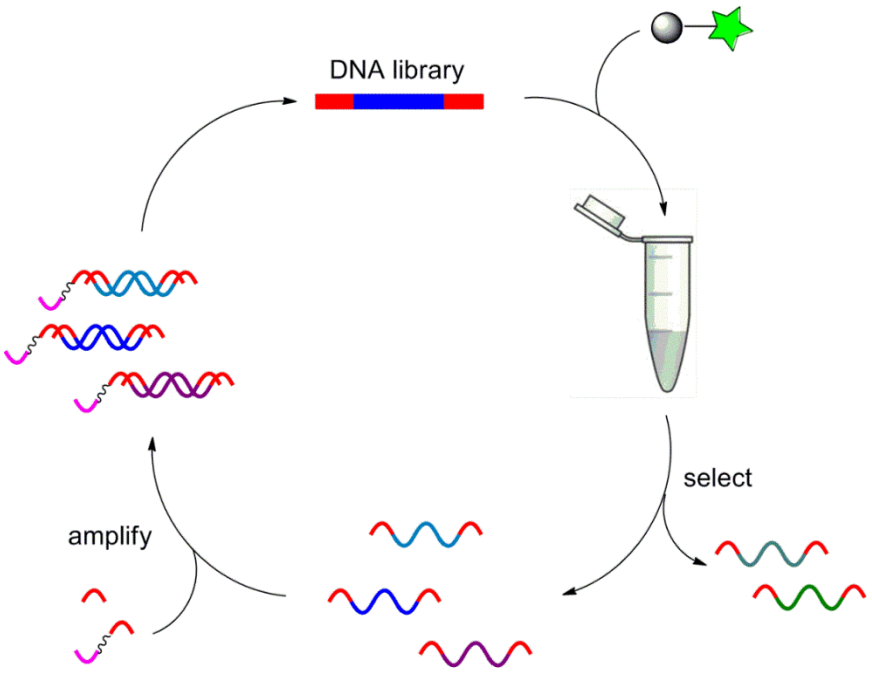

Figure 6.2. The basic cycle FluMag-SELEX. Binding sequences are enriched through a cyclical process of isolating and amplifying binding strands.

target nucleic acid sequence. To prevent nanoparticle aggregation, the PNA can be solubilized using aspartic acid rather than lysine. In the presence of a target sequence, the fluorescence increase due to PNA release is dose dependent. These particles also demonstrate cell permeability. These data are preliminary, and will be repeated in future experiments to accurately characterize this system. Enzymatic degradation studies would also confirm the utility of this system over traditional DNA-DNA-AuNP systems.

Since different batches of AuNPs have given us very different results, future work for this project will begin with the synthesis of AuNPs from $HAuCl_4$ and citrate to ensure consistency in AuNP composition. We would also like to determine the loading of the DNA and PNA on the AuNP. We have attempted to accomplish this by displacing the thiolated DNA using 6-mercapto-1-hexanol and DTT, but this has given very inconsistent results. To overcome this, our next trial will utilize KCN to dissolve the AuNPs in order to isolate and quantify the DNA. This shall be done using fluorescently-labeled DNA and again with fluorescent PNA to determine the loading of each individually. Once the AuNP is dissolved, we will quantify the DNA and PNA using fluorescence measurements. Since PNA should stabilize the duplexes, we will also quantify the digestion using nucleases and proteases. We will use both trypsin and DNase I to measure the degradation of the DNA-PNA-AuNPs. We will compare this to the same studies on the corresponding DNA-DNA-AuNPs. We shall finish the preliminary characterization by repeating the displacement studies with miRNA-221 to determine reproducibility and the platform's detection range.

Following the studies to assess cell permeability, we will verify that the PNA-

DNA-AuNPs are indeed entering the cells, rather than simply sticking to the surface. This will be done by adding the PNA-DNA-AuNPs to the cells shortly before the washing and trypsinization steps. After confirming cellular entry, we will need to verify that the PNA is not being removed prior to cellular entrance of the complex. This can be done by using cells that have varying expression levels of miRNA-221 and measuring fluorescence. Specifically, we will use the prostate cell lines, LNCaP and PC3, to study nanoparticle permeabilities and relative fluorescence values. PC3 cells are aggressive cancer cell lines and have shown a >10-fold increase in miRNA-221 concentrations compared to LNCaP cells, an indolent form of prostate cancer. After incubating the cells with our PNA-DNA-AuNP constructs, cellular fluorescence will be measured using fluorescence-activated cell sorting (FACS). Ultimately, these experiments will be considered successful if fluorescence measurements are able to distinguish LNCaP cells PC3 cell lines due to AuNP internalization and PNA release.

Throughout this dissertation, electrostatic interactions play an important role in the functionality of nucleic acids and their assembly properties. In DNA-based nanostructures, the electrostatics must be properly tuned in order to avoid agglomeration such as the case of the AuNPs. DNA biosensors do not function in the presence of CTAB; however, they maintain their binding abilities in the presence of negative and neutral surfactants. Further, SDS micelles are capable of modulating the binding of target molecules with different hydrophobicities. When incorporating nucleic acids into sensing and drug delivery applications, the electrostatics must be properly tuned to give the desired functionality while preventing undesired effects.

References

(1) Gundry, R. L.; Fu, Q.; Jelinek, C. A.; Van Eyk, J. E.; Cotter, R. J. Investigation of an albumin-enriched fraction of human serum and its albuminome. *Proteomics Clin. Appl.* **2007**, *1*, 73-88.

(2) Feagin, T. A.; Olsen, D. P. V.; Headman, Z. C.; Heemstra, J. M. High-Throughput Enantiopurity Analysis Using Enantiomeric DNA-Based Sensors. *J. Am. Chem. Soc.* **2015**, *137*, 4198-4206.

(3) Stoltenburg, R.; Reinemann, C.; Strehlitz, B. FluMag-SELEX as an advantageous method for DNA aptamer selection. *Anal. Bioanal. Chem.* **2005**, *383*, 83-91.